Fachbereich Erziehungswissenschaft und Psychologie

der Freien Universität Berlin

A core organizing axis of the human cerebral cortex

Dissertation

zur Erlangung des akademischen Grades

Doktorin der Philosophie (Dr. phil.)

vorgelegt von

Julia M Huntenburg, M. Sc.

Berlin 2017

Erstgutachter:	Prof. Dr. Felix Blankenburg
Zweitgutachter:	Dr. Daniel S Margulies
Datum der Disputation:	12. Dezember 2017

Acknowledgments

I would like to thank :

Daniel Margulies and Pierre-Louis Bazin for sharing their knowledge and contagious passion for Science, and for supporting me in all of my endeavors.

The groups for Neuroanatomy & Conntectivity and Algorithms, Morphometrie &Plasticity for stimulating meetings, heartfelt colleagueship and many good laughs.

The Brainhack community for proving that there is hope for Science.

The Max Planck Society, Studienstiftung des Deutschen Volkes and Google Summer of Code for funding me with a Scholarship.

My family, Ulla, Kadl, and chosen family, Eric, Bjørt, Bene, Jake, ... for relentless encouragement and for having my back.

Was unser Geist der Wirrnis abgewinnt,
kommt irgendwann Lebendigem zugute;
wenn es auch manchmal nur Gedanken sind,
sie lösen sich in jenem großen Blute,
das weiterrinnt.
R.M.Rilke

Contents

Zusammenfassung

Klassische Arbeiten in der Neuroanatomie legen nahe, dass die Anordnung von Rindenfeldern in räumlichen Gradienten ein zentrales Organisationsmerkmal der Großhirnrinde darstellt. Räumliche Gradienten in kortikaler Mikrostruktur und Konnektivität konnten in Versuchstieren eindeutig nachgewiesen werden. Entsprechende Studien im menschlichen Gehirn waren hingegen bisher nicht praktikabel. Daher bleibt auch die Bedeutung struktureller Gradienten für den funktionellen Aufbau des menschlichen Kortex derzeit ungeklärt.

Die vorliegende Dissertation macht sich aktuelle Fortschritte in der Magnetresonanztomographie und neue analytische Ansätze zunutze um räumliche Gradienten im menschlichen Kortex *in vivo* zu untersuchen. Wir führen zunächst einige sachdienliche Werkzeuge ein und weisen anschließend nach, dass verschiedene kortikale Eigenschaften in einem Gradienten zwischen sensomotorischen und transmodalen Regionen organisiert sind. Dieser Gradient findet in der Verteilung des intrakortikalen Myelingehalts Ausdruck und erfasst einen Großteil der Varianz funktioneller Konnektivitätsmuster. Er steht mit der spezifischen Geometrie des Kortex in enger Beziehung und spiegelt sich in einem funktionellen Spektrum zunehmender Abstraktion wider. Wir schlagen schließlich vor, dass dieser Gradient eine grundlegende Organisationsachse des menschlichen Kortex darstellt und arbeiten ein hierauf basierendes intrinsisches kortikales Koordinatensystem aus. Eine Erforschung des Kortex im Hinblick auf seine intrinsischen Dimensionen kann unser Verständnis davon befördern, wie die strukturellen Bedingungen des Kortex sein funktionelles Spektrum hervorbringen.

Abstract

Classical work in neuroanatomy suggests that the spatial arrangement of cortical areas in overarching gradients is a key organizational feature of the cerebral cortex. While studies performed in experimental animals provide strong evidence for spatial gradients in cortical microstructure and connectivity, similar research in humans has been obstructed by methodological challenges. In consequence, the significance of structural gradients for human cortical function remains unaddressed.

The work presented in this dissertation capitalizes on recent advances in magnetic resonance imaging and novel analytic strategies to investigate spatial gradients in the human cerebral cortex *in vivo*. We first introduce a set of relevant tools and proceed to demonstrate a global gradient in cortical features that spans between sensorimotor and transmodal areas. This gradient is reflected in the distribution of intracortical myelin and captures the main axis of variance in functional connectivity patterns. It is spatially embedded in the intrinsic geometry of the cortex and tracks a functional spectrum of increasing abstraction. Finally, we propose that this gradient constitutes a core organizing axis of the human cerebral cortex, and describe an intrinsic cortical coordinate system on its basis. Studying the cortex with respect to its intrinsic dimensions can inform our understanding of how the spectrum of cortical function emerges from structural constraints.

List of original publications

This dissertation is based on the following publications (in the order of appearance):

Technical reports

Huntenburg, J.M., Wagstyl, K., Steele, C.J., Funck, T., Bethlehem, R.A.I., Foubet, O., Larrat, B., Borrell, V. & Bazin, P.-L. (2017a). Laminar Python: tools for cortical depth-resolved analysis of high-resolution brain imaging data in Python. *Research Ideas and Outcomes, 3*(e12346). doi: 10.3897/rio.3.e12346

Huntenburg, J.M., Steele & Bazin, P.-L. (in preparation for GigaScience). Nighres – processing tools for high-resolution neuroimaging.

Huntenburg, J.M., Abraham, A., Loula, J., Liem, F., Dadi, K. & Varoquaux, G. (2017b). Loading and plotting of cortical surface representations in Nilearn. *Research Ideas and Outcomes, 3*(e12342). doi: 10.3897/rio.3.e12342

Margulies, D.S., Falkiewicz, M. & **Huntenburg, J.M**. (2016). A cortical surface-based geodesic distance package for Python. *GigaScience, 5*(1), 1920. doi: 10.1186/s13742-016-0147-0-q

Data paper

Mendes, N., Oligschlaeger, S., Lauckner, M. E., Golchert, J., **Huntenburg, J. M.**, Falkiewicz, M., ... Margulies, D. S. (under review at Scientific Data). A functional connectome phenotyping dataset including cognitive state and personality measures. (Preprint available on *bioRxiv* doi: 10.1101/164764)

Empirical studies

Huntenburg, J.M., Bazin, P.-L., Goulas, A., Tardif, C.L., Villringer, A., Margulies, D.S. (2017c). A systematic relationship between functional connectivity and intracortical myelin in the human cerebral cortex. *Cerebral Cortex, 27*(2), 981-997. doi: 10.1093/cercor/bhx030

Oligschlaeger, S., **Huntenburg, J.M.**, Golchert, J., Lauckner, M.E., Bonnen, T., Margulies, D.S. (2016). Gradients of connectivity distance are anchored in primary cortex. *Brain Structure and Function (222)*(5). doi: 10.1007/s00429-016-1333-7

Margulies, D.S., Ghosh, S.S., Goulas, A., Falkiewicz, M., **Huntenburg, J.M.**, Langs, G., Bezgin, G., Eickhoff, S.B., Castellanos, F.X., Petrides, M., Jefferies, E., Smallwood, J. (2016). Situating the default-mode network along a principal gradient of macroscale cortical organization. *Proceedings of the National Academy of Sciences USA, 113*(44), 12574-12579. doi: 10.1073/pnas.1608282113

Opinion article

Huntenburg, J.M., Bazin, P.-L., Margulies, D.S. (accepted). Large-scale gradients in human cortical organization. *Trends in Cognitive Sciences*.

List of Figures

Abbreviations

AC	anterior commissure
AP	anterior-posterior
CNS	central nervous system
DMN	default mode network
EPI	echoplanar imaging
fMRI	functional magnetic resonance imaging
Hz	Hertz
μm	micrometer
min	minute
mm	millimeter
MP2RAGE	magnetization prepared two rapid acquisition gradient echoes
MRI	magnetic resonance imaging
ms	millisecond
PA	posterior-anterior
PC	posterior commissure
PCC	posterior cingulate cortex
ROI	region of interest
sec	second
T	Tesla
T1(w)	(weighted for) longitudinal relaxation time
T2(w)	(weighted for) transversal relaxation time
TE	echo time
TI	inversion time
TR	repetition time
V1	primary visual cortex

Chapter 1

Introduction

For more than a century, neuroscientists have studied the cerebral cortex by delineating individual cortical areas and mapping their function (Brodmann, 1909; Vogt & Vogt, 1919). This agenda has substantially advanced in recent years, as automated parcellation methods improve and datasets of unprecedented size and quality become available (Amunts & Zilles, 2015; Eickhoff et al., 2017; Glasser et al., 2016). Non-invasive functional neuroimaging has made it possible to associate even high-level human cognitive functions with activity in particular areas or networks. Nevertheless, our understanding of how these complex functions emerge remains fragmentary.

A core tenet of biology is that knowing the structure of a system is essential for a far-reaching understanding of its function (e.g Gudden, 1886). *Knowing the structure* involves a detailed description of the systems individual subunits, such as cortical areas. But it also requires to understand how these subunits are organized in a complex entity from which function arises. The work presented in this dissertation therefore starts from the premise that in order to understand cortical function, we need to complement the characterization of individual cortical areas with a description of their *spatial arrangement*.

Early formulations of this perspective can be found in theories from classical neuroanatomy (Brockhaus, 1940; Pandya & Sanides, 1973; Pandya & Yeterian, 1985; Sanides, 1962, 1969, 1972; Vogt & Vogt, 1919). They state that the spatial layout of

cortical areas is not arbitrary, but a consequence of developmental mechanisms, shaped through evolutionary selection. The location of an area among its neighbors therefore reflects its microstructural characteristics, its connections to other parts of the cortex, and eventually its position in functional processing hierarchies. While these theories are based on qualitative post-mortem studies of mostly non-human species, the papers presented in this dissertation capitalize on state-of-the-art neuroimaging and novel analytic approaches to investigate the spatial organization of the human cerebral cortex *in vivo*. Their common goal is to identify general principles in the spatial layout of the human cortex, that can add to our understanding of how this complex structure gives rise to the spectrum of human cognitive functions.

1.1 Spatial gradients in cortical organization

1.1.1 Progressive microstructural differentiation

A prominent approach to describe cortical organization are architectonic methods, which were established in the early twentieth century by Cécile and Oscar Vogt and their collaborators. The Vogt-Vogt school mainly focused on the meticulous description of individual areas based on their microstructural differentiation in sections stained for cells (cytoarchitectonics, Brodmann, 1909) or myelinated fibers (myeloarchitectonics, Vogt & Vogt, 1919).[1] However, in a short paragraph of their main work the Vogts comment on the spatial arrangement of areas, remarking that an area typically represents the intermediate stage of differentiation between its neighbors (Vogt & Vogt, 1919, p.369, "Die Tatsache einer arealen Gradation"). This concept of *areal gradation* was later revisited by one of the Vogts' collaborators, Harald Brockhaus, who explicitly

[1]Cortical areas vary in terms of how clearly the six major cortical layers and their sublayers can be discerned, in their emphasis on infra- or supragranular layers, and their overall myelin content. A detailed description of areal differentiation can be found e.g. in Nieuwenhuys (2013). In the most general terms, highly differentiated areas present with easily discernible layers, an emphasis on supragranular layers and high myelin content.

traced *directions of differentiation* in his work on the insular cortex (Brockhaus, 1940).

Friedrich Sanides, another collaborator of the Vogts, eventually made the spatial arrangement of cortical areas central to his research. In his comparative studies Sanides recognized that the entire mammalian cortex can be divided in two parallel trends of progressive microstructural differentiation, and proposed that these *Ur-Trends* represent the course of neocortical evolution (Sanides, 1962, 1969, 1972) (Figure 1.1). This thesis was in striking agreement with the *dual origin theory*, previously proposed by Dart (1934) and Abbie (1940, 1942) in more primitive species, and extended it to the mammalian cortex. According to this theory, the neocortex evolved out of two primordial origins: the hippocampal archicortex and the pyriform (or olfactory) paleocortex. Trends of progressive microstructural differentiation can be traced from each of the origins, and the position of an area in these trends reflects when they emerged during evolution. Sanides work in larger mammalian cortices showed that each of the two major trends in fact subsumes multiple sub-progressions in the different cortical lobes (Figure 1.1). Most relevant to the current dissertation is the basic conclusion that the relative spatial position of cortical areas is meaningful as it reflects their microstructural differentiation and phylogenetic history.

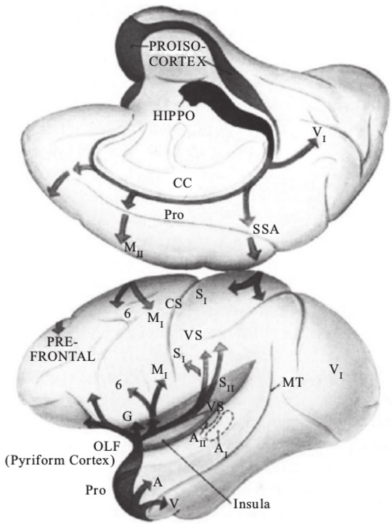

Figure 1.1 Cortical gradients in the macaque monkey cortex. Schematic representation of the progression of the two evolutionary gradients in the macaque monkey. The medial gradient emerges from the hippocampal archicortex (HIPPO), and the lateral gradient from the pyriform or olfactory paleocortex (OLF). Each gradient splits in multiple sub-gradients in the different lobes (Pandya & Yeterian, 1985).

While the observation of an orderly spatial progression in microstructural differentiation is consistent across studies, different researchers have used various terms to refer to this phenomenon (e.g. areal gradation, directions of differentiation, Ur-Trends). For clarity, we will use the term *spatial gradient*, or simply gradient, throughout this dissertation. We define gradients as axes of variance in cortical features along which areas fall in a spatially continuous order. Areas that resemble each other with respect to the feature of interest – here their level of microstructural differentiation – occupy similar positions along the gradient. While the aforementioned literature describes gradients in microstructural features only, the next chapters will discuss evidence that spatial gradients represent a more general organizational principle of the cerebral cortex.[2]

1.1.2 Converging gradients in cortical microstructure and connectivity

While Sanides studied microstructural gradients in the macaque monkey and human frontal lobe, he noted their spatial similarity with the basic dorsal-ventral subdivision that had been described in macaque monkey frontal lobe connectivity by Nauta (1964) (Sanides, 1972). Based on this observation Sanides initiated a collaboration with Deepak Pandya, who was at the forefront of an emerging field studying cortical connections through invasive tract-tracing. Together they investigated the relationship between microstructure and connectivity in the macaque monkey cortex (Pandya & Sanides, 1973). Pandya and his collaborators subsequently pursued this combined approach in numerous studies, which consistently found that microstructural spatial gradients are paralleled by the organization of cortico-cortical connections (reviewed in Pandya et al., 2015). According to these studies, most connections follow a particular microstructural gradient and connect areas in relative close spatial proximity within

[2]Importantly, the concept of spatial gradients does not discount the idea of discrete cortical areas but instead moves their spatial relationship into focus. It remains agnostic regarding the long-standing debate of whether transitions between individual areas are sharp or gradual (e.g. Bailey & von Bonin, 1951).

this gradient. Links between distant areas, and across gradients are less common. Notably, the existing long-range connections preferentially occur between areas that have a comparable level of microstructural differentiation (Pandya & Sanides, 1973; Pandya & Yeterian, 1985, 1990).[3] This last claim in particular has more recently been supported by quantitative analyses of tract-tracing data from the macaque monkey (Beul et al., 2015), cat (Beul et al., 2014), and mouse cortex (Goulas, Uylings, & Hilgetag, 2016), showing that areas with similar microstructural differentiation are more likely to be connected. Microstructural similarity has therefore been suggested as a general wiring rule of the mammalian cortex (Barbas, 2015; Goulas, Werner, et al., 2016; Pandya et al., 2015).

These findings open a new perspective on the concept of spatial gradients. Typically, areas that occupy a similar position along a cortical gradient can be found close to each other on the cortical sheet. This is a plausible consequence of the observations that neighboring areas do not show extreme differences in their level of microstructural differentiation (cf. Vogt & Vogt, 1919) and that most connections are short (cf. Markov et al., 2011; Schüz & Braitenberg, 2002). The findings described in the previous paragraph emphasize that spatially distant areas can also have a similar level of microstructural differentiation and be linked through long-range connections. While such areas have originally been understood to occupy a comparable position along separate gradients, an alternative interpretation is that they occupy a comparable position along a *single gradient spanning the entire cortex*. Proximity in the space of the gradient would still largely reflect proximity on the cortical sheet, but also group distant areas close to each other along the gradient, if they are linked through long-range connections and microstructural similarity. This more global view has not explicitly been stated in the original theories, but constitutes a core concept introduced in this dissertation.

[3]This principle does not generally hold for primary sensorimotor areas, which, with the exception of the somatosensory and motor cores, do not directly connect to each other.

It does, however, resonates with a proposition of Pandya and colleagues, according to which spatially disparate but strongly connected areas represent functional entities. These functional networks are suggested to have emerged in response to the particular environmental challenges placed upon the organism at a specific time in evolution (Pandya et al., 2015). In line with the premise of the dual origin theory – that the microstructural differentiation of an area reflects its phylogenetic age – this view suggests that long-range connections between microstructurally similar areas are rooted in the simultaneous development of these areas during evolution.[4] It also broaches the question in how far the spatial gradients described in microstructure and connectivity are significant for the functional organization of the cortex.

1.1.3 Global functional processing hierarchies

The relationship of spatial gradients and cortical function can be illustrated through the well-researched example of the macaque monkey visual system (Felleman & Van Essen, 1991; Markov et al., 2014). A visual hierarchy has been established by ordering areas based on their microstructural features and classifying their interconnections in feedforward and feedback (cf. Barbas, 1986). Although structurally defined, this hierarchy captures the functional organization of the visual system. Low-level visual features are extracted in early visual areas and get increasingly abstracted and integrated with information from other systems, as they are passed up the hierarchy. This sequence has often been depicted in form of an abstract diagram (Figure 1.2 a, *left*). But when mapped onto the cortex, it becomes obvious that the flow of information along the visual hierarchy follows an orderly spatial progression from one area to the next along the cortical sheet (Figure 1.2 a, *right*). This observation has more recently been quanti-

[4] A complementary theory suggests that long-range connections between distant, but microstructurally similar areas arise through the timing of neurogenesis during ontogenetic development. Areas with similar microstructural differentiation are populated in the same time window and thus represent the most likely connection partners for each other. See Barbas (2015) and Goulas, Uylings, and Hilgetag (2016) for a more detailed account.

fied, by showing that the position of an area in the visual hierarchy is highly correlated to its geodesic distance from the primary visual cortex (Wagstyl et al., 2015) (Figure 1.2 b).[5] The functional specialization of areas in the visual hierarchy is thus strongly related to their spatial arrangement along the cortical sheet. Similar functional processing hierarchies have been described for the somatomotor (Felleman & Van Essen, 1991) and auditory system (Hackett et al., 1998), and show a comparable relationship to the distance along the cortical sheet from respective primary areas (Wagstyl et al., 2015).

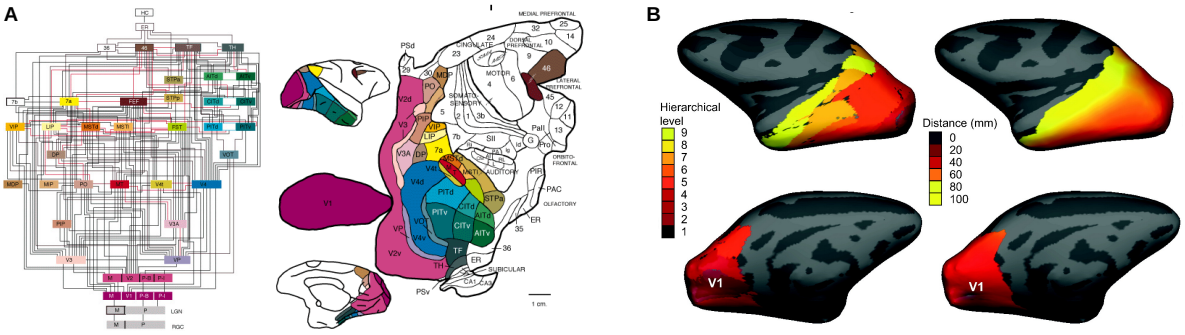

Figure 1.2 The visual hierarchy in the macaque monkey cortex. A functional processing hierarchy in the macaque monkey visual system has been established based on structural features. **A** The visual hierarchy represented as an abstract diagram (*left*) and projected on a cortical flat map (*right*) (Felleman & Van Essen, 1991). **B** The hierarchical level of visual regions (*left*) is strongly related to the geodesic distance from the primary visual cortex V1 (*right*) (Wagstyl et al., 2015)

But how can functional organization be described beyond these sensorimotor hierarchies? Do similar principles hold in regions of the frontal, temporal and parietal cortex, that have been associated with high-level cognitive functions such as social cognition (Spreng & Grady, 2010) or reward-guided decision making (Rushworth et al., 2011)? Marsel Mesulam was one the first to propose that functional processing hierarchies extend beyond sensorimotor systems to transmodal regions (Mesulam, 1998).[6] He suggested that abstract functional categories emerge from the convergence of infor-

[5]Geodesic distance measures the relative position of areas along the cortical sheet, independent of its folding. It will be discussed further in Sections 2.2.2 and 3.2.

[6]Transmodal, in contrast to unimodal, refers to cortical areas whose activity is not specific to a single modality of sensory input or motor output.

mation across different sensory modalities along a global processing hierarchy. From an information theoretical point of view this explanation is compelling. But Mesulam proposed an abstract schematic, similar to the classical diagram of the visual hierarchy, and it remains unaddressed how this global hierarchy is embedded in the space of the cortex. Furthermore, the concept of a global processing hierarchy is to large extents based on empirical data from research in macaque monkeys. Another question is therefore, whether it still applies to the massively expanded transmodal areas in the human cortex.

An interesting perspective on both questions can be found in the recently proposed *tethering hypothesis* (Buckner & Krienen, 2013). It argues that the functional attributes of transmodal areas are in fact a consequence of their increasing spatial distance from molecular patterning centers, which closely regulate the development of sensorimotor regions. Released from such molecular constraints, transmodal regions present with more flexible circuit patterns and in particular form long-range connections. These facilitate the integration of information across systems. This theory supports the idea that the spatial arrangement of cortical areas might play an important role, not only for sensorimotor processing hierarchies (Wagstyl et al., 2015), but for the emergence of a global processing hierarchy spanning the entire cortex. It also offers a framework in which the massive expansion of transmodal areas in humans naturally leads to an extension of this hierarchy, and an increasing emphasis on information integration and abstract representations.

The aforementioned theories suggest a global cortical processing hierarchy, along which information is integrated across multiple domains into progressively more abstract representations. Local gradients within specific cortical systems could be situated and understood as part of this global framework. However, these conclusions are largely deduced from individual findings in different parts of the cortex, many of them obtained in experimental animals. An explicit demonstration of a global functional

hierarchy in the human cortex, and its relationship to spatial gradients, is yet to be provided.

1.2 Studying spatial gradients in the human cerebral cortex *in vivo*

The previous section reviewed comprehensive work on spatial gradients in cortical microstructure and connectivity, and their potential relationship to functional processing hierarchies. Of the studies discussed, the vast majority are based on invasive approaches in experimental animals or post-mortem samples. In addition, they often pursue a qualitative approach and many conclusions remain schematic. The work in this dissertation aims to complement this line of research with a quantitative investigation of spatial gradients in the human cerebral cortex *in vivo*. This endeavor has been enabled through recent advances in neuroimaging technology and analysis, which will be introduced in the following and further discussed throughout the remaining chapters (in particular Section 5.1 and 5.2).

1.2.1 Using high-resolution T1 maps to investigate cortical microstructure

The investigation of cortical microstructure has traditionally been confined to histological studies of post-mortem samples, stained for cells or myelinated fibers. However, with recent developments in ultra-high field ($\geq$ 7 Tesla) and quantitative magnetic resonance imaging (MRI) it is now possible to assess measures related to cortical microstructure *in vivo* (Weiskopf et al., 2015). Specifically, as the longitudinal relaxation time (T1) in MRI is sensitive to gray matter myelin content (Bock et al., 2009; Geyer et al., 2011; Stüber et al., 2014) maps of intracortical T1 have been introduced as an *in vivo* proxy for cortical microstructure, and revived interest in myeloarchitectonic approaches (Glasser et al., 2016; Nieuwenhuys, 2013). Increasingly available quantitative

sequences (e.g. MP2RAGE, Marques et al., 2010) drastically minimize the problem of radio frequency bias fields in T1 images (but see Lutti et al. (2014)) and enable a direct comparison of T1 maps across sessions, subjects and imaging sites (Turner, 2015). In addition, remarkable improvements in the signal-to-noise ratio at high field strength provide increasing spatial resolutions, that allow for intracortical sampling and reduce partial volume effects (Turner, 2013; Zaretskaya et al., 2017).

Taking advantage of these developments, the work presented in the current dissertation uses quantitative T1 maps acquired at 7 Tesla (7T) to estimate intracortical myelin content and draw conclusions about cortical microstructure *in vivo*. T1 maps display a gradient of decreasing myelin density from primary toward transmodal regions which is in line with histological studies (Hopf, 1956; Hopf & Vitzthum, 1957; Sanides, 1962; Vogt & Vogt, 1919). The co-occurrence of local changes in intracortical T1 maps with certain architectonic (Geyer et al., 2011; Glasser & Van Essen, 2011), functional (Bridge et al., 2005; Sigalovsky et al., 2006), and topographic (Dick et al., 2012; Sereno et al., 2013) boundaries, and with rapid changes in functional connectivity patterns (Glasser et al., 2016), exemplifies the meaningful relationship of intracortical T1 to other measures of cortical organization. Moreover quantitative T1 has recently been characterized by the highest intrasubject and intersubject reliability in a comparison of several approaches to map intracortical myelin (Haast et al., 2016). For simplicity, *intracortical T1* and *intracortical myelin content* will be used interchangeably throughout this work, fully acknowledging the serious limitations of measuring myelin using MRI which will further be discussed further in Section 5.1.

1.2.2 Assessing intrinsic cortical organization using resting state functional connectivity

Resting state functional MRI (fMRI) measures spontaneous low-frequency fluctuations in the blood oxygen level dependent signal, in the absence of a specified task demand.

Temporal correlations of these fluctuations across spatially distributed areas are commonly referred to as functional connectivity (Biswal et al., 1995). While functional connectivity also reflects indirect links between areas (Adachi et al., 2012), it is largely constrained by anatomical connections, as demonstrated in several studies in the human brain (Hagmann et al., 2008; Hermundstad et al., 2013; Honey et al., 2009; Skudlarski et al., 2008), as well as on the basis of macaque monkey tract-tracing data (Miranda-Dominguez et al., 2014; Vincent et al., 2007). Functional connectivity patterns robustly reproduce across different sites and protocols (Biswal et al., 2010) and show good test-retest reliability (Shehzad et al., 2009). Resting state functional connectivity has therefore become a widely used measure of the intrinsic organization of the human cortex, which is shaped and constrained by anatomical connections.

When analyzing whole-brain functional connectivity, a temporal correlation value is assigned to each pair of voxels or surface nodes resulting in a high-dimensional connectivity matrix. In order to extract intelligible information from such high-dimensional data, methods for dimensionality reduction are required. The most common approach is to group cortical regions into networks of strongly interconnected areas (e.g Yeo et al., 2011), or into locally confined parcels with high internal connectivity, which have been shown to partly overlap with architectonic areas (e.g. Glasser et al., 2016). These approaches are efficient but typically impose hard cut-offs between, and homogeneity within parcels. By treating parcels as discrete, independent entities the resulting representations fail to capture more gradual changes and overarching spatial relationships (Jbabdi et al., 2013).

More recently, pioneering studies have demonstrated continuous spatial patterns of connectivity in the human cerebral cortex (Atasoy et al., 2016; Haak et al., 2017; Langs et al., 2014, 2015; Sepulcre et al., 2012; Taylor et al., 2015). Instead of parcellating, these studies simplify the complex connectivity matrix to a small set of *connectivity gradients*. The most generic way to derive such gradients is to find the main axes of

variance in the data through decomposition or embedding techniques such as Laplacian Eigenmaps (Belkin & Niyogi, 2003) or diffusion maps (Coifman & Lafon, 2006). In these approaches, the original dimensions of the connectivity matrix are replaced by a set of new dimensions, chosen so that most of the variance in the data is captured by just a few of these dimensions. This can drastically reduce the number of dimensions that are required to represent the data, with few assumptions on its internal organization. Often the new dimensions are inherently ordered, so that the first dimension explains most of the variance in the connectivity matrix (it is sometimes called dominant), the second dimension explains the second most variance, and so on. Each cortical location can now be described by a set of values reflecting where it falls along the new dimensions. Each dimension is a continuous representation of one aspect of connectivity organization, in other words, a connectivity gradient. Areas that occupy a similar position on one of these gradients resemble each other in the aspect of connectivity the gradient represents.

A set of gradients derived from a decomposition represents superimposed aspects of connectivity organization. The interpretation of these gradients can be challenging because the decomposition does not provide information about the particular connectivity features that are reflected in each gradient. A recent study demonstrated that in the case of the primary visual cortex, connectivity gradients reflect important aspects of functional organization (Haak et al., 2017): the decomposition of primary visual cortex functional connectivity yielded two dominant gradients, one reflecting eccentricity and the other reflecting polar angle (Figure 1.3 a-b). Importantly, when the gradients were superimposed and a clustering algorithm was applied, the resulting parcellation did not reflect either of the retinotopic aspects (Figure 1.3 c). It thus appears that decomposing functional connectivity patterns into overlapping gradients is a promising new approach to investigate cortical organization, and a fruitful complement to spatially discrete parcellations. However, similar studies attempting to relate connectivity gradients to other structural or functional features on the scale of the entire cortex have

not yet been performed.

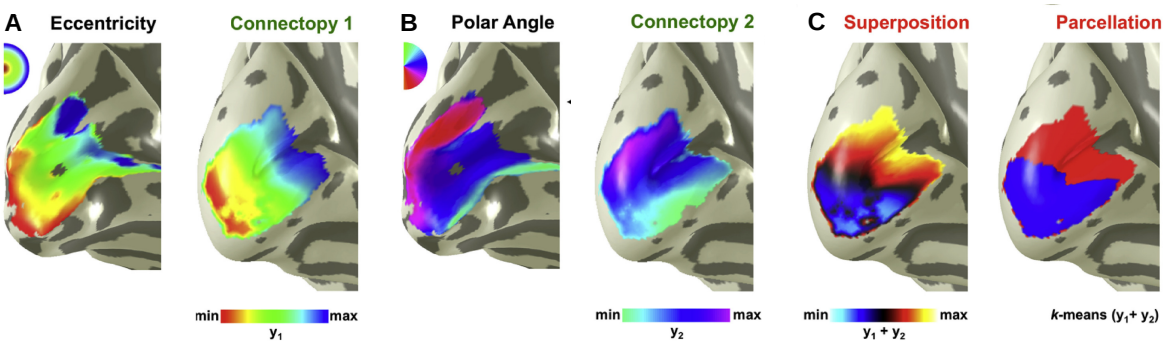

Figure 1.3 Connectivity gradients reflect functional organization in V1. The two dominant gradients (here called "connectopies") of group-level primary visual cortex (V1) functional connectivity reflect stimulus-based retinotopic organization. **A** The first connectivity gradient has a strong spatial correlation to V1's eccentricity map. **B** The second connectivity gradient has a strong spatial correlation to V1's polar angle map. **C** A parcellation based on the superimposed gradients is not meaningfully related to the functional organization of V1. (Haak et al., 2017)

1.3 Aim of the dissertation

The core aim of this dissertation was to apply the concept of spatial gradients in cortical organization – theoretically founded in classical neuroanatomy – to human neuroimaging. A first step towards this goal was to investigate the relationship between cortical microstructure, assessed using quantitative T1 maps, and gradients in resting state functional connectivity in the human cerebral cortex. A second step aimed to further characterize functional connectivity gradients, their relationship to the intrinsic cortical geometry, and to a putative global hierarchy in human cortical function. Given the novelty of the data and methods employed, an important aspect of this work was to develop the required image processing tools and to make them accessible to the scientific community.

Chapter 2

Methodological work

The aforementioned aims entail a set of empirical questions that we pursued in three studies discussed in Chapter 3. Yet, a large part of the work towards these aims was methodological. The questions we were interested in required access to high-quality data sets and specialized software tools. While we made use of several pre-existing open data sets and toolboxes, we also put a strong emphasis on making our own contribution to the scientific community. We released the data that we acquired for public use, made our analysis code openly available and developed significant parts of it into well-documented open source software.

Towards this last goal, we chose Python as our programming language. In recent years, Python has repeatedly been ranked as the most popular programming language[1] and a vibrant community has built around its application to scientific computing[2]. Especially in the field of neuroscience, Python has enjoyed a growing success (Muller et al., 2015). For example, *Nipy*[3] is a community of practice devoted to the development of versatile open source packages for the analysis of neuroimaging data in Python. Projects under the Nipy umbrella include Nibabel (Brett et al., 2016), which supports reading and writing of common neuroimaging data formats in Python, Nipype (Gorgolewski et al., 2011), which provides a uniform interface to combine existing software tools

[1] `https://spectrum.ieee.org/computing/software/the-2017-top-programming-languages`

[2] `https://www.scipy.org/`

[3] `http://nipy.org/`

in efficient pipelines, Nilearn (Abraham et al., 2014), a machine learning toolbox for neuroimaging data, and many others. We aimed to closely integrate our development efforts with this community to maximize the usefulness of our code to other researchers and ensure sustainability by winning active contributors.

Below, we summarize several coding projects relevant to the empirical work discussed in this dissertation. Section 2.1 describes the development of Python tools for processing of high-resolution neuroimaging data. Starting out with a set of functions serving a specific application (Huntenburg et al., 2017a), we subsequently developed this project into a comprehensive software framework for high-resolution image processing, that also provides a platform for future contributions from other researchers (Huntenburg, Steele & Bazin, in preparation). In Section 2.2 we describe our efforts to integrate support for cortical surface representations, essential to studying the spatial layout of cortical features, in Python-based neuroimaging software. In particular, we initiated cortical surface support in Nilearn (Huntenburg et al., 2017b), and introduced a package which facilitates the calculation of geodesic distance along the cortical sheet (Margulies, Falkiewicz & Huntenburg, 2016). Finally, we published a large data set, containing raw and preprocessed structural and resting state MRI data as well as a range of phenotypic measures (Mendes et al., under review), which we describe in Section 2.3.

2.1 Processing tools for high-resolution neuroimaging in Python

As discussed in the introduction, recent advances in high-field and quantitative MRI make it possible to image the whole brain at an unprecedented level of detail (Weiskopf et al., 2015). This data allows researchers to ask new questions about brain structure and function *in vivo*, particularly taking into account the intracortical distribution

of features (Trampel et al., 2017). Concurrently, the amount of neuroimaging data collected per subject in any given experiment increases considerably at this resolution. While the availability of ultra-high field scanners is growing and first 7T MRI data sets have been made publicly available (Forstmann et al., 2014; Gorgolewski et al., 2015; Tardif et al., 2016), software tools are lagging behind. Standard neuroimaging software is often challenged by the new data, resulting in an urgent demand for dedicated tools that can leverage the anatomical detail of high-resolution MRI data and scale well with their increasing size (see also Goebel, 2012; Zaretskaya et al., 2017). CBS High-Res Brain Processing Tools (CBS Tools) is a software suite which addresses this gap by providing cutting-edge methods for efficient processing of MR images at sub-millimeter resolution (Bazin et al., 2014). CBS Tools have been developed in Java as a set of plugins for the MIPAV software package (McAuliffe et al., 2001) and the JIST pipeline environment (Lucas et al., 2010). Unfortunately, this rather complex design can make the installation and handling of CBS Tools challenging for naive users and impedes contribution of other researchers. Since rapid methodological advances in the dynamic field of high-resolution neuroimaging are to be expected, we perceived a growing need for a transparent software platform, through which newly developed methods can be made available to the community and improved collaboratively. We therefore started a new software project in Python pursuing two major goals. First, we aimed to provide an easy-to-use and well-documented implementation of CBS Tools, which eliminates heavy dependencies and facilitates interactive data exploration and integration with popular Python-based neuroimaging tools. Second, we paid particular attention to setting up a project that encourages contributions by other researchers in either Python or Java.

2.1.1 Laminar Python (Technical report 1)

In a first step (Huntenburg et al., 2017a), we built the code repository *Laminar Python*[4], which is dedicated to disseminating one of CBS Tools' most differentiating features – the volume-preserving modeling of cortical laminae. For sampling data at different levels of intracortical depths, it is a common approach to construct multiple surfaces, or *cortical laminae*, between the white matter boundary and the pial surface. These laminae have previously been defined by simply keeping a constant distance between the boundaries (equidistant approach), or by computing equipotentials using the Laplacian equation. In contrast, the implementation in CBS Tools is based on the neuroanatomical work by Bok (1929), who observed that the thickness of architectonically defined layers changes throughout the cortex to compensate for cortical folding, while the volume of cortical segments remains stable (Figure 2.1 a). CBS Tools takes into account the local curvature of the cortical sheet and models cortical laminae which obey Bok's volume-preserving principle (Figure 2.1 b). These laminae provide an anatomically meaningful coordinate system of intracortical depth, which outperforms equidistant and Laplacian approaches in representing ground-truth architectonic layers in post-mortem samples (Waehnert et al., 2016, 2014).[5]

Laminar Python is a standalone package which provides user-friendly Python interfaces to the volume-preserving modeling of cortical laminae and associated CBS Tools functions. We used the JCC package[6] to encapsulate the original CBS Tools Java classes with C++ code, making them available to the Python interpreter. We then implemented a Python wrapper function around each encapsulated class to convert the

[4] `https://github.com/juhuntenburg/laminar_python`

[5] It is important to distinguish between the architectonically defined cortical layers (typically six in neocortical areas) and the analytically defined laminae of which an arbitrary number can be modeled between the white matter and pial surface. While laminae modeled using the volume-preserving approach do not themselves represent individual layers, they provide a coordinate system which realistically follows the course of the layers throughout the cortex.

[6] `http://lucene.apache.org/pylucene/jcc/index.html`

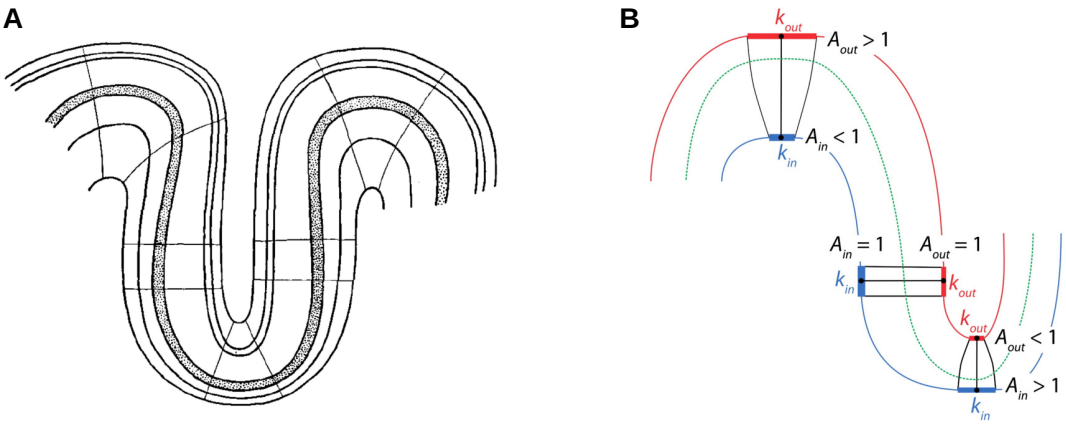

Figure 2.1 Volume-preserving principle of cortical laminae. According to Bok (1929), the thickness of cortical layers changes to compensate for stretching and compression due to the curvature of the cortical sheet. Thus, the volume fraction of each layer in a cortical segment, delimited by radial principal dendrites, remains constant (**A**). The volume-preserving model of intracortical depth proposed by Waehnert et al. (2014) implements this principle by dividing the cortex into segments and modeling laminar compartments with equal volumes within those segments. The distance of a given reconstructed intracortical surfaces from the pial and white matter boundaries therefore varies with cortical curvature (**B**).

input data to Java structures, initiate a Java virtual machine, call the main Java class with the specified parameters, collect, convert and return the output data. Thus, the actual processing still relies on the same, extensively optimized and tested Java code as the original CBS Tools. But since the interfacing between Python and Java is entirely taken care of inside the function, the user only interacts with Python code. Additional input and output functions in pure Python are designed to automatically recognize and load most commonly used data formats, while maintaining flexibility to accommodate loading of non-standard data formats using custom scripts. Data is internally represented as Nibabel SpatialImages (volumes) or dictionaries (surfaces, cf. Section 2.2) and can be passed in the form of file names or memory objects.

We chose to include a set of CBS Tools functions that enables the user to start from a simple tissue classification, compute cortical laminae using the volume-preserving approach, and sample at the different depth levels given by these laminae from any intensity image that is aligned with the tissue classification. This workflow is illustrated

in an example included in the repository[7] which uses 7T MRI data of an adult ferret (voxel size = 120 μm isotropic), testifying that CBS Tools is not only applicable to human neuroimaging data. We used Nilearn (Abraham et al., 2014) for visualization to demonstrate the straightforward integration of our package with other popular Python-based neuroimaging software.

In sum, Laminar Python provides an easy-to-use implementation of the CBS Tools functions necessary to construct and sample from volume-preserving cortical laminae. It no longer requires installation of MIPAV and JIST, and allows for interactive data exploration in Python at each processing stage. The transparent Python interfaces and comprehensive example make the new tools intuitive to use, and the adoption of standardized data objects enables easy integration with other popular Python-based neuroimaging software tools.

2.1.2 Nighres (Technical report 2)

After we had established the feasibility of our approach with Laminar Python, a more complete migration of CBS Tools' functionality to Python was a logical next step. We therefore launched *Nighres*[8], an entire software framework for processing of high-resolution and quantitative neuroimaging data in Python (Huntenburg, Steele & Bazin, in preparation). While building on the same basic design, Nighres was developed to solve a set of open issues that had remained unaddressed in Laminar Python. First, we wanted to provide a more comprehensive set of processing tools for a range of applications. Second, the package should be set up with continuous integration, automated builds and straightforward installation via the pip installation tool[9]. Third, a major goal was to build an extensive online documentation that includes step-by-step exam-

[7] `https://github.com/juhuntenburg/laminar_python/blob/master/examples/laminar_python_demo.ipynb`

[8] `https://github.com/nighres/nighres`

[9] `https://pip.pypa.io/en/stable`

ples showcasing the usage of different functions with publicly available data. Fourth, it was particularly important for us to create a framework that can flexibly be extended by other researchers and to provide thorough instructions for developers.

The initial release of Nighres satisfies these four core demands. The toolbox provides functions for skull stripping, atlas-guided tissue classification using the MGDM algorithm (Bogovic et al., 2013; Fan et al., 2008), cortex extraction using CRUISE (Han et al., 2004), creation of level set surface representations, volume-preserving modeling of cortical laminae (Waehnert et al., 2014), cortical depth-dependent intensity sampling and basic bandpass filtering. The majority of these tools represent Python wrappers around original CBS Tools Java classes and follow the same basic structure as described above for Laminar Python. However, Nighres also includes first tools that are written in pure Python. This illustrates how we envision Nighres to develop, as a flexible framework to which new or existing tools can easily be added in a variety of formats, depending on the specific requirements of the operation and the preferences of the contributing researcher. Nighres uses the same basic data handling conventions as Laminar Python, although we made an effort to improve the input and output functions and raise more informative errors upon incorrect usage.

While both Python and Java are cross-platform languages, the JCC package that we used to encapsulate the CBS Tools Java classes generates C++ code and thus makes the compilation platform-specific. We therefore implemented an automated build script that compiles the original CBS Tools Java code and builds the wrappers using JCC. For Nighres, this process i completely independent of the heavy MIPAV and JIST dependencies, while Laminar Python sidestepped only the installation of these packages but still required their libraries during the build process. We set up continuous integration using Travis CI[10] to test the build upon any changes to the code base and,

[10] `https://travis-ci.org/`

for any tagged releases, deploy the package to the Python Package Index (PyPI)[11]. The user can then download the package, run the fully automated build script to recompile the Java code and C++ wrappers on their platform, and finally use pip to install the modules and all their dependencies. Subsequently, Nighres can simply be imported into any Python environment.

A major advance compared to Laminar Python and CBS Tools is Nighres' extensive online documentation.[12] We used Sphinx[13] to create a documentation that automatically parses the docstrings of all Nighres functions. This simplifies the maintenance of an online documentation that is always up to date with the code, and encourages writing code with comprehensive docstrings. The documentation is hosted on readthedocs.org, which automatically updates it upon changes to the github repository. Beside the documentation of the individual functions, we also implemented detailed examples that demonstrate the usage of different tools combined in small workflows. The examples are based on publicly available data that we host on NITRC (Kennedy et al., 2016). When an example is run for the first time, the data is automatically downloaded so that users can familiarize themselves with Nighres immediately after installation, using examples with known outcome.

Finally, the online documentation contains an in-depth developer's guide that leads contributors through all steps necessary to submit code changes, new Python functions, new wrappers for CBS Tools functions or improvements of the documentation, to the Nighres github repository. We aimed to write a guide that makes it feasible for any researcher working with high-resolution neuroimaging data to contribute to Nighres, even without much previous experience in software development.

---

[11] `https://pypi.python.org/pypi`

[12] `http://nighres.readthedocs.io/en/latest/`

[13] `http://www.sphinx-doc.org/en/stable/`

With Nighres we thus built a user-friendly and well-documented Python package that makes high-resolution image processing tools available to the research community. The existing toolbox is easy to install and provides a comprehensive set of advanced techniques that enable segmentation and laminar analysis of cortical MRI at sub-millimeter resolutions in reasonable times. While the current functionality is largely based on CBS Tools, we hope that the flexible framework and the extensive developer's guide encourage contribution of new tools in a variety of formats, stimulate collaboration and accelerate progress in the promising field of high-resolution neuroimaging.

2.2 Cortical surface representations and geodesic distance

The research questions of this dissertation focus on the spatial layout of the human cerebral cortex. Since the human cortex is highly convoluted, surface representations are essential for exposing cortical regions that are buried in sulcal depths, and studying how features change along the cortical sheet. Moreover, as discussed in Section 2.1.1, intracortical surface reconstructions are used to sample data at different levels of intracortical depths. Cortical surfaces are most commonly represented as triangular meshes.[14] In a triangular mesh, a set of nodes (or vertices) is linked through edges in many small, connected triangles (or faces) which together build a three-dimensional shape. A cortical surface representation thus consists of a set of nodes, defined by three-dimensional coordinates in space, and a set of triangles, defined by the indices of the nodes that form their three corners. A description of how cortical surfaces can be derived from anatomical MRI scans is beyond the scope of this summary. But once a

[14]An alternative is the volumetric representation of cortical surfaces as signed distance functions, or level sets. Such representations have favorable mathematical properties and several Nighres processing tools rely on level sets internally. However, mesh representations are advantageous for the purposes discussed in this chapter and a more in-depth discussion of level sets can be found elsewhere (e.g. Bazin et al., 2014).

cortical surface has been constructed, any volumetric MRI data can be sampled on the surface by assigning to each surface node the data point (or data vector, for example a time series) of the voxel that the three-dimensional coordinates of the node fall into.

Surface-based approaches have traditionally been implemented in dedicated, heavy-weight software suites (e.g. Dale et al., 1999; Fischl et al., 1999; Goebel, 2012; Ramachandran & Varoquaux, 2011), which provide excellent tools for standard analyses of cortical surface data. However, due to rigid data organization, extensive dependencies, or closed source code these packages can be difficult to integrate with other tools and to adapt for new applications or unusual data types. As pointed out above, the development of flexible, open source Python tools for neuroimaging analysis has recently gained momentum. However, these tools focus almost exclusively on volumetric data.[15] In two small software projects we therefore initiated the development of flexible and light-weight functions to explore, analyze and visualize cortical surface data in Python.

2.2.1 Loading and plotting of cortical surface representations in Nilearn (Technical report 3)

Two core functionalities that will invariantly be required for a software framework to support cortical surfaces are, first, to load surface data for processing and, second, to plot the processing results on a cortical surface. We implemented respective functions in Nilearn, a toolbox for machine learning applications in neuroimaging (Huntenburg et al., 2017b). Nilearn shapes neuroimaging data into a feature matrix suited for statistical learning using the more general machine learning framework scikit-learn (Pedregosa et al., 2011). This design lends itself to be adapted for additional data formats such as cortical surfaces. Furthermore, Nilearn is a mature open source project with an active community, making it likely that the support for cortical surface data will be maintained

[15] Exceptions are tools like Nipype (Gorgolewski et al., 2011) and PySurfer (`https://pysurfer.github.io/`) , which provide functionality to process and visualize cortical surfaces, but depend on FreeSurfer software to do so.

and extended in the future.

In order to limit external dependencies to standard Python libraries, we implemented loading of surface mesh geometries and data sampled on the surface using Nibabel (Brett et al., 2016) and rendering using Matplotlib's *plot_trisurf* function (Droettboom et al., 2016). Beyond these two libraries, only Numpy (der Walt et al., 2011) is required. A considerable challenge was posed by the multitude of surface file formats currently in use, and the absence of an obvious community standard. Our loading functions automatically determine the input type and convert the data to standard Python objects. Mesh geometries are internally represented as a list of two Numpy arrays (nodes coordinates and triangle indices), and data to be displayed on the mesh as a single N-dimensional Numpy array. It is also possible to pass these data structures directly, allowing the user to load non-standard file formats with custom scripts. The core plotting function initiates a figure, renders the mesh and calculates the color for each triangle from the node-wise sampled data. This function provides maximal flexibility as almost all common Matplotlib parameters, such as colormaps or thresholds, can be adapted. We additionally implemented wrapper functions with sensible default parameters for common use cases such as plotting a region of interest (ROI, Figure 2.2 a) or a statistical map (Figure 2.2 b). Finally, we included extensive examples in the Nilearn online documentation to demonstrate the application of the new functions based on publicly available data.[16]

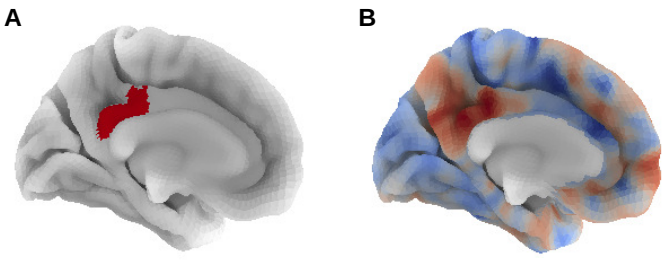

Figure 2.2 Surface plotting in Nilearn. Example output of the functions for plotting surface representations in Nilearn. **A** ROI in the posterior cingulate cortex (PCC) **B** Map of functional connectivity to the PCC seed region (Huntenburg et al. 2017b).

[16] http://nilearn.github.io/auto_examples/01_plotting/plot_surf_stat_map.html#sphx-glr-auto-examples-01-plotting-plot-surf-stat-map-py,
http://nilearn.github.io/auto_examples/01_plotting/plot_surf_atlas.html#sphx-glr-auto-examples-01-plotting-plot-surf-atlas-py

In this project, we implemented light-weight functions for loading and plotting of cortical surface data. The functions are easy to use but flexible enough to adapt to a range of use cases. The current code was developed as part of the Nilearn package but its transparent structure and minimal dependencies make it suitable to be reused for other packages. While our project only provides basic functionality, it represents a first step towards supporting cortical surface data in Python-based neuroimaging tools.

2.2.2 A cortical surface-based geodesic distance package for Python (Technical report 4)

In volumetric data representations the distance between two data points (voxels) is given by their Euclidean distance in the acquisition space (Figure 2.3). In contrast, surface representations make it possible to analyze the distance between two data points (surface nodes) in the anatomically meaningful space of the cortical sheet. For example, two data points located at the opposite walls of a deep sulcus will be close in voxel space, but much further apart on the surface. When studying the spatial organization of cortical features in gradients, we are interested in the relative position of different regions along the cortical sheet, which can be captured by their *geodesic distance* (Figure 2.3). Geodesic distance refers to the shortest distance between two locations along the surface mesh. It is independent of the external configuration of the cortical sheet, such as specific folding patterns, and therefore represents a measure of the *intrinsic geometry* of the cortex (Griffin, 1994).[17] As discussed in Section 1.1.3, geodesic distance from primary sensorimotor regions has been shown to capture progressive differentiation in structural hierarchies (Wagstyl et al., 2015). We suggest that the relative position of areas along the cortical sheet can also be useful to approximate developmental trajecto-

[17]Griffin provides an intuitive explanation of the difference between intrinsic and extrinsic properties in his work *The intrinsic geometry of the cerebral cortex*: "Properties of surfaces can be divided into two classes: intrinsic and extrinsic. Intrinsic properties are invariant under transformations that do not stretch or tear the surface. Extrinsic properties are dependent on the particular configuration of the surface in space. Thus a sheet of paper has the same intrinsic properties whether it is flat or crumpled but not the same extrinsic properties." (Griffin, 1994, p.262)

ries of cortical expansion. While common approaches to characterize cortical expansion focus on local increases in surface area (e.g Winkler et al., 2012), we are particularly interested in the geometric relationships between areas that result from this expansion, and can be described by their geodesic distance. We will further discuss our applications of the geodesic distance measure in Section 3.2.

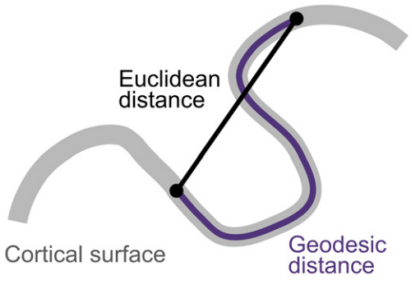

Figure 2.3 Geodesic distance. While Euclidean distance is measured along a straight line between two points in three-dimensional space (*black*), geodesic distance measures the shortest path along the cortical surface (*purple*) (Oligschlaeger et al., 2016).

Because no specific tool for analyzing geodesic distance along cortical surface representations was available, we developed a small Python package called *SurfDist*[18] tailored to this application (Margulies, Falkiewicz & Huntenburg, 2016). It is based on an exact geodesic distance implementation that measures the shortest path between two locations on a surface mesh, independent of the mesh resolution (Mitchell et al., 1987). This is particularly important in the case of neuroimaging data, where the mesh resolution depends on the original resolution of the acquired data and thus might be sub-optimally coarse. We adapted this exact geodesic distance calculation for easy application to common surface formats used in neuroimaging and implemented a solution to prevent the shortest path from passing through non-cortical regions such as the medial wall. The package also includes a Nipype pipeline for group-level batch processing and functions for visualization of the results based on the code discussed in Section 2.2.1.

Taken together, geodesic distance is a measure of the intrinsic cortical geometry, which is particularly useful to capture spatial relationships along the cortical sheet. SurfDist facilitates straightforward calculation of the exact geodesic distance on com-

[18] `http://github.com/margulies/surfdist`

monly used cortical surface meshes.

2.3 Data paper

All data used in this work is openly available. Two of our empirical studies (Study 1 and 3) are based on previously published data sets that have been described in detail elsewhere (Glasser et al., 2013; Gorgolewski et al., 2015; Tardif et al., 2016; Van Essen et al., 2013). We further made an extended version of the data used in Study 2 publicly available, as discussed below (Mendes et al., under review). In addition, all code we used for data processing and analyses can be found online, as will be pointed out in the respective sections throughout. We thereby ensure that our entire research process is transparent to other researchers for reproduction and critical discussion.

The data set we published includes structural and functional MRI and extensive phenotypic data from 194 healthy participants in an age range of 20 to 75 years. All MRI data were acquired using a whole-body 3T scanner (Magnetom Verio, Siemens Healthcare, Erlangen, Germany) equipped with a 32-channel Siemens head coil. The MRI data for each participant comprises a structural scan acquired using a three-dimensional MP2RAGE sequence (Marques et al. 2010, voxel size = 1.0 mm isotropic, TR = 5000 ms, TE = 2.92 ms, TI1/2 = 700/2500 ms, flip angle 1/2 = 4/5°, scan duration = 8.22 min) and four resting state fMRI scans acquired using a multiband gradient echo EPI sequence (Feinberg et al. 2010; Moeller et al. 2010, voxel size = 2.3 mm isotropic, TR = 1400 ms, TE = 39.4 ms, flip angle = 69°, multiband acceleration factor = 4, scan duration = 15 min 30 sec). Sequences were identical across the four resting state runs, with the exception of alternating slice orientation and phase-encoding direction, to vary the spatial distribution of distortions and signal loss. Thus, the y-axis was aligned parallel to the AC-PC axis for runs 1 and 2, and parallel to orbitofrontal cortex for runs 3 and 4. The phase-encoding direction was AP for runs 1 and 3, and

PA for runs 2 and 4. Before each pair of runs with the same y-axis orientation (run 1-2 and run 3-4) an additional gradient echo fieldmap (voxel size = 2.3 mm isotropic, TR = 680 ms, TE1/2 = 5.19 / 7.65 ms, flip angle = 60°, scan duration = 2.03 min) and a pair of spin echo images with reversed phase encoding directions (voxel size = 2.3 mm isotropic, TR = 2200 ms, TE = 52 ms, flip angle = 90°, echo spacing = 0.67 ms, phase encoding = AP / PA, scan duration = 0.20 min each) were acquired, providing two alternative means of distortion correction of the resting state fMRI data. The four resting state scans can be concatenated to obtain a long time series of over one hour which is advantageous for many analysis strategies. Alternatively, within-session test-retest analyses can be performed, for example to assess the impact of the mid-session repositioning. 109 of the subjects also took part in a second study, in which an additional resting state scan was acquired using the same sequence. This data provides the opportunity for cross-session test-retest analyses and will be published soon.

We released all raw MRI data in the standardized brain imaging data structure (BIDS, Gorgolewski et al., 2016). In addition, we provided a carefully preprocessed and quality controlled version of the data. Reusable preprocessing pipelines were implemented in Nipype (Gorgolewski et al., 2011) and all code is openly available.[19] A detailed description of the preprocessing strategy and all employed tools can be found in the data paper. In short, the structural scan of each participant was used to obtain a cortical surface reconstruction and a nonlinear transformation to MNI152 space. Spatial transformations of the resting state data included motion corrected, distortion correction using the gradient echo fieldmap, and boundary-based registration to the structural scan, and were applied in a single interpolation. The time series were denoised using a general linear model with the following nuisance regressors: six motion parameters and their first derivatives, intensity outliers, linear and quadratic trends

[19] `https://github.com/NeuroanatomyAndConnectivity/pipelines/tree/master/src/lsd_lemon`

and six regressors representing physiological noise as identified from signal fluctuations in the white matter and cerebrospinal fluid using the aCompCor approach (Behzadi et al., 2007). Finally, the time series were bandpass filtered (0.01 – 0.1 Hz), mean centered and variance normalized. The published data includes the denoised time series in native subject space and MNI152 space, as well as brain masks and all nuisance regressors. We created quality reports for each individual resting state scan illustrating subject motion, coregistration quality and temporal signal-to-noise ratio. All quality reports were inspected by at least two researchers. Where issues with individual data could not be fixed, preprocessed data was excluded from the release (5 subjects). The data set also includes extensive phenotypic assessment comprising a range of self-reported personality measures, features of self-generated mental experience and cognitive abilities. In total, participants filled out 31 questionnaires, performed 7 behavioral tasks and reported 4 probes of in-scanner mind wandering. Because these data are not used in the current work, we refer to the data paper for further details.

In sum, we published a large data set combining high-quality MRI data with broad state and trait phenotypic assessments. Extensive preprocessing and quality control pipelines for the MRI data were implemented as part of this dissertation (Study 2) and have been made available online for reference and reuse. This code and data permits reproduction of our results obtained in Study 2. It further enables a multitude of future studies exploring the intrinsic functional architecture of the brain and its potential relationship to higher-order cognitive faculties, self-generated mental experience and personality features.

In this chapter we described several methodological contributions that were part of the current dissertation. We developed open source software tools for processing of high-resolution neuroimaging data and for the analysis of cortical surface representations. Further, we published a large MRI data set along with extensive pipelines for prepro-

cessing and quality control. In Chapter 3, we will discuss three empirical studies in which we employed these resources to address the research questions outlined in the introduction.

Chapter 3

Empirical studies

The research compiled in the introduction suggests that the arrangement of cortical areas in spatial gradients is a fundamental principle of cortical organization. While most of the underlying studies have been performed in experimental animals, the core aim of this dissertation was to apply the idea of spatial gradients to human neuroimaging. This chapter summarizes three empirical studies in which we investigated the spatial layout of cortical microstructure and functional connectivity, and related it to the intrinsic geometry and functional specialization of the human cerebral cortex.

A crucial indicator that spatial gradients might indeed be a general principle of cortical organization is the convergence of gradients across two important aspects: cortical microstructure and connectivity (Section 1.1.2, Pandya et al., 2015). In Study 1 (Huntenburg et al., 2017c), we asked whether this fundamental link also holds in the human cortex *in vivo*. We used high-resolution quantitative T1 to estimate intracortical myelin content and resting state functional connectivity to approximate the organization of cortico-cortical connections. Via the decomposition of the functional connectivity matrix into a set of gradients, we found a strong correspondence between the distribution of intracortical myelin and a principal gradient of variance in functional connectivity. Our findings lead us to hypothesize that the particular spatial layout of this principal gradient represents an important organizing axis[1] of the human cortex.

[1]Throughout this dissertation, we will use the terms *global gradient, organizing axis* and *intrinsic dimension* roughly interchangeable.

In Study 2 (Oligschlaeger et al., 2016), we specifically focused on predictions of the tethering hypothesis introduced in Section 1.1.3 (Buckner & Krienen, 2013). This theory points out that the disproportionate expansion of transmodal areas positions them in increasing distance to molecular patterning centers, which constrain the organization of sensorimotor regions. As a result, transmodal areas acquire novel characteristics, for example the formation of connections to distant areas, that facilitate integration of information across systems. This hypothesis offers a potential insight into the specific connectional and functional features that vary between the sensorimotor and the transmodal extreme of the principal gradient of functional connectivity from Study 1. Employing geodesic distance to describe trajectories of cortical expansion, we investigated the distribution of local to distant functional connectivity. In line with the tethering hypothesis, we found that the distance-to-connected-areas gradually increased with increasing geodesic distance from primary sensorimotor areas, and peaked in regions of transmodal cortex. We further demonstrated that the spatial gradient of distance-to-connected-areas provides a meaningful order for the major functional subdivision of the cortex, represented by canonical resting state networks.

The gradient in distance-to-connected-areas from Study 2 showed a strong spatial resemblance to the principal gradient of functional connectivity described in Study 1. We therefore hypothesized that the principal gradient, too, is closely linked to the intrinsic geometry of the cortex and its functional specialization. In Study 3 (Margulies et al., 2016), we examined these relationships explicitly and extended the analysis of cortical function to a more comprehensive and fine-grained approach. We demonstrated that the spatial layout of the principal gradient can essentially be reproduced from the geodesic distance between primary sensorimotor areas and the peaks of transmodal regions. In line with the results from Study 2, we found that the spatial layout of this gradient provides an organizing framework for resting state networks, ordering them along a hierarchy of increasing abstraction. Here, we additionally performed a meta-

analysis which confirmed that the principal gradient of functional connectivity tracks a continuous spectrum from activation patterns elicited by direct perception and action to those associated with abstract and internally-directed functions. We suggested that this layout provides a spatial embedding for the global functional processing hierarchy proposed by Mesulam (Section1.1.3, Mesulam, 1998) and a potential explanation for the distinctive role of the default mode network (DMN) in cognition. Additionally, we described a secondary gradient of functional connectivity which separates different sensorimotor modalities and aligns with a second dimension of Mesulam's schematic. Both gradients are consistent across human functional connectivity and macaque monkey tract-tracing data, indicating that they represent two fundamental, phylogenetically conserved axes of cortical organization

3.1 A systematic relationship between functional connectivity and intracortical myelin in the human cerebral cortex (Study 1)

As described in the introduction, there is strong evidence for a link between the spatial organization of microstructure and connectivity in the mammalian cortex. In particular, long-range connections preferentially occur between regions that show a similar degree of microstructural differentiation. This principle has been established through studies of the mouse (Goulas, Uylings, & Hilgetag, 2016), cat (Beul et al., 2014) and macaque monkey cortex (Beul et al., 2015; Pandya et al., 2015; Scholtens et al., 2014), employing a combination of invasive tract-tracing and post-mortem histology. But the invasive nature of such methods has so far impeded systematic research into the relationship between cortical microstructure and connectivity in the human brain. Recent studies have addressed this challenge by comparing MRI-based measures of cortical connectivity to cytoarchitectonic atlas information (von Economo & Koskinas, 1925), demonstrating a relationship between connectivity and supragranular neuron complexity (van den

Heuvel et al., 2016, 2015) or supragranular cell density (Goulas, Werner, et al., 2016). However, spatial accuracy is limited when mapping atlas information from tables or two-dimensional drawings in stereotactic space, and the discrete parcellation scheme prohibits the analysis of gradual changes.

In Study 1, we built on recent developments in high-resolution and quantitative MRI to overcome these limitations. Using MRI data acquired at ultra-high field (7T) enabled us to compare *in vivo* measures reflecting cortical microstructure and connectivity in the same group of individuals at high spatial resolution. Specifically, we assessed the relationship between quantitative T1 maps, which are sensitive to intracortical myelin, acquired using the MP2RAGE sequence (Marques et al. 2010, 0.5 mm isotropic voxel size) and resting state functional connectivity acquired using a custom EPI sequence (1.5 mm isotropic voxel size, 3000 ms repetition time, 4x15 min scan duration).[2] The data had been published previously (Gorgolewski et al., 2015; Tardif et al., 2016) and we used data sets of 9 subjects for which both types of images were available. To preserve the exceptional spatial precision provided by this data, we implemented a specialized image processing pipeline employing the tools described in Section 2.1 (Figure 3.1). This pipeline included nonlinear coregistration of the functional to the structural data to correct for the significant distortions caused by strong field inhomogeneities at 7T (cf. Huntenburg et al., 2014). To sample intracortical T1, we constructed 11 intracortical depth levels using a volume-preserving approach (Waehnert et al., 2014). As described in Section 2.1.1 this method accounts for the influence of local cortical curvature on laminar thickness and thus provides an anatomically correct intracortical coordinate system (Figure 2.1). We then averaged the T1 values of the five central levels of intracortical depths to obtain a map of intracortical T1 for each subject, which is minimally biased by partial volume effects with the white matter and cerebrospinal

[2]In this section, scanning parameters are reduced to the most essential information for readability. More information can be found in the original papers in the appendix.

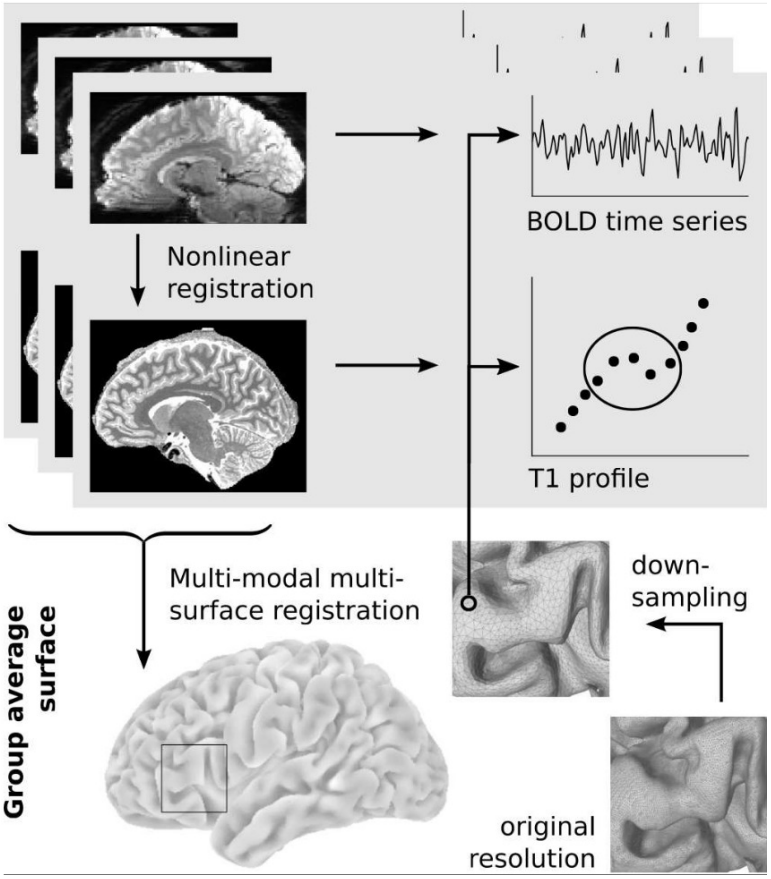

Figure 3.1 Image processing pipeline for Study 1. Resting state images were nonlinearly coregistered to the structural space of the same subject. A group-specific surface template was created using mid-cortical surfaces and intracortical T1 contrasts of all subjects in a multi-modal multi-surface registration approach. The group-average surface was downsampled and projected into the space of each subject for sampling of resting state time series and T1 profiles. Cortical depth profiles were sampled according to a volume-preserving principle; only the central values were averaged to minimize partial volume effects (Huntenburg et al., 2017c).

fluid.[3] For the resting state fMRI data we employed a denoising strategy that minimizes the impact of head motion and physiological fluctuations. We sampled the denoised time series data on the subject's mid-cortical surface. For each pair of surface nodes we computed the temporal correlation of the associated time series, yielding the subject level functional connectivity matrix. A multi-modal multi-surface registration approach was to used to align the mid-cortical surfaces of all subjects and create a study-specific surface template (Tardif et al., 2015). This technique combines information about cortical curvature and the distribution of intracortical T1 to optimize the registration, and preserves more of the original cortical geometry than other popular algorithms. The intracortical T1 maps and the functional connectivity matrices were averaged across all subjects.

[3]As further discussed in Section 5.1, we did not analyze the distribution of intracortical T1 across different cortical laminae in this study, but used the layering approach to obtain an unbiased estimate of average intracortical T1.

Functional connectivity was overall higher between areas that resembled each other in their estimated myelin content, than between areas with rather different myelin content. This relationship showed substantial spatial variation, with a strong correlation between the two measures in unimodal sensorimotor regions and low correlation in several transmodal regions. To investigate this relationship further, we aimed to identify specific aspects functional connectivity patterns that show a particularly strong link to intracortical myelin content. We therefore performed nonlinear dimensionality reduction using diffusion maps (Coifman & Lafon, 2006) to extract gradients of functional connectivity as described in Section 1.2.2. The first – or principal – gradient of functional connectivity showed a substantially higher correlation to intracortical T1 than we had observed when considering the entire functional connectivity matrix. This gradient spans between primary visual, auditory and somatomotor areas at one end and transmodal regions such as the angular gyrus, anterior cingulate and posteromedial cortex, middle temporal gyrus and middle and superior frontal gyri at the other end (Figure 3.2 b). The principal gradient thus captures an aspect of functional connectivity organization which is maximally different between primary sensorimotor and transmodal regions and strongly related to the distribution of intracortical myelin content. In other words, areas that resemble each other in the aspect of functional connectivity that is represented by the principal gradient, also have a similar intracortical myelin content. However, some deviations remained in regions of the posteromedial cortex and the angular gyrus (Figure 3.2, white circles). Employing a formal model comparison procedure we found that these deviations could be alleviated by combining the principal gradient with two additional gradients (gradient 4 and 5). Thus, particular aspects of functional connectivity, in our approach captured mainly in gradient 1 and to some extent in gradient 4 and 5, show a spatial distribution that is strongly related to that of intracortical myelin. At the same time, a substantial amount of variance in the functional connectivity data, captured in gradient 2, 3, and ≥ 6, cannot be explained by the distribution of intracortical myelin. This finding illustrates how decomposing functional connectiv-

ity into separate one-dimensional gradients can help to identify links between specific aspects of this high-dimensional data and a second variable, which might be obscured when considering all functional connections at once (cf. Sections 1.2.2., Figure 1.3).

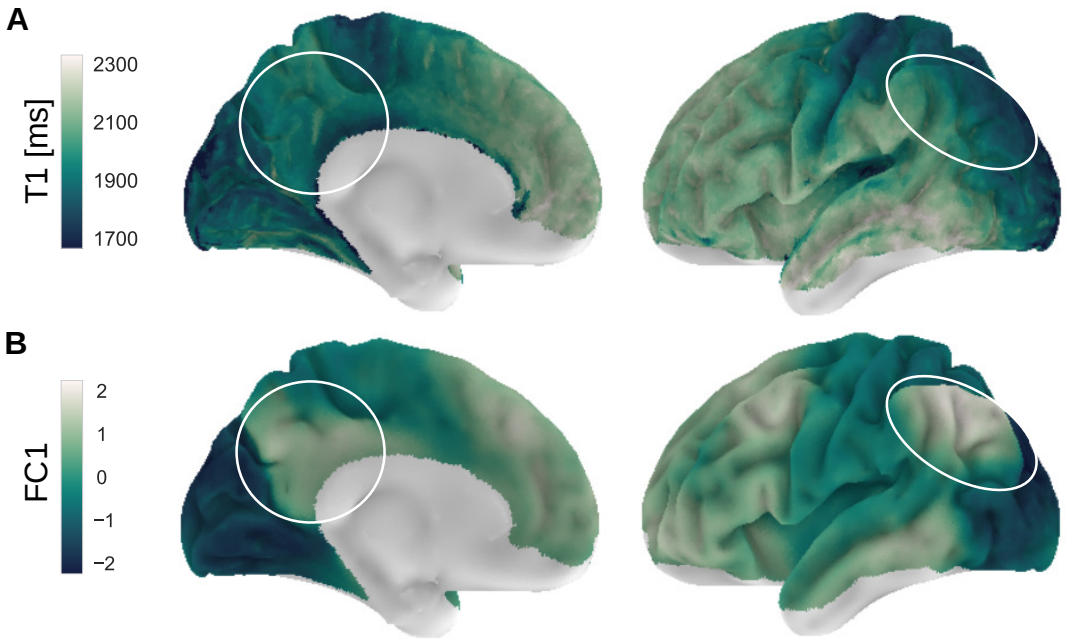

Figure 3.2 Gradients in intracortical T1 and functional connectivity. The group-level map of intracortical T1 (**A**) and the principal gradient of group-level functional connectivity (FC1, **B**) show similar spatial distributions. Deviations can be observed especially in posteromedial cortex and the inferior parietal lobe (*white circles*). Nodes with low signal quality in either imaging modality were excluded from the analysis (Huntenburg et al., 2017c).

To corroborate our findings, we showed that the observed relationship between functional connectivity and intracortical myelin was not driven by the spatial smoothness of the maps nor an underlying common dependency of both measures on spatial proximity or cortical thickness. Moreover, we were able to replicate the relationship between estimated intracortical myelin and functional connectivity in general, and the strong link to the principal gradient of functional connectivity in particular, in a second publicly available data set acquired at 3T (Glasser et al., 2013; Van Essen et al., 2013). While this data set provided a lower spatial resolution (0.7 mm and 2 mm isotropic voxel size, respectively, for the structural data and resting state data), and a more indirect measure of intracortical myelin (the ratio of T1-weighted over T2-weighted images) it

contained data from 820 subjects and thus allowed us to confirm our core findings in a larger sample.

In sum, we demonstrated a systematic relationship between the spatial distribution of functional connectivity and intracortical myelin in the human cerebral cortex. Our findings are in agreement with comprehensive reports linking histologically assessed microstructure and connectivity in different mammalian species. Using high-resolution and quantitative MRI data, as well as specialized image processing tools, we were able to extend these findings to the human cerebral cortex *in vivo*. In particular, we identified a principal gradient of functional connectivity that captures a spectrum of connectivity patterns between primary sensorimotor areas and transmodal regions and is strongly related to intracortical myelin content (Figure 3.2). While two additional gradients of functional connectivity were found to relate to intracortical myelin, the principal gradient undoubtedly showed the strongest link in two independent data sets. These findings lead us to conclude that the principal gradient of functional connectivity captures an important spatial axis of cortical organization, reflected in connectivity and microstructure. We were now interested in understanding more about the potential roots of this organizing axis (Study 2) and its significance for cortical function (Study 3).

3.2 Gradients of connectivity distance are anchored in primary cortex (Study 2)

In Study 1, we identified a principal spatial gradient which spans between primary sensorimotor areas and transmodal regions and represents the main axis of variance in functional connectivity patterns across the cortex. However, the decomposition approach used to derive this gradient does not provide information about the specific features of functional connectivity that vary along its spectrum. In Study 2 (Oligschlaeger et al.,

2016), we examined one candidate feature more closely – a region's spatial distance to its connection partners. While unimodal sensorimotor areas demonstrate a strong preference to form local connections with neighboring regions, typically organized in strict feedforward-feedback patterns (Felleman & Van Essen, 1991), transmodal areas often connect to each other over long distances (Sepulcre et al., 2010). As discussed in Section 1.1.3, the tethering hypothesis (Buckner & Krienen, 2013) has linked this observation to the massive expansion of transmodal regions during human evolution and ontogenetic development (Hill et al., 2010). The disproportionate growth of transmodal areas substantially increases their distance to molecular patterning centers which determine the hierarchical organization of sensorimotor areas (Buckner & Krienen, 2013). Released from these molecular constraints, transmodal regions have been suggested to acquire more flexible properties and, for example, form long-range connections without clear hierarchical patterns. As described in Section 2.2.2, geodesic distance is a measure of the intrinsic cortical geometry which captures the relative spatial position of areas along the cortical sheet. According to the dual origin theory (Section 1.1.1), this relative spatial position reflects the sequence in which areas arose through cortical expansion during evolution. We therefore suggested that geodesic distance is a useful proxy to describe the trajectory of cortical expansion. The tethering hypothesis adds that the spatial position of an area influences its connectional characteristics via distance to developmental patterning centers. Based on this premise, we hypothesized that the prevalence of long-range connections increases continuously with increasing geodesic distance from primary sensorimotor areas – representing the location of maximum influence of molecular patterning centers – and peaks in late developing transmodal regions. The tethering hypothesis also proposes that the trajectory of cortical expansion is significant for the differences in functional attributes between sensorimotor and transmodal regions. We aimed to test this prediction by examining if an increasing emphasis on distant over local connections provides an organizing framework for canonical resting state networks, which have consistently been associated with distinct functional domains (Smith et al.,

2009).

Towards these goals we characterized each point on the cortical surface based on its average geodesic distance to its highly connected areas ("distance-to-connected-areas"). It is important to highlight, that the distance-to-connected-areas does not reflect the average length of white matter fibers between connected regions, but instead captures how far connected areas are positioned from each other on the cortical surface. We used the MRI data described in Section 2.3 from a subsample of 77 healthy adults. This subsample was obtained by restricting the age range to 18-40 years in order to mitigate developmental and aging-related variance. Details on image acquisition and processing can be found in Section 2.3 and the associated data paper (Mendes et al., under review). We computed a functional connectivity matrix for each subject based on over one hour of resting state fMRI data (2.3 mm isotropic voxel size, 1400 ms repetition time, 4 x 15 min 30 sec scan duration). Further, we used each subject's structural scan (1 mm isotropic voxel size) to reconstruct the cortical surface and quantify the geodesic distance between each pair of nodes on this surface (Section 2.2.2). For each surface node, distance-to-connected-areas was calculated by first thresholding its functional connectivity to the top 2% strongest connections and then averaging its geodesic distance to all nodes that survived this threshold.[4] The distance-to-connected-areas thus represents a node's average geodesic distance from the areas it is most strongly connected to. As we wanted to know how the distance-to-connected-areas relates to a node's spatial separation from primary sensorimotor regions, we also assigned to each node its geodesic distance to the closest of three cortical landmarks in primary regions: the calcarine sulcus, the temporal transverse sulcus, and the central sulcus. For visualization purposes, all maps were projected on a standard surface template and averaged across subjects. We also used a canonical resting state network parcellation (the 17-network template by Yeo et al., 2011) to sample the network-specific distributions of distance-to-connected-areas.

[4]The results were robust for a range of thresholds (5, 10, 15, 20, 25 and 30%)

Sorting distributions by increasing mean suggested three groups of networks. To confirm this observation, distributions were then compared between each pair of networks using the Jensen-Shannon divergence measure. K-means clustering was applied to the Jensen-Shannon divergence matrix to group the networks.

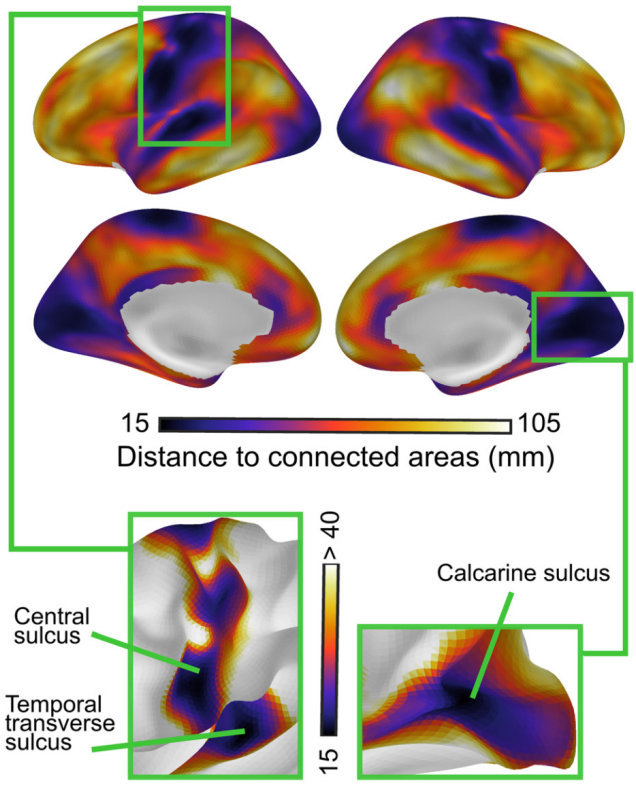

Figure 3.3 A gradient in connectivity distance. The group-level map of the distance-to-connected-areas shows a gradient from the shortest distances in primary cortex to the longest distances in transmodal regions. The shortest distances delineate primary auditory, somatosensory (*left box*), and visual (*right box*) areas (Oligschlaeger et al., 2016).

Confirming our hypothesis, the distance-to-connected-areas was shortest in primary sensorimotor regions and increased nearly linearly with geodesic distance from primary landmarks, peaking in transmodal regions (Figure 3.3). In fact, the shortest values of distance-to-connected areas precisely delineated cortical landmarks of primary areas (Figure 3.3, boxes). This observed distribution of distance-to-connected-areas is strikingly similar to the spatial layout of the principal gradient of functional connectivity (Figure 3.2 b), indicating that at least on important features that is reflected in the principal gradient is a transition from local to distant connections. Furthermore, using an established resting state network parcellation, we were able show that distance-to-connected-areas provides an order for the major functional subdivisions of the cerebral

cortex: it is shortest in unimodal networks, such as the visual and the somatomotor network, intermediate in dorsal and ventral attention networks, and highest in fronto-parietal control networks and the DMN. We will return to this observation and its potential interpretation in Study 3.

Taken together, we demonstrated a continuous spatial distribution of a specific aspect of functional connectivity – the distance-to-connected-areas – which is anchored in primary sensorimotor regions and progresses towards transmodal areas. Our finding is line with the idea that the preference for local hierarchies, comprised of short feedforward-feedback connections, vanishes with increasing spatial separation from primary regions and connections between distant regions begin to emerge (Buckner & Krienen, 2013). Moreover, the spatial gradient between primary and transmodal regions also captures major functional subdivisions of the cortex, pointing towards a role of cortical location in shaping functional specialization that will be discussed further in Study 3. A remarkable similarity of the map of distance-to-connected-areas (Figure 3.3) to the principal gradient of functional connectivity (Figure 3.2 b) allows for some tentative conclusions. First, the variance in functional connectivity captured by the principal gradient represents – at least in part – a continuous transition from local to distant connectivity patterns, rooted in developmental gradients. Second, the principal gradient of functional connectivity is strongly related the intrinsic geometry of the cortex as measured with geodesic distance. Third, this core axis of cortical organization is not only reflected in cortical microstructure (Study 1) but also captures a functional spectrum from direct environmental in- and output to high-level cognitive functions. These observations prompted us to explicitly investigate the relationship of the principal gradient of functional connectivity with intrinsic geometry and distributed function in greater detail in the following.

3.3 Situating the default mode network along a principal gradient of macroscale cortical organization (Study 3)

Study 1 demonstrated a systematic link between the principal gradient of functional connectivity and the distribution of intracortical myelin. The findings from Study 2 further indicated that an area's position along this principal gradient is related to its geodesic distance from primary regions and its functional role. These last two conclusions, however, were based on the spatial similarity of the principal gradient of functional connectivity to the distribution of distance-to-connected-areas alone. In Study 3 (Margulies et al., 2016), we strove for an explicit investigation of the proposed relationships between the principal gradient of functional connectivity, the intrinsic geometry of the cortex and distributed functional specialization. In particular, we wanted to know if the principal gradient could provide a spatial embedding for the global functional processing hierarchy proposed by Mesulam (Section 1.1.3, Mesulam, 1998).

We used a publicly available data set comprising preprocessed MRI data from 820 healthy adult subjects (Glasser et al., 2013; Van Essen et al., 2013).[5] Specifically, we obtained subject-level functional connectivity matrices from one hour of preprocessed resting state fMRI data, acquired using a multiband EPI sequence (Uğurbil et al. 2013, 2 mm isotropic voxel resolution, 700 ms repetition time, 4x15 min scan duration). The resting state time series had been sampled on cortical surface reconstructions derived from a combination of two structural scans acquired using a T1-weighted (T1w) and T2-weighted (T2w) sequence, respectively (Glasser et al. 2013, both 0.7 mm isotropic voxel resolution). All data were provided on a standard cortical surface and we averaged

[5]The same data set was used for replication in Study 1.

the functional connectivity matrices across subjects for our analyses.

Like in Study 1, we used diffusion maps for dimensionality reduction of the functional connectivity data. The resulting principal gradient of functional connectivity, accounting for most of the variance in functional connectivity patterns, showed the same distribution as described in Study 1. It was anchored at one end by primary visual, somatomotor, and auditory regions. The other extreme of the gradient was located in transmodal regions of the frontal, parietal and temporal lobe, in humans collectively described as the DMN. In this study, we also described a secondary gradient that separated different unimodal regions from each other, with visual areas in the occipital cortex at one end, and somatosensory and motor regions surrounding the central sulcus, as well as the auditory cortex in the temporal perisylvian region at the opposite end.[6] Notably, we could reproduce the spatial distribution of both gradients in a publicly available data set of macaque monkey cortico-cortical connections based on tract-tracing experiments (Bakker et al., 2012; Stephan et al., 2001).

As stated above, one of our main interests was to find out whether the principal gradient indeed tracks the spatial trajectories of geodesic distance between primary sensorimotor and transmodal regions. We selected seven spatially separate peak nodes at the transmodal extreme of the gradient and calculated the minimum geodesic distance from all other nodes on the cortex to any of these peak nodes. With striking spatial precision, these transmodal peaks were located at the maximum possible distance along the cortex from morphological landmarks in primary sensorimotor regions (Figure 3.4). More generally, gradient values varied continuously with geodesic distance between transmodal peaks and primary sensory landmarks.

The other major question we wanted to address in Study 3 was if the position of

[6]The same secondary gradient had been observed in both data sets in Study 1, but since it did not substantially correlate with the distribution of intracortical myelin, we did not focus on it then.

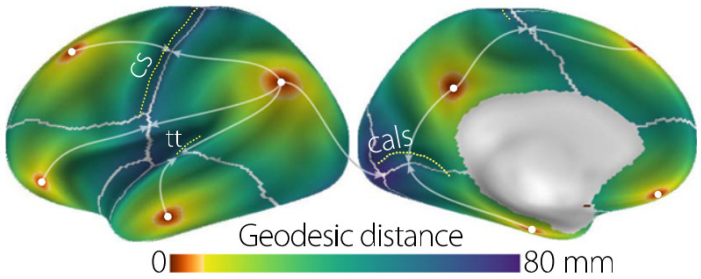

Figure 3.4 Geodesic distance from transmodal peak regions. Minimum geodesic distance was measured from peak nodes at the transmodal end of the principal gradient of functional connectivity (*red*). The highest distances precisely converge at landmarks in primary sensorimotor areas (*dotted lines*). Gray arrows indicate equidistance from different peak nodes. cs, central sulcus; cals, calcarine sulcus; tt, transverse temporal gyrus (Margulies et al., 2016).

cortical regions along the principal gradient is related to their functional specialization. Similar to Study 2, we initially focused on major functional subdivisions represented in a widely used resting state network parcellation (7-network parcellation by Yeo et al., 2011). While these large-scale networks are highly reproducible and have robustly been associated with distinct functional domains, an organizing framework explaining their spatial organization has so far been lacking. We were able to show that the principal gradient of functional connectivity can provide such an organizing axis. Cortical nodes assigned to the same network were found to cluster at similar positions along the gradient, even if they were spatially far apart. In particular, nodes of the DMN grouped at one extreme of the gradient, maximally separated from the visual and the somatomotor networks (Figure 3.5 a). Between these two extremes, the dorsal attention and salience networks occupied positions closer to the sensorimotor modalities while the fronto-parietal network was positioned towards the DMN. Based on the functional domains typically associated with these networks, our findings indicate that the principal gradient of functional connectivity provides a spatial axis along which cortical function orderly progresses from direct environmental in- and output, through functions related to attention and cognitive control, towards abstract, stimulus-independent domains. To provide a more direct link between the principal gradient and these cognitive domains, we next performed a meta-analysis using the Neurosynth database (Yarkoni et al., 2011).[7] We binned the principal gradient in five-percentile increments and sorted

[7]We obtained similar results when repeating the analysis using the BrainMap database (Fox &

Neurosynth topic terms according to their weighted average z-statistic associating them with each of these bins. This analysis revealed a spectrum of increasing functional abstraction that follows the spatial layout of the gradient from unimodal to transmodal regions. Confirming our findings from the network analysis, topic terms progressed from those related to direct perception and action, through domain-general terms related to attention, inhibition and working memory, to abstract concepts such as social cognition, semantics or autobiographical memory (Figure 3.5 b).

Collectively, our findings in Study 3 manifest the principal gradient of functional connectivity as a core axis of human cortical organization. The spatial layout of this gradient accounts for the relative position of canonical networks and captures a functional spectrum from perception and action to more abstract cognitive functions. This organization aligns with the global functional processing hierarchy proposed by Mesulam (1998). While Mesulam's proposal remained schematic, our findings indicate that the principal gradient of functional connectivity and its close relationship to the intrinsic geometry of the cortex provide the spatial embedding for this global hierarchy. As a concrete example we suggest that the position of the DMN at one extreme end of the principal gradient, and at maximum geodesic distance from primary sensorimotor regions, can help to understand its special role in cognition. Initially identified through a tendency to deactivate during tasks, the DMN has been associated with a variety of stimulus-independent cognitive domains, such as thinking about one's own past or future, considering mental states of others, mind wandering and creative thinking (Raichle, 2015; Spreng & Grady, 2010). Such processes require the integration of information from different systems and abstraction from concrete content. We propose that the *spatial insulation* of DMN regions from areas that operate on direct environmental input is crucial for these high-level functions to emerge (see Section 5.3 for further discussion).

Lancaster, 2002).

The converging findings from our three empirical studies provide strong evidence for a spatial gradient spanning between sensorimotor and transmodal regions, that constitutes a core axis of human cortical organization. While we initially discovered this gradient by decomposing functional connectivity data, we subsequently accumulated evidence that its spatial layout captures important aspects of cortical microstructure and functional specialization. The gradient can essentially be reconstructed from the simple measure of geodesic distance between primary sensorimotor areas and transmodal peak regions. We additionally described a secondary gradient of functional connectivity which separates different sensory domains from each other. Both gradients were consistent across human functional connectivity and macaque monkey tract-tracing data, indicating that they might represent phylogenetically conserved axes of cortical organization.[8] We found our observation regarding these two gradients to align with other recent demonstrations of global trends in cortical organization and, based on this cumulative evidence, developed the concept of an intrinsic coordinate system of the human cerebral cortex, which will be discussed in the next chapter.

[8]This finding also lends further support for the validity of using resting state functional connectivity to assess the organization of cortico-cortical connections.

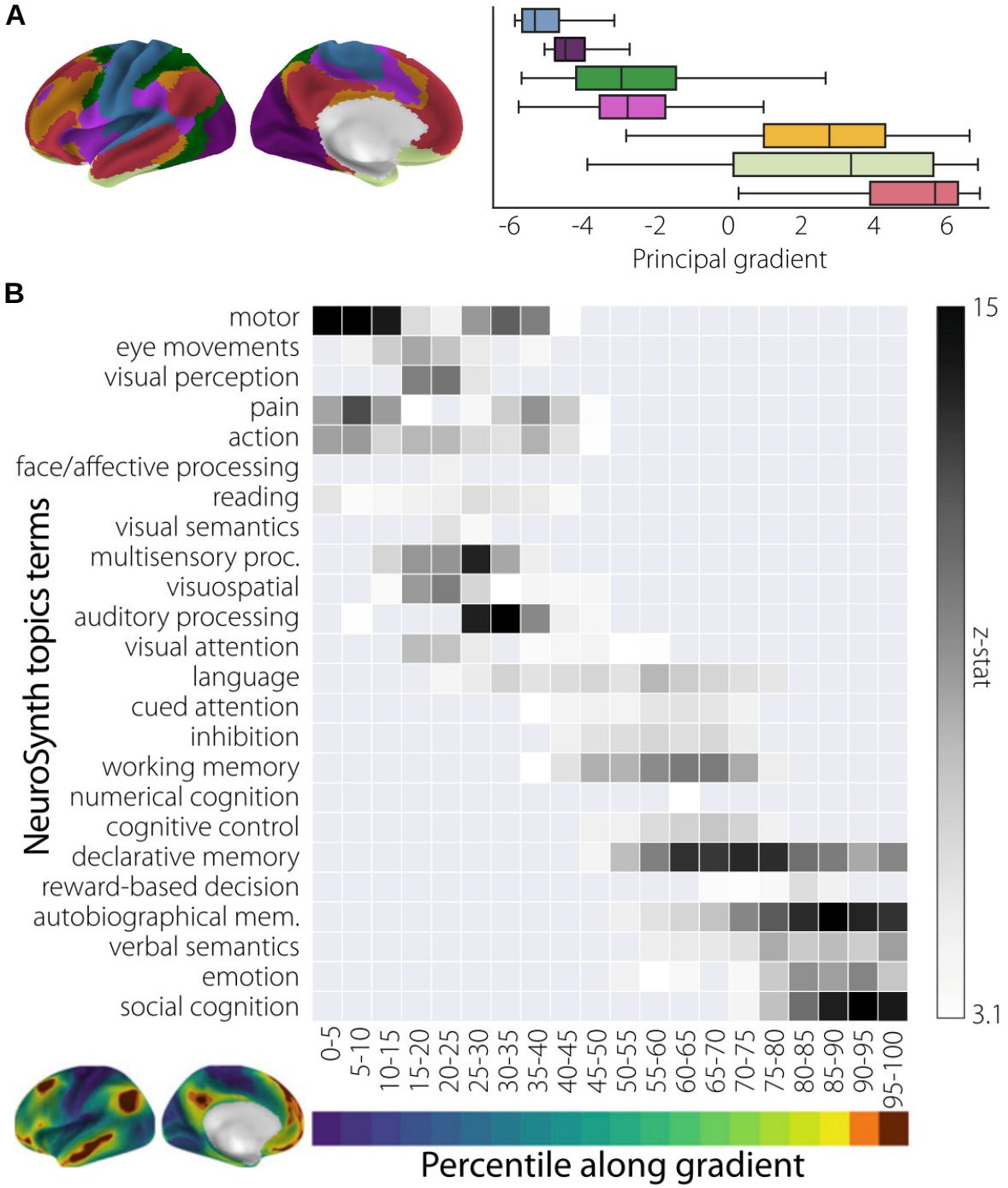

Figure 3.5 Functional abstraction increases along the principal gradient. A The principal gradient of functional connectivity provides an organizing framework for canonical resting state networks (*left*). Box plots represent the seven networks and are ordered by the mean principal gradient value of all nodes that fall within a network (*right*) (blue-somatomotor, purple-visual, green-dorsal attention, pink-salience, yellow-fronto-parietal, beige-limbic, red-default mode) **B** Meta-analysis results using 24 Neurosynth topic terms show that the principal gradient reflects a functional processing hierarchy of increasing abstraction. Topic terms are ordered by their weighted average association with maps representing 5-percentile bins along the principal gradient. autobiographical mem., autobiographical memory; multisensory proc., multisensory processing (Margulies et al., 2016).

Chapter 4

Opinion article

The approach to understand cortical organization in terms of spatial gradients is historically based in post-mortem studies and has rarely been adopted in current human neuroimaging. In three MRI studies we accumulated evidence for a dominant spatial gradient in the human cerebral cortex *in vivo*, which spans between primary sensorimotor and transmodal regions. This gradient is present in the spatial distribution of functional connectivity and intracortical myelin, shows a strong relationship to the intrinsic geometry of the cortex and captures a functional spectrum of increasing abstraction. Motivated by our own results and converging findings from the recent literature we aspired to lift the cortical gradient framework from classical neuroanatomy literature and increase its visibility in current human neuroimaging. In our opinion article (Huntenburg et al., accepted), we drew together different lines of research in support of the notion that cortical features are organized in large-scale spatial gradients, and proposed that these gradients build the dimensions of an intrinsic coordinate system of the human cerebral cortex.

We began by discussing a rostrocaudal gradient in cortical microstructure which has been described in the cortex of different mammalian species (Cahalane et al., 2012; Charvet et al., 2015, 2017; Collins et al., 2010). The rostrocaudal organization aligns with known neurodevelopmental gradients and there is strong evidence that it arises from the temporal sequence of neurogenesis (Cahalane et al., 2012, 2014; Charvet &

Finlay, 2014).[1] However, deviations from this organization have been reported in multiple species. Especially in the human cortex, a rostrocaudal gradient is not sufficient to explain the distribution of microstructural features. Instead, we and others have demonstrated a gradient in MRI-based markers of cortical microstructure which is anchored in primary sensorimotor regions and radiates towards higher-order areas in parietal, temporal and prefrontal cortex (Huntenburg et al., 2017c, Burt et al., 2017; Glasser et al., 2016; Rowley et al., 2015; Tardif et al., 2015; Whitaker et al., 2016) (Figure 4.1 a). Similarly, gene expression gradients in the cortex of more primitive mammals show a rostrocaudal organization (Krienen et al., 2016), while dimensionality reduction of gene expression data in the human cortex has revealed a principal gradient spanning from primary sensorimotor to transmodal temporal and frontal areas (Hawrylycz et al., 2012). Cortical development is far less understood in humans as compared to other mammals. However, based on the aforementioned evidence we raised the possibility that the deviation from purely rostrocaudal patterns in the adult human cortex could be rooted in spatially more complex developmental gradients. As previously discussed in Study 2, the distribution of these gradients might be influenced by the massive and disproportionate expansion of transmodal areas in the human lineage, which increases their distance from molecular patterning centers (Buckner & Krienen, 2013).

The opinion article also outlines our findings regarding the principal gradient of functional connectivity, covered in Chapter 3. We will not repeat this discussion here, but point out that our results align with other recent studies, consistently demonstrating sensorimotor-to-transmodal gradients in human cortical connectivity through various methodological approaches (Atasoy et al., 2016; Langs et al., 2014, 2015; Sepulcre et al., 2012; Taylor et al., 2015) (Figure 4.1 b). Likewise, our demonstration of a global functional processing hierarchy along the principal gradient is in line with others

[1] A more detailed account of the proposed developmental mechanism can be found in Section 5.3 and in the original article in the appendix

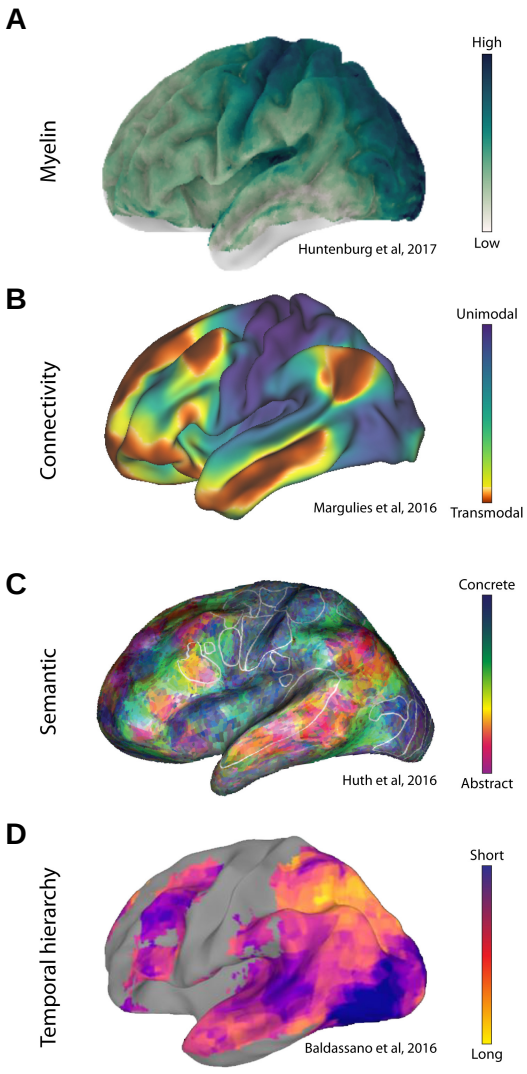

Figure 4.1 A sensorimotor-to-transmodal gradient in the human cerebral cortex. A basic sensorimotor-to-transmodal organization is apparent in different cortical features as assessed with MRI. **A** Intracortical myelin increases along the sensorimotor-to-transmodal gradient (Huntenburg et al., 2017c). **B** The main variance in functional connectivity patterns spans between primary sensorimotor areas and transmodal regions of the DMN. The connectivity gradient does not have a unit, but it is strongly related to a spectrum of concrete-to-abstract cognitive domains (cf. Figure 3.5) (Margulies et al., 2016). **C** The map shows a superposition of the first three semantic category-processing gradients. The largest axis of variation separates perceptual and physical categories in sensorimotor areas from more abstract concepts in transmodal regions (Huth et al., 2016). **D** The length of events that are represented in a given area, here extracted from movie-watching data, varies from short events in sensory areas to long events in transmodal regions (only patterns with high between-subject consistency are shown, for example, somatosensory regions did not respond consistently to the auditory-visual input in this study) (Baldassano et al., 2016).

holding the view that processing hierarchies extend beyond sensorimotor systems into transmodal areas (Badre & D'Esposito, 2009; Chanes & Barrett, 2016). The most direct support comes from a study presenting a principal gradient of semantic categories that varies smoothly from concrete perceptual and quantitative descriptions in sensorimotor areas, to abstract category representations related to emotions and social interactions in transmodal regions (Huth et al., 2016)(Figure 4.1 c).

Together, the aforementioned studies indicate a spatial relationship between gradients in cortical microstructure, gene expression, connectivity and function. Beyond this spatial correlation, we found a potential explanation for how structural and functional

gradients might be linked in recent work on temporal integration hierarchies (Baldassano et al., 2016; Ding et al., 2016; Hasson et al., 2015, 2008; Honey et al., 2012; Lerner et al., 2011). These studies show that the temporal window, across which information is integrated, varies across the cortex. While primary sensory areas, at one extreme, track fast changes of a scene on the order of milliseconds, transmodal association areas, at the other extreme, integrate information across seconds, minutes, or longer, to encode slowly changing states of the world, complex concepts and situations (Figure 4.1 d). There is strong evidence that this temporal hierarchy is based on differences in the frequency of intrinsic fluctuations across cortical areas (Honey et al., 2012; Murray et al., 2014; Stephens et al., 2013). This variation in intrinsic time scales, in turn, has been shown to emerge from the interplay of local microstructural gradients and long-range connections in a computational simulation (Chaudhuri et al., 2015), providing the potential link between structural gradients, temporal hierarchies and eventually functional specialization (see also Section 5.3).

In our view, these collective findings draw a clear picture of an organizing gradient from sensorimotor to transmodal regions that establishes an axis along which all areas of the cerebral cortex can be situated. In the last part of our opinion article, we therefore proposed that this gradient constitutes the core dimension of an *intrinsic coordinate system* of the human cerebral cortex. While it is common practice in human neuroimaging to describe cortical locations with respect to arbitrary coordinates imposed by the measurement techniques, such as voxel grids, intrinsically-defined coordinates are based on the underlying organization of the cortex itself. Instead of indicating the position of a cortical location in three-dimensional space, intrinsic coordinates indicate its relative position along functional hierarchies and gradients of structural features. The exact configuration of such a coordinate system and even the number of its dimensions remain to be resolved, but we proposed a working model in our article. This model is based on the observation that there is a strong relationship between the relative

position of areas along the sensorimotor-to-transmodal gradient, and their relative position along the cortical surface. The first dimension of the intrinsic coordinate system can therefore be constructed from the spatial distance along the cortical surface from transmodal regions to primary areas (Figure 4.2 a, cf. Study 3). Moreover, our model contains a second intrinsic dimension. As described in Study 3, a secondary gradient of connectivity in the human and macaque monkey cortex separates different functional domains from each other. A similar organization has been observed for a secondary gene expression gradient (Hawrylycz et al., 2012), and is reflected in laminar microstructure (Waehnert et al., 2016) as well as dynamically selected temporal integration hierarchies (Chaudhuri et al., 2015). The distinction between sensorimotor modalities thus offers an additional axis of cortical differentiation. Our model demonstrates that this second dimension, too, can be reproduced from geodesic distance along the cortex, describing each cortical location by its relative distance from morphological landmarks in primary auditory, visual and somatomotor areas (Figure 4.2 b). The proposed intrinsic coordinate system is thus entirely constructed from the intrinsic geometry of the cortex, but captures gradients in multiple structural and functional features.

While many questions remain open, our working model provides a starting point for an intrinsic organizational template of the human cerebral cortex. As will be discussed in more depth in Section 5.3, the intrinsic coordinate system can serve as a common space to integrate observations across time points, measurement modalities, subjects (Langs et al., 2014, 2015) and even across species (Charvet & Finlay, 2014), and fosters novel analytic approaches (Falkiewicz et al., 2017; Haak et al., 2017). With our opinion article, we hope to stimulate a new perspective in which we try to understand the cortex with respect to its own, intrinsic dimensions.

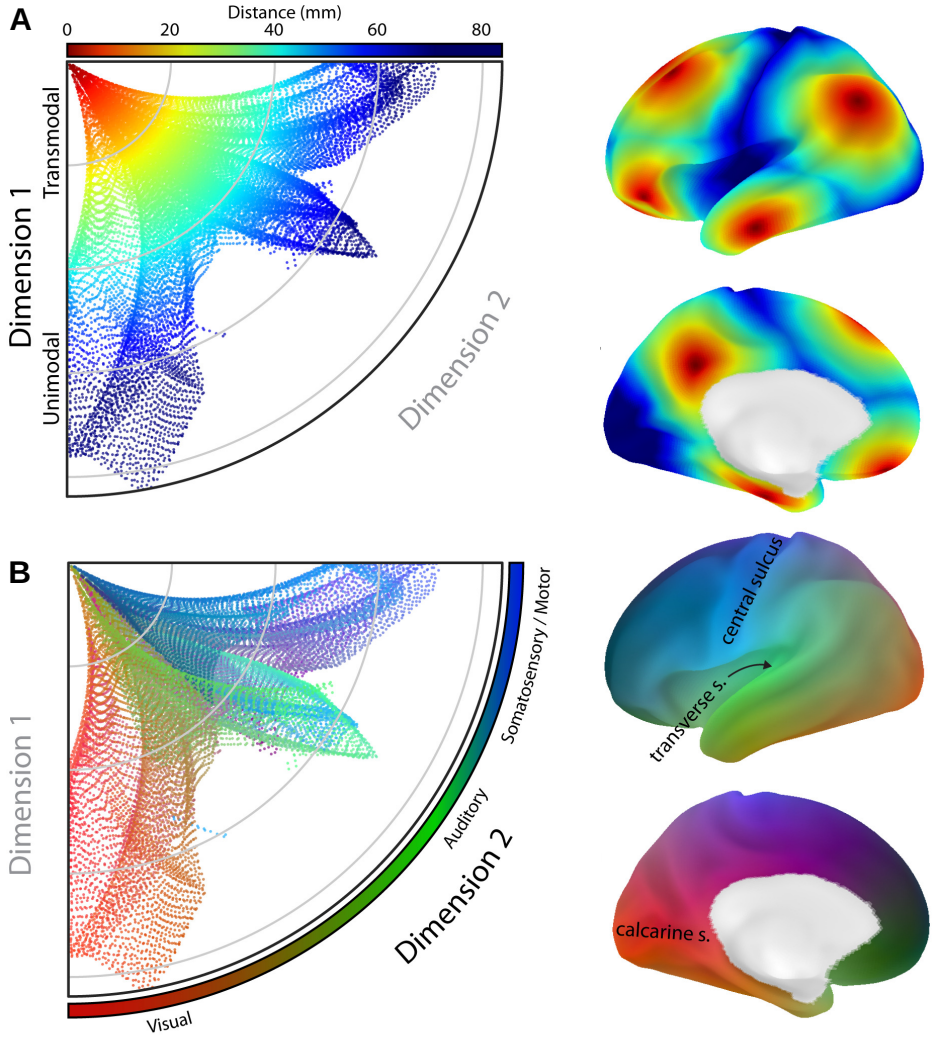

Figure 4.2 A distance-based intrinsic coordinate system of the human cerebral cortex. We propose an intrinsic coordinate system based on the geodesic distance along the cortex. Each data point in the intrinsic coordinate space (*left*) represents a location on the cortical surface (*right*). **A** Data points are colored according to the first intrinsic dimension. This dimension is given by the geodesic distance between sensorimotor and transmodal regions, represented in a color spectrum from red to blue. In other words, the minimum geodesic distance of a cortical location from any of the red transmodal peak regions determines its position along the first intrinsic dimension. In the abstract representation (*left*), this dimension is represented by concentric circles of increasing size. When displayed on the cortical surface (*right*) it largely aligns with the feature maps in Figure 4.1. **B** Data points are colored according to the second intrinsic dimension, which differentiates between the different sensory modalities. The position of a cortical location along this dimension is given by its relative geodesic distance from three morphological landmarks in primary areas. Each cortical location is assigned an RGB value composed of its proximity to each of these landmarks (calcarine sulcus = red, transverse sulcus = green, central sulcus = blue). That means, the closer a cortical location is to the calcarine sulcus, the higher its R-value, and so on. The second dimension is captured by the distance along the arc of the abstract representation of the intrinsic coordinate space (*left*) (Huntenburg et al., accepted).

Chapter 5

General discussion

The main aim of this dissertation was to apply the concept of spatial gradients in cortical organization – emanating from classical neuroanatomical studies in experimental animals – to the human cerebral cortex *in vivo*. This goal was realized in three empirical studies, which employed state-of-the-art neuroimaging technology and novel analysis strategies to investigate the spatial distribution of different cortical features in the human cortex (Chapter 3). The current dissertation additionally presented a set of technical reports introducing open source software tools and data that may serve future research interests in this evolving field (Chapter 2).

Our findings confirmed the general idea of a significant spatial arrangement of cortical areas and extended it to the human cortex. Going beyond the original accounts, our studies provided converging evidence that a global gradient between sensorimotor and transmodal regions captures a core axis of human cortical organization. This global spatial gradient was reflected in the distribution of intracortical myelin, assessed using high-resolution quantitative T1 maps (Study 1), and in the principal spatial motif of functional connectivity patterns, extracted using dimensionality reduction (Study 1 and 3). A link to the intrinsic cortical geometry was established by employing geodesic distance as a proxy for trajectories of cortical expansion between primary sensorimotor and transmodal regions (Study 2 and 3). This approach illustrated that geodesic distance essentially reproduces the principal gradient of functional connectivity. A key feature varying along its spatial axis was found to be the increasing distance to func-

tionally connected areas with increasing distance from primary sensorimotor regions (Study 2). Finally, the sensorimotor-to-transmodal gradient was shown to provide an organizing framework for canonical resting state networks (Study 2 and 3) and a spatial embedding for a global functional hierarchy of increasing abstraction (Study 3).

Taken together, the results of our empirical studies indicated that core aspects of human cortical organization are spatially arranged along a global sensorimotor-to-transmodal gradient. This layout subsumes multiple gradients in individual cortical systems and is embedded in the intrinsic geometry of the cortex. In a subsequent opinion article, we proposed that the sensorimotor-to-transmodal gradient represents the first dimension of a distance-based intrinsic coordinate system of the human cortex (Chapter 4). A second dimension is given by the relative distance between cortical landmarks, representing the different primary sensory domains. This concept entails a new perspective on human cortical organization and gives rise to a range of novel scientific and methodological questions that will be discussed below.

5.1 The potential of *in vivo histology* to investigate microstructural gradients

Spatial gradients were originally described in cortical microstructure (Section 1.1.1). Until recently, this aspect of cortical organization was exclusively accessible through histological studies on post-mortem samples. However, substantial advances in high-resolution and quantitative MRI now facilitate non-invasive assessment of microstructural features in the human brain (Paus, 2017; van der Zwaag et al., 2016; Weiskopf et al., 2015). Because the signal-to-noise ratio in MRI scales supra-linearly with the strength of the static magnetic field, increasingly available ultra-high field scanners provide good image quality even at sub-millimeter resolutions (Pohmann et al., 2016). Furthermore, quantitative sequences yield individual maps of the parameters underlying

the image contrast – such as the different relaxation time constants or susceptibility effects – in physical units. This makes it possible to compare absolute values across brain areas, sessions, subjects and imaging sites (Turner, 2015). It also enables a more direct inference about how different microstructural components influence individual MR parameters, which can be hard to disentangle in standard weighted images. Quantitative, high-resolution MRI therefore provides a new tool for mapping biologically relevant variables such as relative axonal myelination (g-ratio, Paus & Toro, 2009), macromolecular tissue volume (Mezer et al., 2013), iron and myelin concentration (Stüber et al., 2014). Questions about the brain's microstructure, that had previously required histological approaches, can thus be addressed non-invasively in humans (sometimes referred to as *in vivo histology*, Weiskopf et al. 2015). Nevertheless, quantitative MRI is not a direct measure of microstructural components, and its spatial resolution is still low compared to histology. A crucial advantage of MRI over histology in the current context is that it does not require the slicing of brain tissue. It is thus ideally suited to capture global gradients in three-dimensional space.

In this dissertation, we specifically used quantitative T1 acquired at 7T to investigate the distribution of intracortical myelin content in the human cerebral cortex (Study 1). Overall myelination has been described to increase along gradients of microstructural differentiation (Hopf, 1956; Hopf & Vitzthum, 1957; Sanides, 1962), making it a suitable measure to describe such gradients. We acquired quantitative T1 maps using the MP2RAGE sequence (Marques et al., 2010) which have been shown to reflect gray matter myelin content (Stüber et al., 2014) and were used in many recent works (Lutti et al., 2014; Sereno et al., 2013; Tardif et al., 2015; Waehnert et al., 2016). Alternative quantitative MRI techniques, such as magnetization transfer imaging (Dousset et al., 1992) and myelin water imaging (Mackay et al., 1994) are more specific to myelin than T1 but provide lower spatial resolution. Another popular approach to assess intracortical myelin, the ratio of T1w over T2w images (Glasser et al., 2016, 2014; Glasser &

Van Essen, 2011), has not yet been validated against histological data and shows a lower intra- and intersubject reproducibility than quantitative T1 (Haast et al., 2016). Yet, the spatial distribution of the T1w/T2w ratio generally appears similar to quantitative T1, and we were able to confirm our main results in Study 1 using T1w/T2w-based estimates of intracortical myelin. Of note, quantitative T1 is also influenced by the concentration of intracortical iron (Stüber et al., 2014), which however is strongly colocalized to intracortical myelin (Fukunaga et al., 2010). Ferritin particles embedded in the myelin sheath function as a storage for oligodendrocytes, that require iron for the production and repair of myelin (Connor & Menzies, 1996; Todorich et al., 2009). Therefore, independent of the exact contributions of iron and myelin, it appears justified to interpret T1 as to largely reflect the distribution of intracortical myelin.

For the analyses presented in Study 1, we used the *average* intracortical myelin content as a proxy for microstructural differentiation. The high spatial resolution of the underlying T1 maps helps to obtain an unbiased estimate of this average, by improving the definition of cortical boundaries to the white matter and cerebrospinal fluid and reducing partial volume effects (Zaretskaya et al., 2017). Defining anatomically meaningful intracortical depth levels through a volume-preserving approach (Section 2.1.1) further aids in sampling T1 from consistent layers throughout the cortex (Waehnert et al., 2014). However, in contrast to classic myeloarchitectonic techniques, we did not analyze the radial distribution of myelin across the cortical depth. Radial differences in myelin content can be comparable in size to horizontal differences between cortical areas (Lutti et al., 2014), and the increasing spatial resolution in MRI has fostered new approaches to investigate the laminar distribution of intracortical myelin (see Trampel et al. 2017 for a review). While early studies mainly focused on detecting the conspicuous stria of Gennari in the primary visual cortex (Duyn et al., 2007; Sánchez-Panchuelo et al., 2012; Turner et al., 2008), more recent work has demonstrated differences in the laminar myelin distribution across multiple areas of the human cerebral cortex (Dinse

et al., 2015; Fracasso et al., 2016; Marques et al., 2017; Waehnert et al., 2016; Whitaker et al., 2016). Methods to extract and analyze radial myelin profiles are still in their infancy, but more elaborate and robust approaches are likely to emerge from this line of research soon (e.g. Kok et al., 2016). It will then be possible to expand the global spatial gradient in intracortical average myelin, presented here, with a more detailed examination of how the laminar distribution of intracortical myelin changes along the cortical sheet.

Taken together, high-resolution and quantitative MRI represent essential tools for the investigation of global microstructural gradients in the human cerebral cortex *in vivo*. Intracortical myelin in particular has been described to vary along such gradients, can reliably be assessed using quantitative T1 maps, and will likely yield further insights when studied at laminar resolution in the future. At the same time, it is crucial to appreciate that there is no simple one-to-one relationship between the measured MR signal and underlying microstructural components. In order to draw neurobiological conclusions, for example about the mechanisms through which spatial gradients emerge during development, or how they give rise to differences in functional specialization, progress in two domains will be critical. First, the contribution of different microstructural features to MRI-based measures needs to be evaluated against *ex vivo* data (e.g Fracasso et al., 2016; Leuze et al., 2017; Stüber et al., 2014). Second, biophysical models linking microstructural phenomena and MRI readout have to be improved or newly developed (Lerch et al., 2017; Weiskopf et al., 2015). Only under these prerequisites, *in vivo histology* will be able to fully live up to its promise and provide fundamental insights about the human brain at a biologically relevant level. Such insights will be essential to uncover the cellular and molecular basis of spatial gradients observed in MR images.

5.2 Spatial motifs in cortical connections

Research investigating cortical connectivity focuses on the relationship between pairs of locations on the cortex, and thereby yields complex, high-dimensional data in the form of connectivity matrices. The premise of any connectivity analysis is to break down this complexity and extract interpretable patterns. Influenced by the dominant approach of studying cortical organization through a division into spatially discrete areas (Vogt & Vogt, 1919), connectivity analyses have often aimed at deriving discrete network parcellations (e.g. Power et al., 2011; Yeo et al., 2011). These parcellations provide converging information about the organization of cortical regions in spatially distributed, but strongly interconnected networks, which overlap with functionally defined activation patterns (Smith et al., 2009). However, parcellations describe networks as homogeneous and independent entities. This prevents the detection of spatial regularities in connectivity patterns within a parcel, and between different parcels (Jbabdi et al., 2013).

Another widely-used method to analyze connectivity data are graph-theoretical approaches (e.g Bullmore & Sporns, 2009; van den Heuvel & Sporns, 2013). These typically require pre-existing cortical parcellations to define the nodes of the graph. A graph provides an abstract description of the cortical network along with topological measures such as degree, path length or hubness. While such descriptions can be illuminating regarding the flow of information, they classically disregard spatial information altogether and neglect that the cortical network is embedded in anatomical space. Including spatial features in graph-theoretical models leads to the revision of some current assumptions about cortical networks (Knoblauch et al., 2016). For example, it has been shown that the often cited *small-world properties* (Watts & Strogatz, 1998) of the cortex arise from its distribution of connection lengths by necessity, without implying a particular clustering pattern as typically assumed (Lang et al., 2017). This illustrates that

spatial aspects can inform and refine existing descriptions of connectivity organization.

As standard analysis strategies focus on dividing the cortex in discrete networks, or describing its topological properties, they fall short of capturing the spatial arrangement of connections central to the concept of gradients in cortical organization. On the other hand, the classical studies on gradients in connectivity do not provide an alternative analytic approach. While they report the specific projection patterns of injected tracers in detail, the descriptions of the overarching spatial gradients remain qualitative and schematic (cf. Figure 1.1). One core aspect of these descriptions, the preference on long-range connections to occur between regions of similar microstructural differentiation, has subsequently been confirmed in a quantitative fashion (Beul et al., 2015, 2014; Goulas, Uylings, & Hilgetag, 2016). But analytical approaches to characterize *spatial motifs* in connectivity patterns emerged only most recently (Atasoy et al., 2016; Haak et al., 2017; Langs et al., 2014, 2015; Sepulcre et al., 2012; Taylor et al., 2015). A particularly promising method is the decomposition of the connectivity matrix into a set of superimposed gradients (Section 1.2.2). The work presented in this dissertation was the first to show that such connectivity gradients, derived on the scale of the entire cortex, capture core aspects of cortical organization reflected in microstructure (Study 1) and functional specialization (Study 3). Study 2 furthermore presented a first indication that connectivity gradients in the adult brain might arise from the influence of molecular gradients during development. While the conceptual implication of these findings will be discussed in Section 5.3, the following highlights some of the methodological advancements that this new strategy to analyze cortical connections entails.

One question that arises when characterizing connectivity gradients is how to compare them statistically across subjects or sessions. In their study examining connectivity gradients in the visual and motor cortex, Haak et al. (2017) proposed to exploit statistical tools from a spatial inference technique called *trend surface analysis* (Gelfand

et al., 2010). In this approach, spatial gradients are parameterized using polynomial base functions to model the main surface trend, and a Gaussian process to model small variations. Differences between gradients can then be tested for via statistical inference on the model coefficients. While common statistical approaches used in neuroimaging are based on voxel- or node-wise comparisons, tools to statistically compare the *spatial layout* of cortical maps have so far been lacking. The potential impact of this new approach therefore extends far beyond the comparison of connectivity gradients to virtually any measure that can be mapped onto the cortex.

A particularly innovative application of connectivity gradients is to model task activation patterns as the weighted sum of a set of gradients (Falkiewicz et al., 2017). Activity patterns can then be compared across task conditions and across subjects through statistical inference on the gradient weights. The underlying idea is similar to the hyperalignment approach, initially proposed by Haxby et al. (2011) for the human ventral temporal cortex. These authors acquired fMRI data while subjects were exposed to long and complex stimuli. They then created a high-dimensional representational space from the activation patterns across time, to which all subjects were aligned (hyperalignment). Individual task activation patterns were modeled as a weighted sum of the dimensions of this representational space (basis functions). Task activation patterns could be predicted across subjects at a much higher accuracy using hyperalignment as compared to anatomical alignment. Instead of extracting basis functions from extensive experiments with complex stimuli, connectivity gradients derived from resting state fMRI could be used in a similar way in the future. In support of this idea, the work presented in this dissertation indicates that connectivity gradients capture core organizing axes of the human cerebral cortex, which are likely to shape functional response patterns (see also Tavor et al., 2016).

Both aforementioned use cases are based on the idea that the overall spatial layout of a connectivity gradient is more meaningful than its exact anatomical manifestation

in an individual cortex. The same notion is the basis for another important application – the alignment of subjects via gradient-matching. Langs et al. (2015) showed that aligning connectivity gradients across individuals improves matching accuracy of functionally equivalent areas compared to morphological alignment. This approach even facilitated mapping of functional networks from healthy individuals to those whose networks are disrupted by tumors (Langs et al., 2014). Gradient matching also has the potential to ease the integration of data from different modalities for intersubject alignment. Dominant connectivity gradients, along with maps of morphology, task activation and intracortical myelin content, could represent different dimensions to be aligned simultaneously. This method would be similar to the one recently proposed by Glasser et al. (2016), but avoids a discrete parcellation scheme. Moreover, as indicated by the results of Study 3, connectivity gradients might be phylogenetically conserved and could represent a novel approach for interspecies alignment independent of area definition and homology (Charvet et al., 2017).

Characterizing spatial motifs in cortical connectivity through gradients thus presents a fruitful complement to parcellations and graph-theoretical analyses. The spatial perspective fosters methodological innovations that bring the layout of cortical maps into focus, and inspires fresh approaches to longstanding challenges such as cortical alignment. The basic idea of decomposing high-dimensional data into superimposed spatial gradients, and the associated analytical tools, can be extended to other high-dimensional data such as gene expression, functional co-activation, or laminar profiles.

5.3 A core intrinsic dimension of the human cerebral cortex

A key contribution of this dissertation is the proposal of an intrinsic coordinate system of the human cerebral cortex with a sensorimotor-to-transmodal core dimension (Chapter

4). This approach is inspired by the concept of a natural coordinate system of the vertebrate central nervous system (CNS) by Nieuwenhuys and Puelles (2015). Instead of using Cartesian coordinates, the natural coordinate system describes CNS organization along three built-in dimensions: the curved long axis of the neural tube and two limiting curved planes, given by the ventricular and the meningeal surfaces. These organizing axes manifest themselves during CNS development through the orientation of blood vessels and fibers, and the migratory paths of neurons. Simple rostrocaudal patterns found in the cerebral cortex of more primitive mammals align with the long axis of the natural coordinate system. However, Chapter 3 and 4 have presented evidence that the core axis of the human cerebral cortex deviates from this rostrocaudal organization. The concept of the intrinsic coordinate system thus borrows from the basic idea of the natural coordinate system – to use a structures intrinsic, naturally occurring axes for describing its organization – and applies it to the specific case of the human cerebral cortex.[1]

The work discussed in Chapter 3 and 4 has shown that important aspects of cortical organization – such as microstructure, gene expression, connectivity and function – are organized along a gradient from primary sensorimotor areas to transmodal regions. Furthermore, there is a strong relationship between the relative position of areas along this gradient and their relative position along the cortical surface. Chapter 4 therefore proposed that the first intrinsic dimension of the human cerebral cortex is given by the geodesic distance between transmodal and primary areas (Figure 4.2). This global gradient extends the classical studies on cortical gradients by unifying the multiple

[1]Using the term *intrinsic coordinate system*, rather than *natural coordinate system* aims to differentiate this proposition from the original concept by Nieuwenhuys and Puelles (2015). While the natural coordinate system is directly deduced from detailed knowledge about CNS development, the gradients discussed in this dissertation are inferred from various, often indirect, measures of cortical organization in the adult brain, and retrospectively associated with developmental processes. This is not to imply that the intrinsic coordinate system of the cerebral cortex is categorically different from the natural coordinate system of the CNS. In contrast, the developmental processes which establish cortical gradients might eventually be uncovered and facilitate an integration between both coordinate systems.

individual progressions that they describe (e.g Pandya et al., 2015; Sanides, 1962) in a single dimension. While such an overarching framework was implied in the classical work, it had never actually been shown analytically. As indicated in the previous two sections, this advancement has at least partly been enabled by new tools. Detecting global gradients in a complete reconstruction of the cortical sheet, obtained from a three-dimensional MRI scan, is more feasible than combining information from post-mortem samples, in which gradients had to be traced through stacks of adjacent slices. Similarly, the analytical and computational means to decompose high-dimensional connectivity data into superimposed spatial gradients were not available when the classical studies were performed. This latter innovation in particular, has enabled the insight that long-range connections represent an additional layer of organization which links local gradients. Spatially distant areas that share a similar microstructure and long-range connections thus get situated at a comparable position of *one global gradient*, instead of a comparable position along separate gradients (cf. Section 1.1.2).

The sensorimotor-to-transmodal core axis of the human cortex offers a concrete spatial implementation of the global processing hierarchy suggested by Mesulam (1998)(Section 1.1.3). Local hierarchies, for example in the visual system (Felleman & Van Essen, 1991), have been vital for understanding the functional role of individual cortical areas. A global processing hierarchy, embedded in the intrinsic geometry of the cortex, has the potential to particularly elucidate the role of the DMN in human cognition, which remains incompletely understood (Raichle, 2015; Spreng & Grady, 2010). Study 3 showed that DMN regions are positioned at a maximum geodesic distance from primary sensorimotor areas (Figure 3.4). We suggested that this spatial insulation of the DMN from the direct environmental in- and output, processed in sensorimotor regions, enables functions that require the abstraction from concrete content such as mind wandering (Mason et al., 2007) or creative thought (Beaty et al., 2014). Furthermore, Study 2 demonstrated that regions of the DMN show the highest average distance to

their functionally connected partners (Figure 3.3). This makes them ideally suited to integrate information across systems in complex tasks such as considering the mental states of others (Amft et al., 2015). According to the tethering hypothesis, the emergence of long-range connections in DMN regions is a result of their distance from the constraints of molecular patterning centers (Buckner & Krienen, 2013). This release from developmental determination could also underlie the flexible and learning-related properties of the DMN that enable the generation of alternative behavioral strategies (Haggard, 2008). Finally, Hasson et al. (2015) have proposed that the representation of complex concepts in the DMN can be explained from its position at the top of a sensorimotor-to-transmodal hierarchy of temporal integration (cf. Chapter 4). These authors suggest that each region along the hierarchy segregates incoming information into discrete events at its preferred intrinsic timescale. This leads to representation of short sensory events, and respective memory traces, in primary regions, and encoding of abstract concepts that build on many pieces of information, or situations that unfold over a longer time span, in regions of the DMN (Figure 4.1 d)(Baldassano et al., 2016; Hasson et al., 2015; Yeshurun et al., 2017). This model specifically explains the involvement of DMN regions in thinking about the past and imagining the future (Schacter & Addis, 2007). The position of the DMN at one extreme of the sensorimotor-to-transmodal core axis can thus provide new insights into the functional role of these regions, which can be difficult to understand via task-based activation studies.

Functions commonly associated with the DMN, such as social cognition, remembering the past and planning the future, are often described as hallmarks of human cognition. The sensorimotor-to-transmodal gradient offers a new perspective on the emergence of such functions through phylogeny and ontogeny. It has been suggested that microstructural gradients in the mammalian cortex result from the temporal sequence of neurogenesis (Cahalane et al., 2012, 2014; Charvet & Finlay, 2014), which begins uniformly across the cortex but terminates later in primary sensorimotor re-

gions (Rakic, 2002). Primary areas therefore undergo a higher number of cell cycles, producing a high number of small neurons. In transmodal regions, neurogenesis likely terminates much earlier (although the exact numbers for the human brain are unknown), so that more time can in turn be devoted to the growth of large neurons with dense and complex dendritic trees (Elston, 2000, 2003). The sensorimotor-to-transmodal gradient thus signifies a shift in computational capacity, from a high number of units processing high frequency input in primary sensorimotor areas, to a lower number of highly connected units ideally suited for information integration in transmodal regions (Cahalane et al., 2012). This gradient is more pronounced in species with larger cortices and longer developmental schedules, leading to greater differences in neurogenesis termination across areas (Cahalane et al., 2014; Charvet et al., 2015; Charvet & Finlay, 2014). A possible implication is that the specific functional spectrum of the human cortex results from an evolutionary selection on an extended developmental schedule – which is indeed considerably longer in humans as compared to all other mammals (Workman et al., 2013) – that leads to steeper structural gradients (Cahalane et al., 2014). The functional attributes of DMN regions could consequently be explained from an amplified emphasis on highly connected processing units at the expanded transmodal end of this gradient. While the resulting cognitive capacities could plausibly present an evolutionary advantage, the underlying adaptations would not be found in some uniquely human property of respective regions, but in genes determining the developmental schedule of the cortex (Buckner & Krienen, 2013). Importantly, these considerations are based on dispersed pieces of evidence from different species in various contexts and remain hypothetical for now. Yet, they point to an interesting research avenue, exploring the differences of cortical gradients across species and investigating if an adaptive pressure on steeper cortical gradients might indeed underlie the evolution towards an extended spectrum of cognitive functions.

In sum, this dissertation presented evidence for a core axis in human cortical orga-

nization which is embedded in a spatial gradient between sensorimotor and transmodal areas. This gradient, and a secondary gradient separating different sensory modalities, build the dimensions of the proposed intrinsic coordinate system of the human cerebral cortex. Much like cortical surface representations have been introduced to analyze neuroimaging data in the space of the folded cortical sheet itself, rather than an arbitrary voxel grid, a gradient-based intrinsic coordinate system is a next step towards describing the cortex in reference to its internal organization, rather than the way we measure it. This perspective facilitates the integration of findings in a common conceptual framework and reinforces their interpretation in the context of cortical development and evolution.

5.4 Open questions and future prospects

How do we understand one of our bodies' most remarkable systems – the human cerebral cortex? The work presented in this dissertation started from the premise that profound knowledge about the general principles governing a system's structure is vital for understanding its function (Gudden, 1886). In human neuroscience, the functions in question are our own cognitive abilities, functions so elaborate and integral to our perception of what makes us human, that it can be hard to imagine them arising through the right configuration of cells and fibers, or – on the spatial scale on which we operate – the right arrangement of cortical areas. Human neuroimaging has yielded a plethora of studies associating areas or networks with specific cortical functions. Yet, the general principles of how these areas and networks are arranged to form a highly integrated entity, and how this organization gives rise to the spectrum of human cognitive functions, remain largely unsettled. This might in part be because our view on the cortex is shaped and constrained by the techniques we use to measure it. With the intrinsic coordinate system of the human cerebral cortex this dissertation aims to stimulate a shift in perspective towards "meeting the brain on its own terms" (Haueis, 2014), that is, ana-

lyzing the cortex with respect to its intrinsic organization. The arrangement of areas in spatial gradients, forming the intrinsic dimensions, does not itself constitute an explanation for how the functional spectrum of the cortex arises. But it offers a framework for unifying observations across a variety of domains in order to deduce general rules and construct new models on their basis (e.g. Cahalane et al., 2014; Chaudhuri et al., 2015). A gradient-based intrinsic coordinate system thus constitutes a novel research agenda with diverse applications and new methodological and conceptual challenges.

One fundamental question is how best to construct the intrinsic coordinate system and how many meaningful dimensions it contains. We have suggested a working model with two distance-based dimension which, however, constitutes a starting point rather than a final solution. It is likely that the exact configuration of these dimensions needs to be revised and that further dimensions will be added. Furthermore, it remains to be investigated if brain structures other than the cerebral cortex, such as the cerebellum or the basal ganglia, are organized along corresponding gradients. If so, the next question is how gradients in different structures relate to each other, and if they can be unified into a single coordinate system. The most important methodological challenge related to such gradients might be to optimize techniques for aligning them across individuals (Langs et al., 2015; Lombaert et al., 2015). When decomposing data from individual subjects, matching the gradients is not trivial – signs and order can be flipped or the data can be decomposed along different dimensions altogether. Thorough evaluation studies will be required in order to distinguish meaningful interindividual variation from methodological artifacts.

Assuming that the organization in spatial gradients is not just an evolutionary side effect, but has adaptive value, it can be asked what advantage this arrangement bears for the computational capacities of the cortex. One possibility is that the slow spatial variation of features ensures proximity of strongly connected regions, which perform similar functions, to reduce wiring cost (Charvet et al., 2015, 2017; Jbabdi et al., 2013).

The functional relevance of this arrangement has been illustrated in a study showing that sensory impairment after spinal cord injury is closely related to a discontinuity in somatotopic gradients (Saadon-Grosman et al., 2015). This opens a set of potential research questions, investigating if neurological and psychiatric conditions are associated with specific alterations in cortical gradients. For example, stroke-induced lesions might cause local disruptions or even global reorganization of cortical gradients.

The perhaps most crucial, but most challenging questions to address, concern the emergence of cortical gradients during development. Research into this aspect could substantially enhance our understanding about the significance of the intrinsic cortical dimensions and the mechanisms by which they are determined. Furthermore, the comparison of these dimensions across species could help to uncover the particular changes through which the human cerebral cortex with its unique functional spectrum arose from its phylogenetic predecessors.

5.5 Conclusion

The spatial arrangement of cortical areas is not arbitrary. An area's position along a global organizing gradient, spanning between sensorimotor and transmodal extremes, reflects its structural features and functional role. Recognizing this relationship introduces a new perspective in which cortical organization is described with respect to its own, intrinsic dimensions. It takes us beyond the localization of functions to areas and networks, towards an understanding of how the spectrum of cognitive capacities emerges from the spatial arrangement of structural features. Uncovering the neurodevelopmental basis of these intrinsic dimensions, and exploring their convergence and variation across species, has the potential to demystify the emergence of uniquely human cognitive functions.

References

Abbie, A. A. (1940). Cortical lamination in the monotremata. *J. Comp. Neurol.*, *72*(3), 429–467.

Abbie, A. A. (1942). Cortical lamination in a polyprotodont marsupial, perameles nasuta. *J. Comp. Neurol.*, *76*(3), 509–536.

Abraham, A., Pedregosa, F., Eickenberg, M., Gervais, P., Mueller, A., Kossaifi, J., ... Varoquaux, G. (2014). Machine learning for neuroimaging with scikit-learn. *Front. Neuroinform.*, *8*, 14.

Adachi, Y., Osada, T., Sporns, O., Watanabe, T., Matsui, T., Miyamoto, K., & Miyashita, Y. (2012). Functional connectivity between anatomically unconnected areas is shaped by collective network-level effects in the macaque cortex. *Cereb. Cortex*, *22*(7), 1586–1592.

Amft, M., Bzdok, D., Laird, A. R., Fox, P. T., Schilbach, L., & Eickhoff, S. B. (2015). Definition and characterization of an extended social-affective default network. *Brain Struct. Funct.*, *220*(2), 1031–1049.

Amunts, K., & Zilles, K. (2015). Architectonic mapping of the human brain beyond brodmann. *Neuron*, *88*(6), 1086–1107.

Atasoy, S., Donnelly, I., & Pearson, J. (2016). Human brain networks function in connectome-specific harmonic waves. *Nat. Commun.*, *7*, 10340.

Badre, D., & D'Esposito, M. (2009). Is the rostro-caudal axis of the frontal lobe hierarchical? *Nat. Rev. Neurosci.*, *10*(9), 659–669.

Bailey, P., & von Bonin, G. (1951). *The isocortex of man.* University of Illinois Press.

Bakker, R., Wachtler, T., & Diesmann, M. (2012). CoCoMac 2.0 and the future of tract-tracing databases. *Front. Neuroinform.*, *6*, 30.

Baldassano, C., Chen, J., Zadbood, A., Pillow, J. W., Hasson, U., & Norman, K. A.

(2016). Discovering event structure in continuous narrative perception and memory. *bioRxiv*.

Barbas, H. (1986). Pattern in the laminar origin of corticocortical connections. *J. Comp. Neurol.*, *252*(3), 415–422.

Barbas, H. (2015). General Cortical and Special Prefrontal Connections: Principles from Structure to Function. *Annu. Rev. Neurosci.*, *38*(1), 269–289.

Bazin, P.-L., Weiss, M., Dinse, J., Schäfer, A., Trampel, R., & Turner, R. (2014). A computational framework for ultra-high resolution cortical segmentation at 7Tesla. *Neuroimage*, *93 Pt 2*, 201–209.

Beaty, R. E., Benedek, M., Wilkins, R. W., Jauk, E., Fink, A., Silvia, P. J., ... Neubauer, A. C. (2014). Creativity and the default network: A functional connectivity analysis of the creative brain at rest. *Neuropsychologia*, *64*, 92–98.

Behzadi, Y., Restom, K., Liau, J., & Liu, T. T. (2007). A component based noise correction method (CompCor) for BOLD and perfusion based fMRI. *Neuroimage*, *37*(1), 90–101.

Belkin, M., & Niyogi, P. (2003). Laplacian eigenmaps for dimensionality reduction and data representation. *Neural Comput.*, *15*(6), 1373–1396.

Beul, S. F., Barbas, H., & Hilgetag, C. C. (2015). A predictive structural model of the primate connectome. *arXiv*, *1511*, 07222.

Beul, S. F., Grant, S., & Hilgetag, C. C. (2014). A predictive model of the cat cortical connectome based on cytoarchitecture and distance. *Brain Struct. Funct.*, *220*(6), 3167–3184.

Biswal, B. B., Mennes, M., Zuo, X.-N., Gohel, S., Kelly, C., Smith, S. M., ... Milham, M. P. (2010). Toward discovery science of human brain function. *Proc. Natl. Acad. Sci. U. S. A.*, *107*(10), 4734–4739.

Biswal, B. B., Yetkin, F. Z., Haughton, V. M., & Hyde, J. S. (1995). Functional connectivity in the motor cortex of resting human brain using echo-planar MRI. *Magn. Reson. Med.*, *34*(4), 537–541.

Bock, N. A., Kocharyan, A., Liu, J. V., & Silva, A. C. (2009). Visualizing the entire cortical myelination pattern in marmosets with magnetic resonance imaging. *J. Neurosci. Methods*, *185*(1), 15–22.

Bogovic, J. A., Prince, J. L., & Bazin, P.-L. (2013). A multiple object geometric deformable model for image segmentation. *Comput. Vis. Image Underst.*, *117*(2), 145–157.

Bok, S. (1929). Der Einfluß der in den Furchen und Windungen auftretenden Krümmungen der Großhirnrinde auf die Rindenarchitektur. *Arch. Psychiatr. Nervenkr. Z. Gesamte Neurol. Psychiatr.*, *12*, 682–750.

Brett, M., Hanke, M., Cipollini, B., Côté, M.-A., Markiewicz, C., Gerhard, S., ... Others (2016). nibabel: 2.1. 0. *Zenodo*.

Bridge, H., Clare, S., Jenkinson, M., Jezzard, P., Parker, A. J., & Matthews, P. M. (2005). Independent anatomical and functional measures of the V1/V2 boundary in human visual cortex. *J. Vis.*, *5*(2), 93–102.

Brockhaus, H. (1940). Die Cyto-und Myeloarchitektonik des Cortex claustralis und des Claustrum beim Menschen. *J Psychol Neurol*, *49*(4-6), 249–348.

Brodmann, K. (1909). *Vergleichende lokalisationslehre der grosshirnrinde in ihren prinzipien dargestellt auf grund des zellenbaues*. Leipzig (Germany): Johann Ambrosius Barth.

Buckner, R. L., & Krienen, F. M. (2013). The evolution of distributed association networks in the human brain. *Trends Cogn. Sci.*, *17*(12), 1–18.

Bullmore, E., & Sporns, O. (2009). Complex brain networks: graph theoretical analysis of structural and functional systems. *Nat. Rev. Neurosci.*, *10*(3), 186–198.

Burt, J. B., Demirtas, M., Eckner, W. J., Navejar, N. M., Ji, J. L., Martin, W. J., ... Murray, J. D. (2017). Hierarchy of transcriptomic specialization across human cortex captured by myelin map topography. *bioRxiv*.

Cahalane, D. J., Charvet, C. J., & Finlay, B. L. (2012). Systematic, balancing gradients in neuron density and number across the primate isocortex. *Front. Neuroanat.*,

6, 28.

Cahalane, D. J., Charvet, C. J., & Finlay, B. L. (2014). Modeling local and cross-species neuron number variations in the cerebral cortex as arising from a common mechanism. *Proc. Natl. Acad. Sci. U. S. A.*, *111*(49), 17642–17647.

Chanes, L., & Barrett, L. F. (2016). Redefining the role of limbic areas in cortical processing. *Trends Cogn. Sci.*, *20*(2), 96–106.

Charvet, C. J., Cahalane, D. J., & Finlay, B. L. (2015). Systematic, cross-cortex variation in neuron numbers in rodents and primates. *Cereb. Cortex*, *25*(1), 147–160.

Charvet, C. J., & Finlay, B. L. (2014). Evo-devo and the primate isocortex: the central organizing role of intrinsic gradients of neurogenesis. *Brain Behav. Evol.*, *84*(2), 81–92.

Charvet, C. J., Stimpson, C. D., Kim, Y. D., Raghanti, M. A., Lewandowski, A. H., Hof, P. R., ... Sherwood, C. C. (2017). Gradients in cytoarchitectural landscapes of the isocortex: Diprotodont marsupials in comparison to eutherian mammals. *J. Comp. Neurol.*, *525*(8), 1811–1826.

Chaudhuri, R., Knoblauch, K., Gariel, M.-A., Kennedy, H., & Wang, X.-J. (2015). A Large-Scale circuit mechanism for hierarchical dynamical processing in the primate cortex. *Neuron*, *88*(2), 419–431.

Coifman, R. R., & Lafon, S. (2006). Diffusion maps. *Appl. Comput. Harmon. Anal.*, *21*(1), 5–30.

Collins, C. E., Airey, D. C., Young, N. A., Leitch, D. B., & Kaas, J. H. (2010). Neuron densities vary across and within cortical areas in primates. *Proc. Natl. Acad. Sci. U. S. A.*, *107*(36), 15927–15932.

Connor, J. R., & Menzies, S. L. (1996). Relationship of iron to oligodendrocytes and myelination. *Glia*, *17*(2), 83–93.

Dale, A. M., Fischl, B., & Sereno, M. I. (1999). Cortical Surface-Based Analysis: I. Segmentation and Surface Reconstruction. *Neuroimage*, *9*(2), 179–194.

Dart, R. A. (1934). The dual structure of the neopallidum: its history and significance. *J. Anat.*, *69*, 3–19.

der Walt, S. v., Colbert, S. C., & Varoquaux, G. (2011). The NumPy array: A structure for efficient numerical computation. *Computing in Science Engineering*, *13*(2), 22–30.

Dick, F., Tierney, A. T., Lutti, A., Josephs, O., Sereno, M. I., & Weiskopf, N. (2012). In vivo functional and myeloarchitectonic mapping of human primary auditory areas. *J. Neurosci.*, *32*(46), 16095–16105.

Ding, N., Melloni, L., Zhang, H., Tian, X., & Poeppel, D. (2016). Cortical tracking of hierarchical linguistic structures in connected speech. *Nat. Neurosci.*, *19*(1), 158–164.

Dinse, J., Härtwich, N., Waehnert, M. D., Tardif, C. L., Schäfer, A., Geyer, S., ... Bazin, P.-L. (2015). A cytoarchitecture-driven myelin model reveals area-specific signatures in human primary and secondary areas using ultra-high resolution in-vivo brain MRI. *Neuroimage*, *114*, 71–87.

Dousset, V., Grossman, R. I., Ramer, K. N., Schnall, M. D., Young, L. H., Gonzalez-Scarano, F., ... Cohen, J. A. (1992). Experimental allergic encephalomyelitis and multiple sclerosis: lesion characterization with magnetization transfer imaging. *Radiology*, *182*(2), 483–491.

Droettboom, M., Caswell, T. A., Firing, E., McDougall, D., Ivanov, P., Giuca, M., ... May, R. (2016). *matplotlib: matplotlib v1.5.1.*

Duyn, J. H., van Gelderen, P., Li, T.-Q., de Zwart, J. A., Koretsky, A. P., & Fukunaga, M. (2007). High-field MRI of brain cortical substructure based on signal phase. *Proc. Natl. Acad. Sci. U. S. A.*, *104*(28), 11796–11801.

Eickhoff, S. B., Constable, R. T., & Yeo, B. T. T. (2017). Topographic organization of the cerebral cortex and brain cartography. *Neuroimage*.

Elston, G. N. (2000). Pyramidal cells of the frontal lobe: all the more spinous to think with. *J. Neurosci.*, *20*(18), RC95.

Elston, G. N. (2003). Cortex, cognition and the cell: new insights into the pyramidal neuron and prefrontal function. *Cereb. Cortex*, *13*(11), 1124–1138.

Falkiewicz, M., Jefferies, E., Ghosh, S., Langs, G., Baczkowski, B., Bzdok, D., ... Margulies, D. M. (2017). Gradients of functional connectivity predict task condition and working memory performance. *Poster presented at the 2017 Annual Meeting of the Organization for Human Brain Mapping, Vancouver, Canada*.

Fan, X., Bazin, P.-L., & Prince, J. L. (2008). A Multi-Compartment segmentation framework with homeomorphic level sets. *Proc. IEEE Comput. Soc. Conf. Comput. Vis. Pattern Recognit.*, 1–6.

Feinberg, D. A., Moeller, S., Smith, S. M., Auerbach, E., Ramanna, S., Gunther, M., ... Yacoub, E. (2010). Multiplexed echo planar imaging for sub-second whole brain FMRI and fast diffusion imaging. *PLoS One*, *5*(12), e15710.

Felleman, D. J., & Van Essen, D. C. (1991). Distributed hierarchical processing in the primate cerebral cortex. *Cereb. Cortex*, *1*(1), 1–47.

Fischl, B., Sereno, M. I., & Dale, A. M. (1999). Cortical Surface-Based Analysis: II: Inflation, Flattening, and a Surface-Based Coordinate System. *Neuroimage*, *9*(2), 195–207.

Forstmann, B. U., Keuken, M. C., Schafer, A., Bazin, P.-L., Alkemade, A., & Turner, R. (2014). Multi-modal ultra-high resolution structural 7-tesla MRI data repository. *Sci Data*, *1*, 140050.

Fox, P. T., & Lancaster, J. L. (2002). Opinion: Mapping context and content: the BrainMap model. *Nat. Rev. Neurosci.*, *3*(4), 319–321.

Fracasso, A., van Veluw, S. J., Visser, F., Luijten, P. R., Spliet, W., Zwanenburg, J. J. M., ... Petridou, N. (2016). Lines of baillarger in vivo and ex vivo: Myelin contrast across lamina at 7T MRI and histology. *Neuroimage*, *133*, 163–175.

Fukunaga, M., Li, T.-Q., van Gelderen, P., de Zwart, J. A., Shmueli, K., Yao, B., ... Duyn, J. H. (2010). Layer-specific variation of iron content in cerebral cortex as a source of MRI contrast. *Proc. Natl. Acad. Sci. U. S. A.*, *107*(8), 3834–3839.

Gelfand, A. E., Diggle, P., Guttorp, P., & Fuentes, M. (2010). *Handbook of spatial statistics*. CRC Press.

Geyer, S., Weiss, M., Reimann, K., Lohmann, G., & Turner, R. (2011). Microstructural Parcellation of the Human Cerebral Cortex - From Brodmann's Post-Mortem Map to in vivo Mapping with High-Field Magnetic Resonance Imaging. *Front. Hum. Neurosci.*, *5*, 19.

Glasser, M. F., Coalson, T. S., Robinson, E. C., Hacker, C. D., Harwell, J., Yacoub, E., ... Van Essen, D. C. (2016). A multi-modal parcellation of human cerebral cortex. *Nature*, *536*, 171–178.

Glasser, M. F., Goyal, M. S., Preuss, T. M., Raichle, M. E., & Van Essen, D. C. (2014). Trends and properties of human cerebral cortex: Correlations with cortical myelin content. *Neuroimage*, *93*, 165–175.

Glasser, M. F., Sotiropoulos, S. N., Wilson, J. A., Coalson, T. S., Fischl, B., Andersson, J. L., ... WU-Minn HCP Consortium (2013). The minimal preprocessing pipelines for the human connectome project. *Neuroimage*, *80*, 105–124.

Glasser, M. F., & Van Essen, D. C. (2011). Mapping human cortical areas in vivo based on myelin content as revealed by T1- and T2-weighted MRI. *J. Neurosci.*, *31*(32), 11597–11616.

Goebel, R. (2012). BrainVoyager–past, present, future. *Neuroimage*, *62*(2), 748–756.

Gorgolewski, K. J., Auer, T., Calhoun, V. D., Craddock, R. C., Das, S., Duff, E. P., ... Poldrack, R. A. (2016). The brain imaging data structure, a format for organizing and describing outputs of neuroimaging experiments. *Sci Data*, *3*, 160044.

Gorgolewski, K. J., Burns, C. D., Madison, C., Clark, D., & Halchenko, Y. O. (2011). Nipype : a flexible, lightweight and extensible neuroimaging data processing framework in Python. *Front. Neuroinform.*, *5*(August).

Gorgolewski, K. J., Mendes, N., Wilfling, D., Wladimirow, E., Gauthier, C. J., Bonnen, T., ... Margulies, D. S. (2015). A high resolution 7-Tesla resting-state fMRI test-retest dataset with cognitive and physiological measures. *Sci Data*, *2*, 140054.

Goulas, A., Uylings, H. B. M., & Hilgetag, C. C. (2016). Principles of ipsilateral and contralateral cortico-cortical connectivity in the mouse. *Brain Struct. Funct.*.

Goulas, A., Werner, R., Beul, S. F., Saering, D., van den Heuvel, M., Triarhou, L. C., & Hilgetag, C. C. (2016). Cytoarchitectonic similarity is a wiring principle of the human connectome. *bioRxiv*.

Griffin, L. D. (1994). The intrinsic geometry of the cerebral cortex. *J. Theor. Biol.*, *166*(3), 261–273.

Gudden, B. v. (1886). Über die frage der localisation der functionen der großhirnrinde. *Allg. Z. Psychiatr. Grenzgeb*, *42*, 478–499.

Haak, K. V., Marquand, A. F., & Beckmann, C. F. (2017). Connectopic mapping with resting-state fMRI. *NeuroImage*, *in press*.

Haast, R. A. M., Ivanov, D., Formisano, E., & Uludag, K. (2016). Reproducibility and reliability of quantitative and weighted T1 and t2(???) mapping for Myelin-Based cortical parcellation at 7 tesla. *Front. Neuroanat.*, *10*, 112.

Hackett, T. A., Stepniewska, I., & Kaas, J. H. (1998). Subdivisions of auditory cortex and ipsilateral cortical connections of the parabelt auditory cortex in macaque monkeys. *J. Comp. Neurol.*, *394*(4), 475–495.

Haggard, P. (2008). Human volition: towards a neuroscience of will. *Nat. Rev. Neurosci.*, *9*(12), 934–946.

Hagmann, P., Cammoun, L., Gigandet, X., Meuli, R., Honey, C. J., Wedeen, V. J., & Sporns, O. (2008). Mapping the structural core of human cerebral cortex. *PLoS Biol.*, *6*(7), e159.

Han, X., Pham, D. L., Tosun, D., Rettmann, M. E., Xu, C., & Prince, J. L. (2004). CRUISE: cortical reconstruction using implicit surface evolution. *Neuroimage*, *23*(3), 997–1012.

Hasson, U., Chen, J., & Honey, C. J. (2015). Hierarchical process memory: memory as an integral component of information processing. *Trends Cogn. Sci.*, *19*(6), 304–313.

Hasson, U., Yang, E., Vallines, I., Heeger, D. J., & Rubin, N. (2008). A hierarchy of temporal receptive windows in human cortex. *J. Neurosci.*, *28*(10), 2539–2550.

Haueis, P. (2014). Meeting the brain on its own terms. *Front. Hum. Neurosci.*, *8*, 815.

Hawrylycz, M. J., Lein, E. S., Guillozet-Bongaarts, A. L., Shen, E. H., Ng, L., Miller, J. A., ... Jones, A. R. (2012). An anatomically comprehensive atlas of the adult human brain transcriptome. *Nature*, *489*(7416), 391–399.

Haxby, J. V., Guntupalli, J. S., Connolly, A. C., Halchenko, Y. O., Conroy, B. R., Gobbini, M. I., ... Ramadge, P. J. (2011). A common, high-dimensional model of the representational space in human ventral temporal cortex. *Neuron*, *72*(2), 404–416.

Hermundstad, A. M., Bassett, D. S., Brown, K. S., Aminoff, E. M., Clewett, D., Freeman, S., ... Carlson, J. M. (2013). Structural foundations of resting-state and task-based functional connectivity in the human brain. *Proc. Natl. Acad. Sci. U. S. A.*, *110*(15), 6169–6174.

Hill, J., Inder, T., Neil, J., Dierker, D., Harwell, J., & Van Essen, D. (2010). Similar patterns of cortical expansion during human development and evolution. *Proc. Natl. Acad. Sci. U. S. A.*, *107*(29), 13135–13140.

Honey, C. J., Sporns, O., Cammoun, L., Gigandet, X., Thiran, J. P., Meuli, R., & Hagmann, P. (2009). Predicting human resting-state functional connectivity from structural connectivity. *Proc. Natl. Acad. Sci. U. S. A.*, *106*(6), 2035–2040.

Honey, C. J., Thesen, T., Donner, T. H., Silbert, L. J., Carlson, C. E., Devinsky, O., ... Hasson, U. (2012). Slow cortical dynamics and the accumulation of information over long timescales. *Neuron*, *76*(2), 423–434.

Hopf, A. (1956). Über die Verteilung myeloarchitektonischer Merkmale in der Stirnhirnrinde beim Menschen. *J. Hirnforsch.*, *2*(4), 311–333.

Hopf, A., & Vitzthum, H. G. (1957). Über die Verteilung myeloarchitektonischer Merkmale in der Scheitellappenrinde beim Menschen. *J. Hirnforsch.*, *3*(2/3), 83–104.

Huntenburg, J. M., Gorgolewski, K. J., Anwander, A., & Margulies, D. S. (2014). Evaluating nonlinear coregistration of BOLD EPI and T1 images. *Poster presented at the 20th Annual Meeting of the Organization for Human Brain Mapping, Hamburg, Germany*.

Huth, A. G., de Heer, W. A., Griffiths, T. L., Theunissen, F. E., & Gallant, J. L. (2016). Natural speech reveals the semantic maps that tile human cerebral cortex. *Nature*, *532*(7600), 453–458.

Jbabdi, S., Sotiropoulos, S. N., & Behrens, T. E. (2013). The topographic connectome. *Curr. Opin. Neurobiol.*, *23*(2), 207–215.

Kennedy, D. N., Haselgrove, C., Riehl, J., Preuss, N., & Buccigrossi, R. (2016). The NITRC image repository. *NeuroImage*, *124*(Part B), 1069–1073.

Knoblauch, K., Ercsey-Ravasz, M., Kennedy, H., & Toroczkai, Z. (2016). The brain in space. In H. Kennedy, D. C. Van Essen, & Y. Christen (Eds.), *Micro-, meso- and Macro-Connectomics of the brain.* Cham (CH): Springer.

Kok, P., Bains, L. J., van Mourik, T., Norris, D. G., & de Lange, F. P. (2016). Selective activation of the deep layers of the human primary visual cortex by Top-Down feedback. *Curr. Biol.*, *26*(3), 371–376.

Krienen, F. M., Yeo, B. T. T., Ge, T., Buckner, R. L., & Sherwood, C. C. (2016). Transcriptional profiles of supragranular-enriched genes associate with corticocortical network architecture in the human brain. *Proc. Natl. Acad. Sci. U. S. A.*, *113*(4), E469–78.

Lang, J., De Sterck, H., Kaiser, J. L., & C, M. J. (2017). Random spatial networks: Small worlds without clustering, traveling waves, and Hop-and-Spread disease dynamics. *arxiv.org*.

Langs, G., Sweet, A., Lashkari, D., Tie, Y., Rigolo, L., Golby, A. J., & Golland, P. (2014). Decoupling function and anatomy in atlases of functional connectivity patterns: language mapping in tumor patients. *Neuroimage*, *103*, 462–475.

Langs, G., Wang, D., Golland, P., Mueller, S., Pan, R., Sabuncu, M. R., ... Liu,

H. (2015). Identifying Shared Brain Networks in Individuals by Decoupling Functional and Anatomical Variability. *Cereb. Cortex*, 1–11.

Lerch, J. P., van der Kouwe, A. J. W., Raznahan, A., Paus, T., Johansen-Berg, H., Miller, K. L., ... Sotiropoulos, S. N. (2017). Studying neuroanatomy using MRI. *Nat. Neurosci.*, *20*(3), 314–326.

Lerner, Y., Honey, C. J., Silbert, L. J., & Hasson, U. (2011). Topographic mapping of a hierarchy of temporal receptive windows using a narrated story. *J. Neurosci.*, *31*(8), 2906–2915.

Leuze, C., Aswendt, M., Ferenczi, E., Liu, C. W., Hsueh, B., Goubran, M., ... McNab, J. A. (2017). The separate effects of lipids and proteins on brain MRI contrast revealed through tissue clearing. *Neuroimage*, *156*, 412–422.

Lombaert, H., Arcaro, M., & Ayache, N. (2015). Brain transfer: Spectral analysis of cortical surfaces and functional maps. *Inf. Process. Med. Imaging*, *24*, 474–487.

Lucas, B. C., Bogovic, J. A., Carass, A., Bazin, P.-L., Prince, J. L., Pham, D. L., & Landman, B. A. (2010). The Java Image Science Toolkit (JIST) for rapid prototyping and publishing of neuroimaging software. *Neuroinformatics*, *8*(1), 5–17.

Lutti, A., Dick, F., Sereno, M. I., & Weiskopf, N. (2014). Using high-resolution quantitative mapping of R1 as an index of cortical myelination. *Neuroimage*, *93 Pt 2*, 176–188.

Mackay, A., Whittall, K., Adler, J., Li, D., Paty, D., & Graeb, D. (1994). In Vivo Visualization of Myelin Water in Brain by Magnetic Resonance. *Magn. Reson. Med.*, *31*(10), 673–677.

Markov, N. T., Ercsey-Ravasz, M. M., Ribeiro Gomes, A. R., Lamy, C., Magrou, L., Vezoli, J., ... Kennedy, H. (2014). A weighted and directed interareal connectivity matrix for macaque cerebral cortex. *Cereb. Cortex*, *24*(1), 17–36.

Markov, N. T., Misery, P., Falchier, A., Lamy, C., Vezoli, J., Quilodran, R., ... Knoblauch, K. (2011). Weight consistency specifies regularities of macaque cor-

tical networks. *Cereb. Cortex*, *21*(6), 1254–1272.

Marques, J. P., Khabipova, D., & Gruetter, R. (2017). Studying cyto and myeloarchitecture of the human cortex at ultra-high field with quantitative imaging: R1, R2(*) and magnetic susceptibility. *Neuroimage*, *147*, 152–163.

Marques, J. P., Kober, T., Krueger, G., van der Zwaag, W., Van de Moortele, P.-F., & Gruetter, R. (2010). MP2RAGE, a self bias-field corrected sequence for improved segmentation and t1-mapping at high field. *Neuroimage*, *49*(2), 1271–1281.

Mason, M. F., Norton, M. I., Van Horn, J. D., Wegner, D. M., Grafton, S. T., & Macrae, C. N. (2007). Wandering minds: the default network and stimulus-independent thought. *Science*, *315*(5810), 393–395.

McAuliffe, M. J., Lalonde, F. M., McGarry, D., Gandler, W., Csaky, K., & Trus, B. L. (2001). Medical image processing, analysis and visualization in clinical research. In *Computer-Based medical systems, 2001. CBMS 2001. proceedings. 14th IEEE symposium on* (pp. 381–386).

Mesulam, M. M. (1998). From sensation to cognition. *Brain*, *121 Pt 6*, 1013–1052.

Mezer, A., Yeatman, J. D., Stikov, N., Kay, K. N., Cho, N.-J., Dougherty, R. F., ... Wandell, B. A. (2013). Quantifying the local tissue volume and composition in individual brains with magnetic resonance imaging. *Nat. Med.*, *19*(12), 1667–1672.

Miranda-Dominguez, O., Mills, B. D., Grayson, D., Woodall, A., Grant, K. A., Kroenke, C. D., & Fair, D. A. (2014). Bridging the gap between the human and macaque connectome: a quantitative comparison of global interspecies structure-function relationships and network topology. *J. Neurosci.*, *34*(16), 5552–5563.

Mitchell, J., Mount, D., & Papadimitriou, C. (1987). The discrete geodesic problem. *SIAM J. Comput.*, *16*(4), 647–668.

Moeller, S., Yacoub, E., Olman, C. A., Auerbach, E., Strupp, J., Harel, N., & Uğurbil, K. (2010). Multiband multislice GE-EPI at 7 tesla, with 16-fold acceleration using partial parallel imaging with application to high spatial and temporal whole-brain

fMRI. *Magn. Reson. Med.*, *63*(5), 1144–1153.

Muller, E., Bednar, J. A., Diesmann, M., Gewaltig, M.-O., Hines, M., & Davison, A. P. (2015). Python in neuroscience. *Front. Neuroinform.*, *9*, 11.

Murray, J. D., Bernacchia, A., Freedman, D. J., Romo, R., Wallis, J. D., Cai, X., ... Wang, X.-J. (2014). A hierarchy of intrinsic timescales across primate cortex. *Nat. Neurosci.*, *17*(12), 1661–1663.

Nauta, W. J. H. (1964). Some efferent connection of the prefrontal cortex in the monkey. In J. M. Warren & A. K (Eds.), *The frontal granular cortex and behaviour* (pp. 397–409). New York: McGraw Hill.

Nieuwenhuys, R. (2013). The myeloarchitectonic studies on the human cerebral cortex of the Vogt-Vogt school, and their significance for the interpretation of functional neuroimaging data. *Brain Struct. Funct.*, *218*(2), 303–352.

Nieuwenhuys, R., & Puelles, L. (2015). *Towards a new neuromorphology*. Springer.

Pandya, D. N., & Sanides, F. (1973). Architectonic parcellation of the temporal operculum in rhesus monkey and its projection pattern. *Z. Anat. Entwicklungsgesch.*, *139*(2), 127–161.

Pandya, D. N., Seltzer, B., Petrides, M., & Cipolloni, P. B. (2015). *Cerebral cortex: Architecture, connections, and the dual origin concept*. Oxford University Press.

Pandya, D. N., & Yeterian, E. H. (1985). Architecture and connections of cortical association areas. In A. Peters & E. G. Jones (Eds.), *Association and auditory cortices* (Vol. 4, pp. 3–61). Boston (MA): Springer US.

Pandya, D. N., & Yeterian, E. H. (1990). Prefrontal cortex in relation to other cortical areas in rhesus monkey: architecture and connections. *Prog. Brain Res.*, *85*, 63–94.

Paus, T. (2017). Imaging microstructure in the living human brain: A viewpoint. *Neuroimage*.

Paus, T., & Toro, R. (2009). Could sex differences in white matter be explained by g ratio? *Front. Neuroanat.*, *3*, 14.

Pedregosa, F., Varoquaux, G., Gramfort, A., Michel, V., Thirion, B., Grisel, O., ... Duchesnay, E. (2011). Scikit-learn: Machine learning in Python. *J. Mach. Learn. Res.*, *12*, 2825–2830.

Pohmann, R., Speck, O., Scheffler Magnetic resonance in, K., & 2016. (2016). Signal-to-noise ratio and MR tissue parameters in human brain imaging at 3, 7, and 9.4 tesla using current receive coil arrays. *Wiley Online Library*.

Power, J. D., Cohen, A. L., Nelson, S. M., Wig, G. S., Barnes, K. A., Church, J. A., ... Petersen, S. E. (2011). Functional network organization of the human brain. *Neuron*, *72*(4), 665–678.

Raichle, M. E. (2015). The brain's default mode network. *Annu. Rev. Neurosci.*, *38*, 433–447.

Rakic, P. (2002). Neurogenesis in adult primate neocortex: an evaluation of the evidence. *Nat. Rev. Neurosci.*, *3*(1), 65–71.

Ramachandran, P., & Varoquaux, G. (2011). Mayavi: 3D visualization of scientific data. *Computing in Science Engineering*, *13*(2), 40–51.

Rowley, C. D., Bazin, P.-L., Tardif, C. L., Sehmbi, M., Hashim, E., Zaharieva, N., ... Bock, N. A. (2015). Assessing intracortical myelin in the living human brain using myelinated cortical thickness. *Front. Neurosci.*, *9*, 396.

Rushworth, M. F. S., Noonan, M. P., Boorman, E. D., Walton, M. E., & Behrens, T. E. (2011). Frontal cortex and reward-guided learning and decision-making. *Neuron*, *70*(6), 1054–1069.

Saadon-Grosman, N., Tal, Z., Itshayek, E., Amedi, A., & Arzy, S. (2015). Discontinuity of cortical gradients reflects sensory impairment. *Proc. Natl. Acad. Sci. U. S. A.*, *112*(52), 16024–16029.

Sánchez-Panchuelo, R. M., Francis, S. T., Schluppeck, D., & Bowtell, R. W. (2012). Correspondence of human visual areas identified using functional and anatomical MRI in vivo at 7 T. *J. Magn. Reson. Imaging*, *35*(2), 287–299.

Sanides, F. (1962). *Die architektonik des menschlichen stirnhirns*. Springer.

Sanides, F. (1969). Comparative architectonics of the neocortex of mammals and their evolutionary interpretation. *Ann. N. Y. Acad. Sci.*, *167*(1), 404–423.

Sanides, F. (1972). Representation in the cerebral cortex and its areal lamination patterns. *The Structure and Function of Nervous Tissue*, *5*, 329–453.

Schacter, D. L., & Addis, D. R. (2007). The cognitive neuroscience of constructive memory: remembering the past and imagining the future. *Philos. Trans. R. Soc. Lond. B Biol. Sci.*, *362*(1481), 773–786.

Scholtens, L. H., Schmidt, R., de Reus, M. A., & van den Heuvel, M. P. (2014). Linking macroscale graph analytical organization to microscale neuroarchitectonics in the macaque connectome. *J. Neurosci.*, *34*(36), 12192–12205.

Schüz, A., & Braitenberg, V. (2002). The human cortical white matter: quantitative aspects of cortico-cortical long-range connectivity. *Cortical areas: Unity and diversity*, 377–385.

Sepulcre, J., Liu, H., Talukdar, T., Martincorena, I., Yeo, B. T. T., & Buckner, R. L. (2010). The Organization of Local and Distant Functional Connectivity in the Human Brain. *PLoS Comput. Biol.*, *6*(6), e1000808.

Sepulcre, J., Sabuncu, M. R., Yeo, T. B., Liu, H., & Johnson, K. A. (2012). Stepwise connectivity of the modal cortex reveals the multimodal organization of the human brain. *J. Neurosci.*, *32*(31), 10649–10661.

Sereno, M. I., Lutti, A., Weiskopf, N., & Dick, F. (2013). Mapping the human cortical surface by combining quantitative T1 with retinotopy. *Cereb. Cortex*, *23*(9), 2261–2268.

Shehzad, Z., Kelly, A. M. C., Reiss, P. T., Gee, D. G., Gotimer, K., Uddin, L. Q., ... Milham, M. P. (2009). The resting brain: unconstrained yet reliable. *Cereb. Cortex*, *19*(10), 2209–2229.

Sigalovsky, I. S., Fischl, B., & Melcher, J. R. (2006). Mapping an intrinsic MR property of gray matter in auditory cortex of living humans: A possible marker for primary cortex and hemispheric differences. *Neuroimage*, *32*(4), 1524–1537.

Skudlarski, P., Jagannathan, K., Calhoun, V. D., Hampson, M., Skudlarska, B. A., & Pearlson, G. (2008). Measuring brain connectivity: diffusion tensor imaging validates resting state temporal correlations. *Neuroimage*, *43*(3), 554–561.

Smith, S. M., Fox, P. T., Miller, K. L., Glahn, D. C., Fox, P. M., Mackay, C. E., ... Beckmann, C. F. (2009). Correspondence of the brain's functional architecture during activation and rest. *Proc. Natl. Acad. Sci. U. S. A.*, *106*(31), 13040–13045.

Spreng, R. N., & Grady, C. L. (2010). Patterns of brain activity supporting autobiographical memory, prospection, and theory of mind, and their relationship to the default mode network. *J. Cogn. Neurosci.*, *22*(6), 1112–1123.

Stephan, K. E., Kamper, L., Bozkurt, A., Burns, G. A., Young, M. P., & Kötter, R. (2001). Advanced database methodology for the collation of connectivity data on the macaque brain (CoCoMac). *Philos. Trans. R. Soc. Lond. B Biol. Sci.*, *356*(1412), 1159–1186.

Stephens, G. J., Honey, C. J., & Hasson, U. (2013). A place for time: the spatiotemporal structure of neural dynamics during natural audition. *J. Neurophysiol.*, *110*(9), 2019–2026.

Stüber, C., Morawski, M., Schäfer, A., Labadie, C., Wähnert, M., Leuze, C., ... Turner, R. (2014). Myelin and iron concentration in the human brain: a quantitative study of MRI contrast. *Neuroimage*, *93 Pt 1*, 95–106.

Tardif, C. L., Schäfer, A., Trampel, R., Villringer, A., Turner, R., & Bazin, P.-L. (2016). Open Science CBS Neuroimaging Repository: Sharing ultra-high-field MR images of the brain. *Neuroimage*, *124*, 1143–1148.

Tardif, C. L., Schäfer, A., Waehnert, M., Dinse, J., Turner, R., & Bazin, P.-L. (2015). Multi-contrast multi-scale surface registration for improved alignment of cortical areas. *Neuroimage*, *111*, 107–122.

Tavor, I., Parker Jones, O., Mars, R. B., Smith, S. M., Behrens, T. E., & Jbabdi, S. (2016). Task-free MRI predicts individual differences in brain activity during task performance. *Science*, *352*(6282), 216–220.

Taylor, P., Hobbs, J. N., Burroni, J., & Siegelmann, H. T. (2015). The global landscape of cognition: hierarchical aggregation as an organizational principle of human cortical networks and functions. *Sci. Rep.*, *5*, 18112.

Todorich, B., Pasquini, J. M., Garcia, C. I., Paez, P. M., & Connor, J. R. (2009). Oligodendrocytes and myelination: the role of iron. *Glia*, *57*(5), 467–478.

Trampel, R., Bazin, P.-L., Pine, K., & Weiskopf, N. (2017). In-vivo magnetic resonance imaging (MRI) of laminae in the human cortex. *Neuroimage*.

Turner, R. (2013). Where matters: New approaches to brain analysis. In S. Geyer & R. Turner (Eds.), *Microstructural parcellation of the human cerebral cortex* (pp. 179–196). Berlin, Heidelberg: Springer Berlin Heidelberg.

Turner, R. (2015). Myelin imaging. In *Brain mapping* (pp. 137–142).

Turner, R., Oros-Peusquens, A.-M., Romanzetti, S., Zilles, K., & Shah, N. J. (2008). Optimised in vivo visualisation of cortical structures in the human brain at 3 T using IR-TSE. *Magn. Reson. Imaging*, *26*(7), 935–942.

Uğurbil, K., Xu, J., Auerbach, E. J., Moeller, S., Vu, A. T., Duarte-Carvajalino, J. M., ... WU-Minn HCP Consortium (2013). Pushing spatial and temporal resolution for functional and diffusion MRI in the human connectome project. *Neuroimage*, *80*, 80–104.

van den Heuvel, M. P., Scholtens, L. H., de Reus, M. A., & Kahn, R. S. (2016). Associated microscale spine density and macroscale connectivity disruptions in schizophrenia. *Biol. Psychiatry*, *80*(4), 293–301.

van den Heuvel, M. P., Scholtens, L. H., Feldman Barrett, L., Hilgetag, C. C., & de Reus, M. A. (2015). Bridging Cytoarchitectonics and Connectomics in Human Cerebral Cortex. *J. Neurosci.*, *35*(41), 13943–13948.

van den Heuvel, M. P., & Sporns, O. (2013). Network hubs in the human brain. *Trends Cogn. Sci.*, *17*(12), 683–696.

van der Zwaag, W., Schäfer, A., Marques, J. P., Turner, R., & Trampel, R. (2016). Recent applications of UHF-MRI in the study of human brain function and struc-

ture: a review: UHF MRI: Applications to Human Brain Function and Structure. *NMR in Biomedicine*, *29*(9), 1274–1288.

Van Essen, D. C., Smith, S. M., Barch, D. M., Behrens, T. E. J., Yacoub, E., Ugurbil, K., & WU-Minn HCP Consortium. (2013). The WU-Minn human connectome project: an overview. *Neuroimage*, *80*, 62–79.

Vincent, J. L., Patel, G. H., Fox, M. D., Snyder, A. Z., Baker, J. T., Van Essen, D. C., ... Raichle, M. E. (2007). Intrinsic functional architecture in the anaesthetized monkey brain. *Nature*, *447*(7140), 83–86.

Vogt, C., & Vogt, O. (1919). Allgemeinere Ergebnisse unserer Hirnforschung. *J Psychol Neurol*, *25*, 279–468.

von Economo, C., & Koskinas, G. N. (1925). *Die cytoarchitektonik der hirnrinde des erwachsenen menschen*. Wien (Austria): Springer.

Waehnert, M. D., Dinse, J., Schäfer, A., Geyer, S., Bazin, P.-L., Turner, R., & Tardif, C. L. (2016). A subject-specific framework for in vivo myeloarchitectonic analysis using high resolution quantitative MRI. *Neuroimage*, *125*, 94–107.

Waehnert, M. D., Dinse, J., Weiss, M., Streicher, M. N., Waehnert, P., Geyer, S., ... Bazin, P.-L. (2014). Anatomically motivated modeling of cortical laminae. *Neuroimage*, *93 Pt 2*, 210–220.

Wagstyl, K., Ronan, L., Goodyer, I. M., & Fletcher, P. C. (2015). Cortical thickness gradients in structural hierarchies. *Neuroimage*, *111*, 241–250.

Watts, D. J., & Strogatz, S. H. (1998). Collective dynamics of 'small-world' networks. *Nature*, *393*(6684), 440–442.

Weiskopf, N., Mohammadi, S., Lutti, A., & Callaghan, M. F. (2015). Advances in MRI-based computational neuroanatomy: from morphometry to in-vivo histology. *Curr. Opin. Neurol.*, *28*(4), 313–322.

Whitaker, K. J., Vértes, P. E., Romero-Garcia, R., Váša, F., Moutoussis, M., Prabhu, G., ... Bullmore, E. T. (2016). Adolescence is associated with genomically patterned consolidation of the hubs of the human brain connectome. *Proc. Natl.*

Acad. Sci. U. S. A., *113*(32), 9105–9110.

Winkler, A. M., Sabuncu, M. R., Yeo, B. T. T., Fischl, B., Greve, D. N., Kochunov, P., ... Glahn, D. C. (2012). Measuring and comparing brain cortical surface area and other areal quantities. *Neuroimage*, *61*(4), 1428–1443.

Workman, A. D., Charvet, C. J., Clancy, B., Darlington, R. B., & Finlay, B. L. (2013). Modeling transformations of neurodevelopmental sequences across mammalian species. *J. Neurosci.*, *33*(17), 7368–7383.

Yarkoni, T., Poldrack, R. A., Nichols, T. E., Van Essen, D. C., & Wager, T. D. (2011). Large-scale automated synthesis of human functional neuroimaging data. *Nat. Methods*, *8*(8), 665–670.

Yeo, B. T. T., Krienen, F. M., Sepulcre, J., Sabuncu, M. R., Lashkari, D., Hollinshead, M., ... Buckner, R. L. (2011). The organization of the human cerebral cortex estimated by intrinsic functional connectivity. *J. Neurophysiol.*, *106*(3), 1125–1165.

Yeshurun, Y., Nguyen, M., & Hasson, U. (2017). The butterfly effect: amplification of local changes along the temporal processing hierarchy. *bioRxiv*.

Zaretskaya, N., Fischl, B., Reuter, M., Renvall, V., & Polimeni, J. R. (2017). Advantages of cortical surface reconstruction using submillimeter 7 T MEMPRAGE. *Neuroimage*, *165*, 11–26.

Appendices

Appendix A

Statement of authorship

I hereby declare that this dissertation has been composed by me and is based on my own work. Where I have consulted the work of others, this is always clearly attributed.

Hiermit erkläre ich, dass ich vorliegende Arbeit selbständig verfasst und keine anderen als die angegebenen Quellen und Hilfsmittel benutzt habe. Ideen und Gedanken aus Arbeiten anderer sind eindeutig gekennzeichnet.

_____ _____

Date Signature

Appendix B

Contribution to publications

Erklärung gemäß 7 Abs. 3 der Promotionsordnung über den Eigenanteil an den veröffentlichten oder zur Veröffentlichung vorgesehenen eingereichten wissenschaftlichen Schriften im Rahmen meiner publikationsbasierten Arbeit.

I. Person

Name:	Huntenburg
Vorname:	Julia M
Institut:	Neurocomputation and Neuroimaging
Promotionsfach:	Psychologie
Titel:	M.Sc.

II. Nummerierte Aufstellung der eingereichten Schriften

1. Huntenburg, J.M., Wagstyl, K., Steele, C.J., Funck, T., Bethlehem, R.A.I., Foubet, O., Larrat, B., Borrell, V. & Bazin, P.-L. (2017). Laminar Python: tools for cortical depth-resolved analysis of high-resolution brain imaging data in Python. *Research Ideas and Outcomes, 3*(e12346).
2. Huntenburg, J.M., Steele & Bazin, P.-L. (in preparation, October 2017). Nighres – processing tools for high-resolution neuroimaging. *Gigascience*.
3. Huntenburg, J.M., Abraham, A., Loula, J., Liem, F., Dadi, K. & Varoquaux, G. (2017). Loading and plotting of cortical surface representations in Nilearn.

Research Ideas and Outcomes, 3(e12342).

4. Margulies, D.S., Falkiewicz, M. & Huntenburg, J.M. (2016). A cortical surface-based geodesic distance package for Python. *GigaScience, 5*(1), 1920.
5. Mendes, N., Oligschlaeger, S., Lauckner, M. E., Golchert, J., Huntenburg, J. M., Falkiewicz, M., ... Margulies, D. S. (under review, October 2017). A functional connectome phenotyping dataset including cognitive state and personality measures. *Scientific Data*.
6. Huntenburg, J.M., Bazin, P.-L., Goulas, A., Tardif, C.L., Villringer, A., Margulies, D.S. (2017). A systematic relationship between functional connectivity and intracortical myelin in the human cerebral cortex. *Cerebral Cortex, 27*(2), 981-997.
7. Oligschlaeger, S., Huntenburg, J.M., Golchert, J., Lauckner, M.E., Bonnen, T., Margulies, D.S. (2016). Gradients of connectivity distance are anchored in primary cortex. *Brain Structure and Function (222)*(5).
8. Margulies, D.S., Ghosh, S.S., Goulas, A., Falkiewicz, M., Huntenburg, J.M., Langs, G., Bezgin, G., Eickhoff, S.B., Castellanos, F.X., Petrides, M., Jefferies, E., Smallwood, J. (2016). Situating the default-mode network along a principal gradient of macroscale cortical organization. *Proceedings of the National Academy of Sciences USA, 113*(44), 12574-12579.
9. Huntenburg, J.M., Bazin, P.-L., Margulies, D.S. (accepted, October 2017). Large-scale gradients in human cortical organization. *Trends in Cognitive Sciences*.

III. Darlegung des eigenen Anteils an diesen Schriften

Die Bewertung des Eigenanteils richtet sich nach der Skala: vollständig überwiegend mehrheitlich in Teilen und enthält nur für den jeweiligen Artikel relevante Arbeitsbereiche.

1. Konzeption (überwiegend), Methodenentwicklung (überwiegend), Programmierung

(vollständig), Ergebnisdiskussion (vollständig), Erstellen des Manuskriptes (überwiegend)

2. Konzeption (überwiegend), Methodenentwicklung (überwiegend), Programmierung (vollständig), Ergebnisdiskussion (vollständig), Erstellen des Manuskriptes (überwiegend)
3. Konzeption (überwiegend), Methodenentwicklung (überwiegend), Programmierung (überwiegend), Ergebnisdiskussion (vollständig), Erstellen des Manuskriptes (überwiegend)
4. Konzeption (in Teilen), Methodenentwicklung (in Teilen), Programmierung (in Teilen), Ergebnisdiskussion (in Teilen), Erstellen des Manuskriptes (in Teilen)
5. Konzeption (in Teilen), Versuchsdesign (in Teilen), Programmierung (überwiegend), Datenauswertung (überwiegend), Erstellen des Manuskriptes (in Teilen)
6. Konzeption (überwiegend), Literaturrecherche (vollständig), Methodenentwicklung (überwiegend), Programmierung (vollständig), Datenauswertung (vollständig), Ergebnisdiskussion (vollständig), Erstellen des Manuskriptes (überwiegend)
7. Konzeption (in Teilen), Methodenentwicklung (in Teilen), Programmierung (mehrheitlich), Datenauswertung (mehrheitlich), Ergebnisdiskussion (mehrheitlich), Erstellen des Manuskriptes (in Teilen)
8. Konzeption (in Teilen), Methodenentwicklung (in Teilen), Programmierung (in Teilen), Datenauswertung (in Teilen), Ergebnisdiskussion (mehrheitlich), Erstellen des Manuskriptes (in Teilen)
9. Konzeption (überwiegend), Literaturrecherche (vollständig), Erstellen des Manuskriptes (überwiegend)

_____ _____

Date Signature

Appendix C

Original publications

Laminar Python: tools for cortical depth-resolved analysis of high-resolution brain imaging data in Python

Huntenburg, J.M., Wagstyl, K., Steele, C.J., Funck, T., Bethlehem, R.A.I., Foubet, O., Larrat, B., Borrell, V. & Bazin, P.-L. (2017). Research Ideas and Outcomes, 3 (e12346). http://dx.doi.org/10.3897/rio.3.e12346

Research Ideas and Outcomes 3: e12346
doi: 10.3897/rio.3.e12346

Project Report

Laminar Python: tools for cortical depth-resolved analysis of high-resolution brain imaging data in Python

Julia M Huntenburg[‡,§], Konrad Wagstyl[|,¶], Christopher J Steele[‡,#], Thomas Funck[¶], Richard A.I. Bethlehem[|], Ophélie Foubet[¤], Benoit Larrat[«], Victor Borrell[»], Pierre-Louis Bazin[‡]

‡ Max Planck Institute for Human Cognitive and Brain Sciences, Leipzig, Germany
§ Free University Berlin, Berlin, Germany
| University of Cambridge, Cambridge, United Kingdom
¶ Montreal Neurological Institute, Montreal, Canada
# Douglas Mental Health University Institute of McGill University, Montreal, Canada
¤ Institut Pasteur, Paris, France
« Institut d'Imagerie Biomédicale, CEA, Paris, France
» Instituto de Neurociencias de Alicante, Alicante, Spain

Corresponding author: Julia M Huntenburg (ju.huntenburg@gmail.com)

Reviewed v1

Received: 20 Feb 2017 | Published: 23 Feb 2017

Citation: Huntenburg J, Wagstyl K, Steele C, Funck T, Bethlehem R, Foubet O, Larrat B, Borrell V, Bazin P (2017) Laminar Python: tools for cortical depth-resolved analysis of high-resolution brain imaging data in Python. Research Ideas and Outcomes 3: e12346. https://doi.org/10.3897/rio.3.e12346

Abstract

Increasingly available high-resolution brain imaging data require specialized processing tools that can leverage their anatomical detail and handle their size. Here, we present user-friendly Python tools for cortical depth resolved analysis in such data. Our implementation is based on the CBS High-Res Brain Processing framework, and aims to make high-resolution data processing tools available to the broader community.

Keywords

laminar analysis, high-resolution MRI

Introduction

Recent advances in ultra-high field and quantitative MRI facilitate non-invasive imaging of the whole brain at an unprecedented level of detail (Weiskopf et al. 2015). Standard neuroimaging software is not optimised for processing such images. Thus, there is a growing demand for dedicated tools that can take advantage of the additional information provided by the new data, and scale well with their increasing size. CBS High-Res Brain Processing Tools (CBSTools, Bazin et al. 2014) is a suite of software tools for processing MR images at submillimeter resolution. CBSTools have been developed in Java as a set of plugins for the MIPAV software package and the JIST pipeline environment (https://www.nitrc.org/projects/cbs-tools/).

In this project, we made a subset of CBSTools modules available in Python (https://github.com/juhuntenburg/laminar_python, Huntenburg 2017). The standalone package no longer requires installation of MIPAV and JIST, and allows for interactive data exploration at each processing stage. The Python interfaces also enable easy integration with other popular Python-based neuroimaging software tools such as Nibabel (Brett et al. 2016), Nipype (Gorgolewski et al. 2011) and Nilearn (Abraham et al. 2014). We focused on a set of modules that enable the analysis of multiple horizontal laminae within the cortical sheet (Waehnert et al. 2016). The package implements an equivolumetric approach for generating intracortical laminae (Waehnert et al. 2014), which accounts for the dependence of layer thickness on cortical folding (Bok 1929).

Approach

Our aim was to provide user-friendly Python interfaces to the CBSTools modules and make these available in a platform independent manner with minimal dependencies. We used the JCC package (http://lucene.apache.org/pylucene/jcc/index.html) to encapsulate the original Java classes. We then implemented a set of Python wrapper functions which convert the input data to Java data structures, initiate a Java virtual machine, call the main Java class with the specified parameters, collect, convert and return the output data.

Input and output data can either be passed as files or specific Python data structures. We chose to represent volumetric data as Nibabel SpatialImages (http://nipy.org/nibabel/reference/nibabel.spatialimages.html), in particular Nifti1Images. These standardized objects simplify data exchange with other software tools. Finding a solution to represent surface data proved to be more difficult, since neither a community standard, nor a suitable precedent solution in other Python tools exists. Here, we decided to represent a surface mesh as a dictionary with the entries *coords*, an array containing the coordinates of the mesh vertices, and *faces*, an array containing the vertex indices of the mesh faces.

Functions for loading and saving of volumetric and surface mesh data in various file formats (currently nifti, gifti, ply, vtk, obj and Freesurfer formats) can be called directly by the user, but are also employed by the main processing functions. The loading functions

automatically determine the input type: supported file formats are loaded and Python data structures are tested for compliance with the expected pattern. This approach is inspired by the input and output management in Nilearn. It makes it easy for the user to call the main functions directly on their data files, without further specifications. At the same time, it is flexible to accommodate non-standard data formats, which the user can load into the appropriate Python data structure with custom scripts.

Results

The set of functions implemented in this package enables sampling of a given intensity image on multiple intracortical laminae, starting from a simple tissue classification. We illustrated their usage in an example workflow (https://github.com/juhuntenburg/laminar_python/blob/master/examples/laminar_python_demo.ipynb). Here, the initial inputs are two binary images demarcating the inner and outer boundary of the cortical grey matter of a ferret (*Mustela putorius furo)* brain (Fig. 1a). Both images are converted into levelset representations using the *create_levelsets* function (Fig. 1b). The levelsets are passed to the *layering* function, which subdivides the intracortical space between the two boundaries in equivolumetric laminae. This function outputs three images: a continuous (Fig. 1c) and a discrete (Fig. 1d) representation of equivolumetric intracortical depth, and levelset representations of each of the intracortical surfaces. In the example, the latter output is passed to the *profile_sampling* function, together with an aligned T2 contrast image. T2 values are then sampled at different cortical depths (Fig. 1e). Importantly, the equivolumetric laminae do not represent architectonic layers, but provide an anatomically meaningful coordinate system of cortical depth.

The example data is taken from a 7 Tesla MR scan of an adult ferret (voxel size = 120 µm isotropic). With no additional manipulation, the package was readily applied to the animal data, testifying that it can also be used for cross-species analysis. Nilearn plotting functions were used for visualization, demonstrating the straightforward integration between the two packages.

Limitations and future directions

The current stage of the project faces several limitations, which might be overcome in future work. First, we focused on a subset of CBSTools modules. A more complete migration of CBSTools functionality to Python is a logical next step. Second, platform independence has not yet been achieved and requires pre-compilation of the JCC wrappers on different platforms. Third, atlases, lookup tables and example data are currently located within the GitHub repository. Better solutions for providing these files and other relevant datasets to the user should be found in the long term. Fourth, while our approach ensures general compatibility with other Python-based neuroimaging software, we aim for a closer integration, for instance by providing Nipype interfaces. Fifth, CBSTools are mainly used for processing MRI data, but are generally applicable to other types, such

as histological data. It would be interesting to expand usability to different data types and provide respective examples.

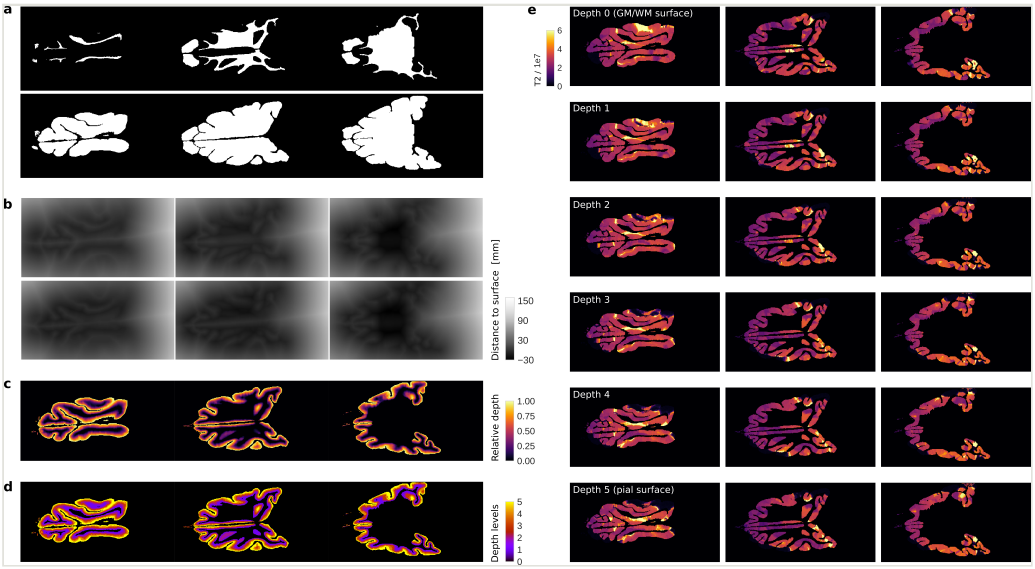

Figure 1.

Laminar python pipeline, demonstrated using high-resolution MR data of a ferret brain. a) Binary images demarcating inner (grey-white matter interface, top) and outer (pial surface, bottom) boundaries of the cortex. b) Levelset representations of the same surfaces, where positive values are assigned to voxels outside of the volume deliminated by the surface, and negative values to voxels inside, each increasing in value with euclidean distance from the surface. c) Continuous equivolumetric intracortical depth, which models the positions of laminae relative to cortical morphology. d) Discrete representations of equivolumetric depth levels. e) T2 values, sampled at the six equivolumetric intracortical depths. Note that the equivolumetric laminae do not represent architectonic layers, but provide an anatomically meaningful coordinate system of cortical depth.

Conclusion

We encapsulated a subset of CBSTools in Python and implemented user-friendly interfaces for the laminar analysis of high-resolution MR images. This is a first step to making high-resolution data processing tools available to the broader community, which also aims to encourage other scientists to contribute with their own code.

Acknowledgements

This work was completed during OHBM Hackathon Lausanne 2016 and Brainhack Anatomy Paris 2016.

Author contributions

JMH and PLB conceived the project. JMH, KW, CJS, TF and PLB contributed to the code. RAIB and OF tested the code and gave feedback for revision. JMH wrote the initial draft of the manuscript. KW, CJS, TF, RB, OF and PLB revised the manuscript. OF, BL and VB provided the example data.

Conflicts of interest

None declared.

References

- Abraham A, Pedregosa F, Eickenberg M, Gervais P, Mueller A, Kossaifi J, Gramfort A, Thirion B, Varoquaux G (2014) Machine learning for neuroimaging with scikit-learn. Frontiers in Neuroinformatics 8 https://doi.org/10.3389/fninf.2014.00014
- Bazin P, Weiss M, Dinse J, Schäfer A, Trampel R, Turner R (2014) A computational framework for ultra-high resolution cortical segmentation at 7Tesla. NeuroImage 93: 201-209. https://doi.org/10.1016/j.neuroimage.2013.03.077
- Bok ST (1929) Der Einfluss der in den Furchen und Windungen auftretenden Kruemmungen der Grosshirnrinde auf die Rindenarchitektur. Zeitschrift für die gesamte Neurologie und Psychiatrie 12: 682-750. https://doi.org/10.1007/bf02864437
- Brett M, Hanke M, Cipollini B, Côté M, Markiewicz C, Gerhard S, Larson E, Lee G, Halchenko Y, Kastman E, cindeem, Morency F, moloney, Millman J, Rokem A, jaeilepp, Gramfort A, den Bosch JFv, Subramaniam K, Nichols N, embaker, bpinsard, chaselgrove, Oosterhof N, St-Jean S, Amirbekian B, Nimmo-Smith I, Ghosh S, Varoquaux G, Garyfallidis E (2016) nibabel: 2.1.0. Zenodo https://doi.org/10.5281/ZENODO.60808
- Gorgolewski K, Burns C, Madison C, Clark D, Halchenko Y, Waskom M, Ghosh S (2011) Nipype: A Flexible, Lightweight and Extensible Neuroimaging Data Processing Framework in Python. Frontiers in Neuroinformatics 5 https://doi.org/10.3389/fninf.2011.00013
- Huntenburg J (2017) juhuntenburg/laminar_python: initial release. v1.0. Zenodo. Release date: 2017 2 02. URL: http://doi.org/10.5281/zenodo.268021
- Waehnert M, Dinse J, Schäfer A, Geyer S, Bazin P, Turner R, Tardif CL (2016) A subject-specific framework for in vivo myeloarchitectonic analysis using high resolution quantitative MRI. NeuroImage 125: 94-107. https://doi.org/10.1016/j.neuroimage.2015.10.001
- Waehnert MD, Dinse J, Weiss M, Streicher MN, Waehnert P, Geyer S, Turner R, Bazin P- (2014) Anatomically motivated modeling of cortical laminae. NeuroImage 93: 210-220. https://doi.org/10.1016/j.neuroimage.2013.03.078
- Weiskopf N, Mohammadi S, Lutti A, Callaghan M (2015) Advances in MRI-based computational neuroanatomy. Current Opinion in Neurology 28 (4): 313-322. https://doi.org/10.1097/wco.0000000000000222

Nighres: processing tools for high-resolution neuroimaging

Huntenburg, J.M., Steele & Bazin, P.-L. (under review). GigaScience.

GigaScience, 2017, 1–7

doi: xx.xxxx/xxxx
Manuscript in Preparation
Technical Note

TECHNICAL NOTE

Nighres: Processing tools for high-resolution neuroimaging

Julia M Huntenburg[1,2,*], Christopher J Steele[3,4,†] and Pierre-Louis Bazin[3,5,6,7,†]

[1]Max Planck Research Group for Neuroanatomy & Connectivity, Max Planck Institute for Human Cognitive and Brain Sciences, Leipzig, Germany and [2]Neurocomputation and Neuroimaging Unit, Department of Education and Psychology, Free University of Berlin, Berlin, Germany and [3]Department of Neurology, Max Planck Institute for Human Cognitive and Brain Sciences, Germany and [4]Cerebral Imaging Center, Douglas Mental Health University Institute, Montreal, QC, Canada and [5]Department of Neurophysics, Max Planck Institute for Human Cognitive and Brain Sciences, Leipzig, Germany and [6]Social Brain Lab, Netherlands Institute for Neuroscience, Amsterdam, Netherlands and [7]Spinoza Centre for Neuroimaging, Amsterdam, Netherlands

[*]Correspondance: huntenburg@cbs.mpg.de
[†]Contributed equally

Abstract

With recent improvements in magnetic resonance imaging (MRI) at ultra-high fields, the amount of data collected per subject in a given MRI experiment has increased considerably. Standard image processing packages are often challenged by the size of these data and dedicated methods are needed to leverage their extraordinary spatial resolution. Here we introduce a flexible Python toolbox which implements a set of advanced techniques for high-resolution neuroimaging. With these tools, segmentation and laminar analysis of cortical MRI data can be performed at resolutions up to 500 μm in reasonable times. Comprehensive online documentation makes the toolbox easy to use and install. An extensive developer's guide encourages contributions of other researchers that will help to accelerate progress in the promising field of high-resolution neuroimaging.

Key words: Neuroimaging in Python; High-resolution MRI; Ultra-high field MRI; Laminar MRI; Python Java integration

Background

Advances in ultra-high field (7 Tesla and above) MRI now make it possible to image the whole brain at an unprecedented level of detail [1]. Submillimeter resolutions and quantitative metrics reveal fine-grained variations in structure and function that were previously undetectable in vivo, and allow researchers to ask new questions about the human brain. Examples include the investigation of intracortical myelin [e.g 2, 3, 4, 5], the laminar organization of the cortical sheet [e.g. 6, 7, 8, 9, 10], feedforward and feedback patterns in cortical connections [11, 12, 13] and the detailed description of small cortical and subcortical structures [14, 15] and their function [16].

While ultra-high field scanners have become increasingly available and the first open 7 Tesla MRI data sets have been released [17, 18, 19], software tools still lag behind. Standard neuroimaging software packages are often not designed to handle the growing data size and new quantitative contrasts. Three-dimensional MRI data grows as a cube of its resolution, and computational complexity generally ranges between

Compiled on: December 20, 2017.
Draft manuscript prepared by the author.

Key Points

- A toolbox dedicated to the processing of high-resolution MRI data
- Lightweight and flexible code written in Python for ease of use, expansion and integration with other tools
- Extensive documentation with developer's guide and usage examples based on open data

$O(N \log N)$ and $O(N^2)$. Therefore, a change in spatial resolution from 1 mm to 0.5 mm easily entails an increase in computational requirements by a factor of 15 to 60, depending on the methods used. Moreover, many new applications, such as laminar analysis, have only become possible with higher resolutions and are not implemented in existing software packages.

CBS High-Res Brain Processing Tools (CBS Tools) is a software suite which addresses this gap by providing cutting-edge methods for efficient processing of MR images at submillimeter resolution [20]. For example, CBS Tools implements routine cortical segmentation at resolutions as high as 400 μm, processing of quantitative MRI sequences such as MP2RAGE, MPM or QSM [20], laminar analysis [7], and small vessel segmentation [21]. While this software has been well-received as a key tool set for quantitative and high-resolution neuroimaging, its adoption has been slowed by the complex infrastructure it builds on. CBS Tools have been developed in Java as a set of plugins for the MIPAV software package [22] and the JIST pipeline environment [23]. The MIPAV / JIST framework provides a graphical interface for building analysis pipelines and implements many convenient tools, but it comes with a complex installation procedure, heavy dependencies, and limited documentation. More importantly, it is difficult to integrate with other popular neuroimaging tools, limiting its software ecosystem.

Meanwhile, a range of versatile, interoperable open source packages for the analysis of neuroscientific data has been developed using the increasingly popular programming language Python [24]. For example, Nipy[1] is a community of practice devoted to the use of Python in the analysis of neuroimaging data, encompassing popular tools such as Nibabel [25], Nipype [26], Nilearn [27] and many others.

Here we present Nighres[2] – a new toolbox that makes the quantitative and high-resolution image processing capabilities of CBS Tools available in Python. Nighres is a user-friendly Python package which interfaces with CBS Tools while avoiding the JIST and MIPAV dependency tree. It facilitates integration with other Python-based neuroimaging tools and interactive data exploration, for example in Jupyter notebooks[3]. Nighres features comprehensive online documentation with usage examples that are based on publicly available data sets. An extensive developer's guide encourages external contributions in Java or Python. With this new package, we aim to make the capacities of CBS Tools accessible to a wider community, highlight the potential of new high-resolution image processing methods, and foster collaboration in this emerging field.

Implementation

Architecture and design

The Nighres package consists of two core Python modules. The module **cbstools** contains the original CBS Tools Java classes that have been encapsulated using the JCC package[4]. JCC encapsulates the Java code with C++ code, to make it accessible to the Python interpreter, and produces a complete Python extension module. The module **nighres** includes the Python interfaces that are exposed to the user. It is organized in submodules that represent different application areas.[5] For example, the submodule *laminar* contains functions related to laminar analysis of the cortical sheet. The Python interfaces in each submodule are currently of two types:

i. Functions that wrap Java classes
ii. Functions in pure Python

Functions that wrap Java classes

The initial motivation to develop Nighres was to provide a user-friendly interface to the functionality of CBS Tools, leveraging the flexibility of Python. Therefore, a majority of the current functions in Nighres constitute Python wrappers which internally execute the original CBS Tools Java classes. These functions generally adhere to the following basic structure (a simple example can be found in the function *probability_to_levelset*):

i. Evaluate input parameters
ii. Start Java virtual machine
iii. Initiate Java class through JCC wrapper
iv. Load input data and cast to Java array
v. Pass additional parameters to Java class
vi. Execute Java class
vii. Collect outputs of Java class and cast back
viii. Return outputs (optional: save outputs)

Thus, the actual processing still relies on the same optimized Java code as in the original CBS Tools. However, since the Nighres function takes care of the interfacing between Python and Java, the user only interacts with Python code.

Functions in pure Python

Our long-term vision is for Nighres to become a central platform for new high-resolution image processing tools as they are developed. As discussed above, Python is rapidly becoming the most popular programming language in the neuroimaging community. The modular design of Nighres allows for easy integration of pure Python processing routines, and for the use of other neuroimaging software that has been (or can be) wrapped in Python independently with pipelining tools such as Nipype [26]. In addition, we have included a core set of lightweight convenience functions for input and output, parameter handling, and file naming in Python to simplify function calls and minimize the integration burden for new methods.

1 http://nipy.org/
2 NeuroImagin**G** at **H**igh **RES**olution
3 http://jupyter.org/
4 http://lucene.apache.org/pylucene/jcc/index.html
5 For consistency the submodule names are based on the original module organization in CBS Tools

Data handling

Data handling within Nighres follows established and widely used standards in the imaging community to ensure maximum interoperability. Where possible, Nighres uses the Nibabel package for handling imaging data [25]. Input and output functions are designed to automatically recognize and load most commonly used data formats, while maintaining flexibility to accommodate loading of non-standard data formats using custom scripts. Data is internally represented as Nibabel *Nifti1Images* (volumes) or Python dictionaries (surfaces) and can be passed in the form of file names or memory objects. Processing results are returned as memory objects, functions with multiple outputs return a dictionary storing the different outputs. Outputs can also be saved to disk. For saving, modifiers are appended to the output file names that refer to the name of the function and the specific output (e.g. *_layering_depth* for the continuous depth output of the volumetric layering function). Output names can be set to have a specific prefix or, by default, append modifiers to the main input file name.

Distribution

While both Python and Java are cross-platform languages, the JCC package that is used to encapsulate the CBS Tools Java classes generates C++ code and thus makes compilation platform-specific. We therefore implemented an automated build script that compiles the original CBS Tools Java code and builds the wrappers using JCC. We set up continuous integration using Travis CI[6] to test the build upon any changes to the code base on Github and, for any tagged releases, deploy the package to the Python Package Index[7]. The user can then download the package, run the fully automated build script to recompile the Java code and C++ wrappers on their platform, and finally use the pip installer[8] to install the modules and all their dependencies. Subsequently, Nighres can simply be imported into any Python environment.

We also provide a container allowing users to test Nighres in a preset environment, without actually installing it on their system. For this option the user only has to install Docker[9], a lightweight container platform that runs on Linux, Windows and Mac OS X. The Nighres Dockerfile[10] can then be used to build an Ubuntu 14 Trusty Docker image that contains a suitable Java installation, Nighres, and Jupyter Notebook.

Dependencies
One goal of Nighres was to reduce external dependencies. We therefore restricted the required packages for Nighres' core functionality to Nibabel, for reading and writing of common neuroimaging data formats [25], and Numpy, for efficient manipulation of data arrays [28]. The functions wrapping CBS Tools code require the CBS Tools Java library as well the Java matrix manipulation[11] and Apache Commons Math[12] libraries. However, these libraries are automatically recompiled, wrapped and installed from the CBS Tools github repository[13] upon installation of Nighres. Our example workflows use Nilearn's [27] plotting functionality for visualizing their results, but will automatically skip plotting if Nilearn is not installed.

Support files
Nighres automatically installs all essential support files including statistical atlases for brain segmentation, look-up tables for topological constraints, templates for high-resolution spatial normalization, and a cerebellar lobular atlas [29]. In addition, example data from publicly released 7 Tesla data sets is hosted on the Nighres project page[14] at the neuroimaging informatics tools and resources clearinghouse [NITRC, 30], and automatically downloaded when running the example workflows (see below).

Documentation

Beyond functional code, clear and concise documentation is one of the most important drivers of software use and longevity. Nighres' online documentation[15] was implemented using the Sphinx documentation tool[16] and automatically generates online content from the original function docstrings, which are written according to the the Numpy/Scipy documentation guidelines[17]. This design ensures that the documentation stays up-to-date with minimal overhead for developers, and is intuitive for users. Extensive example workflows provide users with easily understandable and reproducible code, as described in the following section. Finally, the online documentation contains an in-depth developer's guide that leads contributors through all steps necessary to submit code changes, new Python functions, new wrappers for CBS Tools functions or improvements of the documentation, to the Nighres github repository. We aimed to write a guide that makes it feasible for any researcher working with high-resolution neuroimaging data to contribute to Nighres, even without much previous experience in software development.

Usage example

In the following we present one of Nighres' usage example pipelines. The example shows how to obtain a tissue classification from MP2RAGE data [31] by performing the following steps:

i. Downloading the open MP2RAGE data set from NITRC
ii. Removing the skull and creating a brain mask
iii. Atlas-guided tissue classification using a multiple object geometric deformable model (MGDM) [32]

The outputs of the plotting functions are shown in Figure 1.

Import and download

First we import `nighres` and the `os` module to set the output directory.

```
import nighres
import os

out_dir = os.path.join(os.getcwd(),'nighres_examples/
    ↪ tissue_classification')
```

We also try to import Nilearn plotting functions. If Nilearn is not installed, plotting will be skipped.

```
skip_plots = False
```

6 https://travis-ci.org/nighres
7 https://pypi.python.org/pypi/nighres
8 https://pip.pypa.io/en/stable/
9 https://www.docker.com/
10 https://github.com/nighres/nighres/blob/master/Dockerfile
11 http://math.nist.gov/javanumerics/jama/
12 http://commons.apache.org/proper/commons-math/
13 https://github.com/piloubazin/cbstools-public
14 https://www.nitrc.org/projects/nighres/
15 http://nighres.readthedocs.io/en/latest/
16 http://www.sphinx-doc.org/en/stable/
17 https://numpydoc.readthedocs.io/en/latest/format.html

```
try:
    from nilearn import plotting
except ImportError:
    skip_plots = True
    print('Nilearn could not be imported, plotting will be
        ↪ skipped')
```

Now we download an example MP2RAGE [31] dataset that is hosted on NITRC [30]. It is the structural scan of the first subject, first session of the 7 Tesla Test-Retest dataset published by Gorgolewski et al. [18]

```
dataset = nighres.data.download_7T_TRT(out_dir)
```

Skull stripping

The first processing step is skull stripping. Only the second inversion image of the MP2RAGE sequence is required to calculate the brain mask. But if we input the quantitative T1 map and the T1-weighted image as well, they will be masked for us. We also save the outputs in the `out_dir` specified above and use a subject ID as the base file name.

```
skullstripping_results =
nighres.brain.mp2rage_skullstripping(second_inversion=
    ↪ dataset['inv2'],t1_weighted=dataset['t1w'],t1_map=
    ↪ dataset['t1map'], save_data=True,file_name='
    ↪ sub001_sess1',output_dir=out_dir)
```

To check if the skull stripping worked well ,we plot the brain mask on top of the original image (Figure 1a). Nighres, like Nilearn [27], uses Nibabel [25] *Nifti1Image* objects to pass data internally. Therefore, we can directly pass the outputs to Nilearn's plotting functions without saving and reloading. Alternatively, the images stored in `out_dir` can be opened in any common interactive viewer that can read the Nifti data format.

```
if not skip_plots:
    plotting.plot_roi(skullstripping_results['brain_mask'],
        ↪  dataset['t1w'], annotate=False, black_bg=False
        ↪ , draw_cross=False, cmap='autumn')
```

MGDM classification

Next, we use the masked data as input for tissue classification with the MGDM algorithm [32]. MGDM works with a single contrast, but can be improved with additional contrasts. In this case we use the T1-weigthed image as well as the quantitative T1 map.

```
mgdm_results = nighres.brain.mgdm_segmentation(
contrast_image1=skullstripping_results['t1w_masked'],
    ↪ contrast_type1="Mp2rage7T",contrast_image2=
    ↪ skullstripping_results['t1map_masked'],
    ↪ contrast_type2="T1map7T",save_data=True, file_name
    ↪ ="sub001_sess1", output_dir=out_dir)
```

Now we look at the topology-constrained segmentation that MGDM created (Figure 1b)

```
if not skip_plots:
    plotting.plot_img(mgdm_results['segmentation'], vmin=1,
        ↪  vmax=50, cmap='cubehelix', colorbar=True,
        ↪ annotate=False, draw_cross=False)
```

MGDM also creates an image which represents for each voxel the distance to its nearest border (Figure 1c). It is useful to assess where partial volume effects may occur.

```
if not skip_plots:
    plotting.plot_anat(mgdm_results['distance'], vmin=0,
        ↪ vmax=20, annotate=False, draw_cross=False,
        ↪ colorbar=True)
```

This examples implements a complete workflow for advanced processing of a quantitative MR contrast at high spatial resolution (voxel size = 0.5 mm isotropic). With the openly available and automatically downloaded data, any user can try out Nighres' functionality immediately after installation and then adapt the clearly explained code for their own use case.

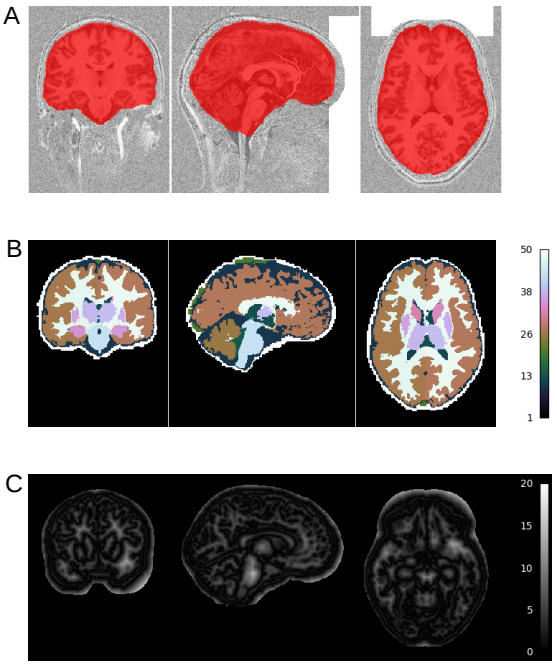

Figure 1. Tissue classification from MP2RAGE data. **A** The brain mask obtained from skull stripping. (Note that the white rectangles in the image occur because the data has been "defaced" for anonymization) **B** The segmented brain structures. **C** A representation of each voxel's distance to their nearest borders for assessing partial volume effects. Visualization performed within the script using Nilearn [27].

Discussion

We developed a Python toolbox that specializes in processing high-resolution brain imaging data. It has been designed with two key purposes in mind:

i. to provide the neuroimaging community with user-friendly access to cutting-edge high-resolution image processing tools,
ii. to create a flexible framework that can be extended by other researchers, along with thorough instructions on how to contribute.

The availability of high-resolution and quantitative MRI data, and the interest in new research directions that this data enables, are rapidly growing [e.g 33, 34]. At the same time, the image processing tools that would be required to leverage the new level of spatial detail provided by this data are largely missing. Only a few major neuroimaging packages have begun to adapt their tools for these purposes [35, 36]. However, these packages are limited by their closed source

code or rigid data organization, while it is crucial that newly emerging methods can be flexibly adapted, collaboratively developed, and integrated with other tools.

CBS Tools provides dedicated open source methods for high-resolution image processing [20]. Unfortunately, its complex design and heavy dependencies can make the installation and handling challenging for naive users, and impede contributions from other researchers. With Nighres we provide a flexible and user-friendly implementation of CBS Tools' functionality, which eliminates the dependency on MIPAV and JIST. Another major advance of Nighres compared to CBS Tools is its extensive online documentation. Besides comprehensives explanation of every function's in- and outputs, carefully documented usage examples provide step-by-step instructions of how the different tools can be combined to create complete processing pipelines.

The current implementation of Nighres contains a set of cutting-edge methods, but rapid methodological advances are to be expected in the dynamic field of high-resolution neuroimaging. We therefore designed Nighres as a transparent software platform through which newly developed methods can be made available to the community and improved collaboratively. New or existing tools can easily be added in a variety of formats, depending on the specific requirements of the operation and the preferences of the developer. The extensive developer's guide aims to encourage contributions even from researchers with little previous experience in software development.

We aimed to closely integrate our package with the existing community around neuroimaging tools in Python. To this end, we adopted standardized objects for internal data handling, which can easily be exchanged with other tools. An example is the seamless visualization of Nighres outputs using Nilearn's [27] plotting functions as showcased in the usage example (Figure 1).

A major limitation of the current package is that it has been developed and tested for common Linux platforms only. The C++ code generated by JCC to interfaces with the CBS Tools Java classes makes the compilation platform dependent. We addressed this issue by providing an automated build script that recompiles this code upon installation. While this process has only been tested on Linux, the design makes a future adaptation to Mac OS X platforms straightforward. Support for Windows is not currently planned. However, the provided Dockerfile enables usage of Nighres in a container on any platform that supports Docker.

Many future extension of the current package can be envisioned. Besides integrating more of the original CBS Tools functions, a main goal is to extend functionality with new tools coded directly in Python. To ensure efficient processing of the large data this might require the implementation of critical processes as C-extension through Cython[18]. Another goal is to provide integration with tools for parallel processing and job management on compute clusters.

In sum, we developed a user-friendly and well-documented Python package that makes cutting-edge high-resolution image processing tools available to the research community. The toolbox is easy to install and provides a comprehensive set of advanced techniques. While the current functionality is largely based on CBS Tools, we hope that the flexible framework encourages contribution of new tools, stimulates collaboration, and accelerates progress in the promising field of high-resolution neuroimaging.

18 http://cython.org/

Availability and requirements

- Project name: Nighres
- Project home page: https://github.com/nighres/nighres
- Operating system(s): Linux
- Programming language: Python, Java
- Other requirements: Java≥1.7, Python≥2.7, Numpy≥1.13, Nibabel≥2.1.0
- License: Apache License 2.0

Availability of supporting data

The data sets supporting the results of this article are available in the NITRC image repository [30] under https://www.nitrc.org/frs/?group_id=1205.

Declarations

List of abbreviations

- MGDM - multiple object geometric deformable model
- MPM - quantitative multi-parameter mapping
- MP2RAGE - magnetization prepared two rapid acquisition gradient echoes
- MRI - magnetic resonance imaging
- NITRC - the neuroimaging informatics tools and resources clearinghouse
- QSM - quantitative susceptibility mapping

Ethical Approval

Not applicable.

Consent for publication

Not applicable.

Competing Interests

The authors declare that they have no competing interests.

Funding

JMH project was partially funded by a stipend from Google via the Google Summer of Code program, with INCF as mentoring organization.

Author's Contributions

JMH, CJS and PLB contributed equally to conceptualization of the project and writing of the manuscript. JMH lead and CJS and PLB supported software development. All authors read and approved the final manuscript.

Acknowledgements

We would like to thank Gilles de Hollander, Nathaniel Kofalt and Rüdiger Meier for their contributions to Nighres, Daniel S. Margulies for his continuous support of this project, and Malin Sandström and the INCF for their coordination of the Google Summer of Code project.

References

1. van der Zwaag W, Schäfer A, Marques JP, Turner R, Trampel R. Recent applications of UHF-MRI in the study of human brain function and structure: a review: UHF MRI: Applications to Human Brain Function and Structure. NMR in Biomedicine 2016 Sep;29(9):1274–1288. http://doi.wiley.com/10.1002/nbm.3275.
2. Lutti A, Dick F, Sereno MI, Weiskopf N. Using high-resolution quantitative mapping of R1 as an index of cortical myelination. NeuroImage 2014 Jun;93:176–188. http://linkinghub.elsevier.com/retrieve/pii/S1053811913006423.
3. Sereno MI, Lutti A, Weiskopf N, Dick F. Mapping the human cortical surface by combining quantitative T1 with retinotopy. Cereb Cortex 2013;23(9):2261–2268.
4. Dick F, Tierney AT, Lutti A, Josephs O, Sereno MI, Weiskopf N. In vivo functional and myeloarchitectonic mapping of human primary auditory areas. J Neurosci 2012;32(46):16095–16105.
5. Huntenburg JM, Bazin PL, Goulas A, Tardif CL, Villringer A, Margulies DS. A Systematic Relationship Between Functional Connectivity and Intracortical Myelin in the Human Cerebral Cortex. Cerebral Cortex 2017 Feb;27(2):981–997. https://academic.oup.com/cercor/article/2981936/A.
6. Dinse J, Härtwich N, Waehnert MD, Tardif CL, Schäfer A, Geyer S, et al. A cytoarchitecture-driven myelin model reveals area-specific signatures in human primary and secondary areas using ultra-high resolution in-vivo brain MRI. NeuroImage 2015 Jul;114:71–87. http://linkinghub.elsevier.com/retrieve/pii/S1053811915003134.
7. Waehnert MD, Dinse J, Schäfer A, Geyer S, Bazin PL, Turner R, et al. A subject-specific framework for in vivo myeloarchitectonic analysis using high resolution quantitative MRI. NeuroImage 2016 Jan;125:94–107. http://linkinghub.elsevier.com/retrieve/pii/S1053811915008897.
8. Fracasso A, van Veluw SJ, Visser F, Luijten PR, Spliet W, Zwanenburg JJM, et al. Lines of Baillarger in vivo and ex vivo: Myelin contrast across lamina at 7T MRI and histology. Neuroimage 2016;133:163–175.
9. Whitaker KJ, Vértes PE, Romero-Garcia R, Váša F, Moutoussis M, Prabhu G, et al. Adolescence is associated with genomically patterned consolidation of the hubs of the human brain connectome. Proc Natl Acad Sci U S A 2016;113(32):9105–9110.
10. Marques JP, Khabipova D, Gruetter R. Studying cyto and myeloarchitecture of the human cortex at ultra-high field with quantitative imaging: R1, R2(*) and magnetic susceptibility. Neuroimage 2017;147:152–163.
11. Kok P, Bains L, vanMourik T, Norris D, deLange F. Selective Activation of the Deep Layers of the Human Primary Visual Cortex by Top-Down Feedback. Current Biology 2016 Feb;26(3):371–376. http://linkinghub.elsevier.com/retrieve/pii/S0960982215015699.
12. Huber L, Handwerker D, Gonzalez-Castillo J, Jangraw MS D, Guidi M, et al, Directional connectivity measured with layer-dependent fMRI in human sensory-motor system;. Talk presented at 3rd Biennial Whistler Scientific Workshop on Brain Functional Organization, Connectivity and Behavior, March 6-9, 2016, Whistler, BC, Canada.
13. Huber L, Handwerker D, Gonzalez-Castillo J, Guidi M, Ivanov D, Poser B, et al., Methods for measuring effective connectivity with high resolution blood volume fMRI;. Talk presented at 24th Annual Meeting of the International Society for Magnetic Resonance in Medicine, May 7-9, 2016, Singapore.
14. Keuken MC, Bazin PL, Crown L, Hootsmans J, Laufer A, Müller-Axt C, et al. Quantifying inter-individual anatomical variability in the subcortex using 7T structural MRI. NeuroImage 2014 Jul;94:40–46. http://linkinghub.elsevier.com/retrieve/pii/S1053811914001797.
15. Steele CJ, Anwander A, Bazin PL, Trampel R, Schaefer A, Turner R, et al. Human Cerebellar Sub-millimeter Diffusion Imaging Reveals the Motor and Non-motor Topography of the Dentate Nucleus. Cerebral Cortex 2017;27(9):4537–4548. +http://dx.doi.org/10.1093/cercor/bhw258.
16. Thürling M, Kahl F, Maderwald S, Stefanescu RM, Schlamann M, Boele HJ, et al. Cerebellar cortex and cerebellar nuclei are concomitantly activated during eyeblink conditioning: a 7T fMRI study in humans. J Neurosci 2015 Jan;35(3):1228–1239.
17. Forstmann BU, Keuken MC, Schafer A, Bazin PL, Alkemade A, Turner R. Multi-modal ultra-high resolution structural 7-Tesla MRI data repository. Sci Data 2014 Dec;1:140050.
18. Gorgolewski KJ, Mendes N, Wilfling D, Wladimirow E, Gauthier CJ, Bonnen T, et al. A high resolution 7-Tesla resting-state fMRI test-retest dataset with cognitive and physiological measures. Sci Data 2015 Jan;2:140054.
19. Tardif CL, Schäfer A, Trampel R, Villringer A, Turner R, Bazin PL. Open Science CBS Neuroimaging Repository: Sharing ultra-high-field MR images of the brain. Neuroimage 2016;124:1143–1148.
20. Bazin PL, Weiss M, Dinse J, Schäfer A, Trampel R, Turner R. A computational framework for ultra-high resolution cortical segmentation at 7Tesla. Neuroimage 2014 Jun;93 Pt 2:201–209.
21. Bazin PL, Plessis V, Fan AP, Villringer A, Gauthier CJ. Vessel segmentation from quantitative susceptibility maps for local oxygenation venography. IEEE; 2016. p. 1135–1138. http://ieeexplore.ieee.org/lpdocs/epic03/wrapper.htm?arnumber=7493466.
22. McAuliffe MJ, Lalonde FM, McGarry D, Gandler W, Csaky K, Trus BL. Medical Image Processing, Analysis and Visualization in clinical research. In: Computer-Based Medical Systems, 2001. CBMS 2001. Proceedings. 14th IEEE Symposium on; 2001. p. 381–386.
23. Lucas BC, Bogovic JA, Carass A, Bazin PL, Prince JL, Pham DL, et al. The Java Image Science Toolkit (JIST) for rapid prototyping and publishing of neuroimaging software. Neuroinformatics 2010 Mar;8(1):5–17.
24. Muller E, Bednar JA, Diesmann M, Gewaltig MO, Hines M, Davison AP. Python in neuroscience. Front Neuroinform 2015 Apr;9:11.
25. Brett M, Hanke M, Cipollini B, Côté MA, Markiewicz C, Gerhard S, et al. nibabel: 2.1. 0. Zenodo 2016;.
26. Gorgolewski KJ, Burns CD, Madison C, Clark D, Halchenko YO. Nipype : a flexible, lightweight and extensible neuroimaging data processing framework in Python. Front Neuroinform 2011;5(August).
27. Abraham A, Pedregosa F, Eickenberg M, Gervais P, Mueller A, Kossaifi J, et al. Machine learning for neuroimaging with scikit-learn. Front Neuroinform 2014;8:14.
28. van der Walt S, Colbert SC, Varoquaux G. The NumPy Array: A Structure for Efficient Numerical Computation. Computing in Science Engineering 2011 March;13(2):22–30.
29. Bazin J P L Kipping, Steele CJ, Margulies D, Turner R, Villringer A, Subject-specific cortical cerebellar mapping at 3T

and 7T;. Poster presented at the 19th Annual Meeting of the Organization for Human Brain Mapping, June 16-20, 2013, Seattle, USA.
30. Kennedy DN, Haselgrove C, Riehl J, Preuss N, Buccigrossi R. The NITRC image repository. NeuroImage 2016;124(Part B):1069–1073.
31. Marques JP, Kober T, Krueger G, van der Zwaag W, Van de Moortele PF, Gruetter R. MP2RAGE, a self bias-field corrected sequence for improved segmentation and T1-mapping at high field. Neuroimage 2010 Jan;49(2):1271–1281.
32. Bogovic J, Prince J, Bazin P. A multiple object geometric deformable model for image segmentation. Computer Vision and Image Understanding 2013;117(2):145–157.
33. Trampel R, Bazin PL, Pine K, Weiskopf N. In-vivo magnetic resonance imaging (MRI) of laminae in the human cortex. Neuroimage 2017 Sep;.
34. Paus T. Imaging microstructure in the living human brain: A viewpoint. NeuroImage 2017;http://www.sciencedirect.com/science/article/pii/S1053811917308261.
35. Goebel R. BrainVoyager–past, present, future. Neuroimage 2012 Aug;62(2):748–756.
36. Zaretskaya N, Fischl B, Reuter M, Renvall V, Polimeni JR. Advantages of cortical surface reconstruction using submillimeter 7 T MEMPRAGE. Neuroimage 2017 Sep;165:11–26.

Loading and plotting of cortical surface representations in Nilearn

Huntenburg, J.M., Abraham, A., Loula, J., Liem, F., Dadi, K. & Varoquaux, G. (2017).

Research Ideas and Outcomes, 3 (e12342).

http://dx.doi.org/10.3897/rio.3.e12342

Research Ideas and Outcomes 3: e12342
doi: 10.3897/rio.3.e12342

Project Report

Loading and plotting of cortical surface representations in Nilearn

Julia M Huntenburg[‡,§], Alexandre Abraham[|,¶], João Loula[|,#], Franziskus Liem[‡], Kamalaker Dadi[|,¶], Gaël Varoquaux[|,¶]

‡ Max Planck Research Group for Neuranatomy and Connectivity, Max Planck Institute for Human Cognitive and Brain Sciences, Leipzig, Germany
§ Neurocomputation and Neuroimaging Unit, Free University Berlin, Berlin, Germany
| Inria Parietal, Saclay, France
¶ CEA Neurospin, Gif-Sur-Yvette, France
# Department of Computer Science, École Polytechnique, Palaiseau, France

Corresponding author: Julia M Huntenburg (ju.huntenburg@gmail.com)

Reviewed v1

Received: 20 Feb 2017 | Published: 23 Feb 2017

Citation: Huntenburg J, Abraham A, Loula J, Liem F, Dadi K, Varoquaux G (2017) Loading and plotting of cortical surface representations in Nilearn. Research Ideas and Outcomes 3: e12342.
https://doi.org/10.3897/rio.3.e12342

Abstract

Processing neuroimaging data on the cortical surface traditionally requires dedicated heavy-weight software suites. Here, we present an initial support of cortical surfaces in Python within the neuroimaging data processing toolbox Nilearn. We provide loading and plotting functions for different surface data formats with minimal dependencies, along with examples of their application. Limitations of the current implementation and potential next steps are discussed.

Keywords

cortical surfaces, surface plotting, Python

Introduction

The human cerebral cortex is highly convoluted. Surface representations of neuroimaging data are essential to study cortical topography and to expose areas buried in sulcal depths. Surface-based approaches have traditionally been implemented in dedicated software suites, that can be hard to integrate with other tools. While the development of versatile Python tools for neuroimaging has recently gained momentum (e.g. http://nipy.org/), most of these tools focus on volumetric data. A notable exception is PySurfer (https://pysurfer.github.io/), a Python package for rendering neuroimaging data on the cortical surface. PySurfer provides high-level functions to visualise data processed with the Freesurfer software (Dale et al. 1999, Fischl et al. 1999a). However, this design complicates adaptation for other input data as it imposes a specific file layout. Moreover, PySurfer requires the Mayavi library (Ramachandran and Varoquaux 2011) which can be complicated to install.

Here we present a project that departs from this landscape in two ways: it strives 1) to provide plotting for cortical surface data in Python *under minimal dependencies*, and 2) to integrate surface data with multivariate processing in the Nilearn toolbox (Abraham et al. 2014).

Approach

In order to limit external dependencies to standard*1 Python libraries, we implemented loading of surface data using Nibabel (Brett et al. 2016) and rendering of the triangular surface meshes using Matplotlib (Hunter 2007). Beyond these two packages, only Numpy (van der Walt et al. 2011) is required.

All functions are integrated in Nilearn's plotting module. The core functionality is implemented in *plot_surf*, which initiates the figure and axes, renders the mesh using Matplotlib's *plot_trisurf* function, and assigns colour for each triangle from the node-wise input data. While *plot_surf* provides maximal parameter flexibility, we complemented it with wrapper functions setting sensible default parameters for most common use cases.

A considerable challenge was posed by the multitude of surface file formats currently in use, and the absence of an obvious community standard. The implemented loading functions automatically determine the input type and convert it to a standard Python structure. Input can be any file that can be read by Nibabel. Internally, surface mesh geometries are represented as a list of two Numpy arrays (vertex coordinates and face indices), and data to be displayed on the mesh as a single Numpy array. It is also possible to pass these data structures directly. This design makes it easy to load common surface file formats, but also allows the user to load other formats with custom scripts.

Results and limitations

The resulting functions are demonstrated in two examples. The example data is hosted on NITRC (https://www.nitrc.org/) and data fetchers for easy download and reuse were implemented as part of this project.

In the first example, the Destrieux atlas (Destrieux et al. 2010) is displayed on Freesurfer's fsaverage5 standard surface (Fischl et al. 1999b) using the *plot_surf_roi* function (Fig. 1). This function is optimised for plotting discrete patches and each triangle is coloured according to the median value of its three nodes. While this strategy prevents blurring between patches, some boundaries appear rugged. This could be addressed in the future by considering edge length during the determination of the triangle colours.

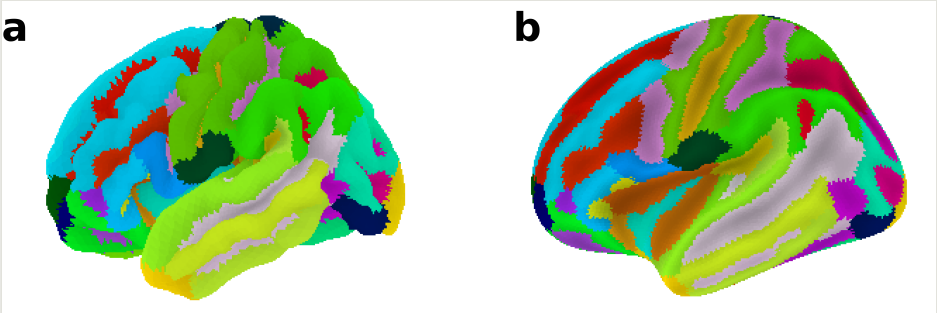

Figure 1.

Destrieux atlas plotted on the fsaverage5 surface template using the *plot_surf_roi* function. **a** Convoluted pial surface geometry of the left hemisphere. **b** Inflated pial surface geometry of the left hemisphere.

The second example uses resting-state fMRI data from 1 out of 102 subjects of the enhanced NKI sample (Nooner et al. 2012), which was preprocessed and sampled on the fsaverage5 surface (https://github.com/fliem/nki_nilearn) using Nipype (Gorgolewski et al. 2011). A seed region in the left posterior cingulate cortex is extracted from the Destrieux atlas and displayed using the *plot_surf_roi* function in a medial view (Fig. 2a). The *view* parameter is currently dependent on user specification of the hemisphere, and optimised for the orientation of Freesurfer templates. Since the orientation of the brain in 3D space can differ for other meshes, a solution which allows to specify elevation and azimuth directly, or determines a sensible view automatically, will be an important next step.

Next in the example, functional connectivity of the seed region to all other cortical nodes in the same hemisphere is calculated using Pearson's product-moment correlation coefficient. The resulting correlation map is plotted using *plot_surf_stat_map* (Fig. 2b), which determines face colours based on a linear interpolation of the node values and defaults to a symmetric diverging colormap. The example also demonstrates how images can be thresholded, plotted in a different colour scheme (Fig. 2c) and saved to disk.

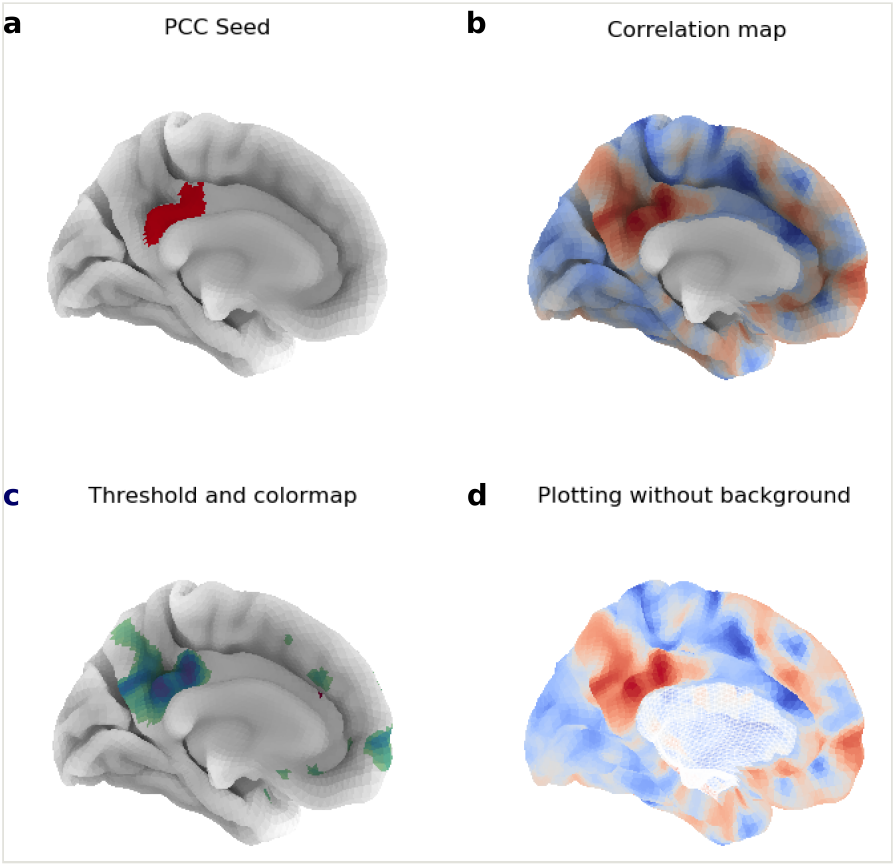

Figure 2.

Seed-based functional connectivity example. **a** Seed region in the posterior cingulate cortex (PCC). **b** Pearson product-moment correlation coefficient from the seed region time series to all other nodes. **c** The same map as in b, thresholded and plotted with a different colour scheme. **d** The same map as in b, plotted without sulcal depth information for shading.

In figures 1 and 2a-c, sulcal depth information is used for shading of the convoluted surface. While the depth data currently has to be provided by the user, it is conceivable to include utilities for calculating sulcal depth internally. If no sulcal depth information is provided, the functions default to displaying a semi-transparent mesh to expose the 3D structure without shading (Fig. 2d). Transparency can also be controlled using the *alpha* parameter.

Beyond the specific limitations discussed above, some general issues remain to be solved in future work. Currently, each figure contains a single view surrounded by a lot of white space. Convenient plotting of more complex scenes, including different views and a colorbar, would be desirable. Moreover, 3D rendering remains relatively slow, a problem which is adressed in an ongoing effort to improve the underlying Matplotlib code (https://github.com/matplotlib/matplotlib/pull/6085). Finally, the present design still requires many low-level inputs from the user. To avoid this, it might be necessary to represent surfaces in a more complex object, such as a Nibabel GiftiImage. A challenge here is the lack of a standard representation of surface data in the community.

Conclusion

We implemented a set of functions to load and plot surface representations of neuroimaging data in Python and demonstrated their application in examples. The functions are easy to use, flexibly adapt to different use cases, and only require Numpy, Matplotlib and Nibabel. While multiple features remain to be added and improved, this work presents a first step towards the support of cortical surface data in Nilearn.

Acknowledgements

This work was completed during Brainhack Paris 2016 and Brainhack Anatomy Paris 2016.

Author contributions

JMH, AA and GV designed the project. JMH, AA and JL contributed to the code. KRD and GV reviewed the code. FL preprocessed the example data. JMH wrote the initial draft of the manuscript. AA, GV, JL, FL and KRD revised the manuscript.

Conflicts of interest

None declared.

References

- Abraham A, Pedregosa F, Eickenberg M, Gervais P, Mueller A, Kossaifi J, Gramfort A, Thirion B, Varoquaux G (2014) Machine learning for neuroimaging with scikit-learn. Frontiers in neuroinformatics 8: 14. https://doi.org/10.3389/fninf.2014.00014
- Brett M, Hanke M, Cipollini B, Côté M, Markiewicz C, Gerhard S, Larson E, Lee G, Halchenko Y, Kastman E, cindeem, Morency F, moloney, Millman J, Rokem A, jaeilepp, Gramfort A, den Bosch JFv, Subramaniam K, Nichols N, embaker, bpinsard, chaselgrove, Oosterhof N, St-Jean S, Amirbekian B, Nimmo-Smith I, Ghosh S, Varoquaux G, Garyfallidis E (2016) nibabel: 2.1.0. Zenodo https://doi.org/10.5281/ZENODO.60808
- Dale A, Fischl B, Sereno M (1999) Cortical Surface-Based Analysis. NeuroImage 9 (2): 179-194. https://doi.org/10.1006/nimg.1998.0395
- der Walt Sv, Colbert SC, Varoquaux G (2011) The NumPy Array: A Structure for Efficient Numerical Computation. Computing in Science & Engineering 13 (2): 22-30. https://doi.org/10.1109/mcse.2011.37
- Destrieux C, Fischl B, Dale A, Halgren E (2010) Automatic parcellation of human cortical gyri and sulci using standard anatomical nomenclature. NeuroImage 53 (1): 1-15. https://doi.org/10.1016/j.neuroimage.2010.06.010

- Fischl B, Sereno M, Dale A (1999a) Cortical Surface-Based Analysis. NeuroImage 9 (2): 195-207. https://doi.org/10.1006/nimg.1998.0396
- Fischl B, Sereno M, Tootell RH, Dale A (1999b) High-resolution intersubject averaging and a coordinate system for the cortical surface. Human Brain Mapping 8 (4): 272-284. https://doi.org/10.1002/(sici)1097-0193(1999)8:43.0.co;2-4
- Gorgolewski K, Burns C, Madison C, Clark D, Halchenko Y, Waskom M, Ghosh S (2011) Nipype: A Flexible, Lightweight and Extensible Neuroimaging Data Processing Framework in Python. Frontiers in Neuroinformatics 5 https://doi.org/10.3389/fninf.2011.00013
- Hunter J (2007) Matplotlib: A 2D Graphics Environment. Computing in Science & Engineering 9 (3): 90-95. https://doi.org/10.1109/mcse.2007.55
- Nooner KB, Colcombe S, Tobe R, Mennes M, Benedict M, Moreno A, Panek L, Brown S, Zavitz S, Li Q, Sikka S, Gutman D, Bangaru S, Schlachter RT, Kamiel S, Anwar A, Hinz C, Kaplan M, Rachlin A, Adelsberg S, Cheung B, Khanuja R, Yan C, Craddock C, Calhoun V, Courtney W, King M, Wood D, Cox C, Clare Kelly AM, Martino AD, Petkova E, Reiss P, Duan N, Thomsen D, Biswal B, Coffey B, Hoptman M, Javitt D, Pomara N, Sidtis J, Koplewicz H, Castellanos FX, Leventhal B, Milham M (2012) The NKI-Rockland Sample: A Model for Accelerating the Pace of Discovery Science in Psychiatry. Frontiers in Neuroscience 6 https://doi.org/10.3389/fnins.2012.00152
- Ramachandran P, Varoquaux G (2011) Mayavi: 3D Visualization of Scientific Data. Computing in Science & Engineering 13 (2): 40-51. https://doi.org/10.1109/mcse.2011.35
- Waehnert MD, Dinse J, Weiss M, Streicher MN, Waehnert P, Geyer S, Turner R, Bazin P- (2014) Anatomically motivated modeling of cortical laminae. NeuroImage 93: 210-220. https://doi.org/10.1016/j.neuroimage.2013.03.078

Endnotes

[*1] where *standard* refers to the context of neuroimaging data analysis

A cortical surface-based geodesic distance package for Python

Margulies, D.S., Falkiewicz, M. & Huntenburg, J.M. (2016). GigaScience, 5 (1), 1920. http://dx.doi.org/10.1186/s13742-016-0147-0-q

Table 6 (abstract A16). User feedback

User Level	EOU	Time	Notes
Novice 1	8	00:35:25	Required walk through support
Novice 2	8	00:52:55	Required support for basic terminal commands only; then was able to complete independently
Moderate 1	3	00:23:45	Required no support
Moderate 2	4	00:22:10	Required no support
Expert 1	3	00:11:34	Required no support
Expert 2 - DE	3	02:00:00	Getting scripts to run took several minutes but reorganizing data and troubleshooting with freesurfer took significant time
Expert 3 – DE	2	01:15:00	Required walk through support

EOU: Ease of Use score (1–10) 1 = easiest, 10 = hardest. Time: the time it took for the user to setup and learn to use the scripts. DE: User's expertise is with a different computational environment than the one required by the scripts

A17

A cortical surface-based geodesic distance package for Python

Daniel S. Margulies, Marcel Falkiewicz, Julia M. Huntenburg
Max Planck Research Group for Neuroanatomy & Connectivity, Max Planck Institute for Human Cognitive and Brain Sciences, Leipzig, Germany
Correspondence: Daniel S. Margulies (margulies@cbs.mpg.de) – Max Planck Research Group for Neuroanatomy & Connectivity, Max Planck Institute for Human Cognitive and Brain Sciences, Leipzig, Germany
GigaScience 2016, **5(Suppl 1):**A17

Introduction
The human cerebral cortex, whether tracing it through phylogeny or ontogeny, emerges through expansion and progressive differentiation into larger and more diverse areas. While current methodologies address this analytically by characterizing local cortical expansion in the form of surface area [1] several lines of research have proposed that the cortex in fact expands along trajectories from primordial anchor areas [2,3] and furthermore, that the distance along the cortical surface is informative regarding cortical differentiation [4]. We sought to investigate the geometric relationships that arise in the cortex based on expansion from such origin points. Towards this aim, we developed a Python package for measuring the geodesic distance along the cortical surface that restricts shortest paths from passing through nodes of non-cortical areas such as the non-cortical portions of the surface mesh described as the "medial wall'.
Approach
The calculation of geodesic distance along a mesh surface is based in the cumulative distance of the shortest path between two points. The first challenge that arises is the sensitivity of the calculation to the resolution of the mesh: the coarser mesh, the longer the shortest path may be, as the distance becomes progressively less direct. This problem has been previously addressed and subsequently implemented in the Python package gdist [https://pypi.python.org/pypi/gdist/], which calculates the exact geodesic distance along a mesh by subdividing the shortest path until a straight line along the cortex is approximated [5]
The second challenge, for which there was no prefabricated solution, was ensuring that the shortest path only traverses territory within the cortex proper, avoiding shortcuts through non-cortical areas included in the surface mesh — most prominently, the non-cortical portions along the medial wall. Were the shortest paths between two nodes to traverse non-cortical regions, the distance between nodes would be artificially decreased, which would have artifactual impact on the interpretation of results. This concern would be especially relevent to the 'zones analysis' described below, where the boundaries between regions would be altered. It was therefore necessary to remove mesh nodes prior to calculating the exact geodesic, which requires reconstructing the mesh and assigning the respective new node indices for any seed regions-of-interest.
Finally, to facilitate applications to neuroscience research questions, we enabled the loading and visualization of data from commonly used formats such as FreeSurfer and the Human Connectome Project (HCP). A Nipype pipeline for group-level batch processing has also been made available [6]. The pipeline is wrapped in a command-line interface and allows for straightforward distance calculations of entire FreeSurfer-preprocessed datasets. Group-level data are stored as CSV files for each requested mesh resolution, source label and hemisphere, facilitating further statistical analyses.
Results
The resultant package, SurfDist, achieves the aforementioned goals of faciliating the calculation of exact geodesic distance on the cortical surface. We present here the distance measures from the central and calcarine sulci labels on the FreeSurfer native surfaces (Fig. 14b). The distance measure provides a means to parcellate the cortex using the surface geometry. Towards that aim, we also implement a 'zones analysis', which constructs a Voronoi diagram, establishing partitions based on the greater proximity to a set of label nodes (Fig. 14c).
Surface rendering of the results draws from plotting functions as implemented in Nilearn [7] and exclusively relies on the common library matplotlib to minimize dependencies. The visualization applies sensible defaults but can flexibly be adapted to different views, colormaps and thresholds as well as shadowing using a sulcal depth map.
Conclusions
The SurfDist package is designed to enable investigation of intrinisic geometric properties of the cerebral cortex based on geodesic distance measures. Towards the aim of enabling applications specific to neuroimaging-based research question, we have designed the package to facilitate analysis and visualization of geodesic distance metrics using standard cortical surface meshes.
Availability of supporting data
More information about this project can be found at: http://github.com/margulies/surfdist

Competing interests
None.

Author's contributions
DSM, MF, and JMH wrote the software and report.

Acknowledgements
Report from 2015 Brainhack Americas (MX). The authors would like to thank the organizers and attendees of Brainhack MX. The visualization functions were originally developed during the Nilearn coding sprint 2015 in Paris, for which we would also like to thank the organizers and participants of this event.

References
1. Winkler Anderson M, Sabuncu Mert R, Yeo BT Thomas, Fischl Bruce, Greve Douglas N, Kochunov Peter, Nichols Thomas E, Blangero John, Glahn David C. Measuring and comparing brain cortical surface area and other areal quantities. Neuroimage. 2012; 61: 1428–1443.
2. Sanides Friedrich. Comparative architectonics of the neocortex of mammals and their evolutionary interpretation. Ann N Y Acad Sci. 1969; 167: 404–423.
3. Buckner R,y L, Krienen Fenna M. The evolution of distributed association networks in the human brain. Trends Cogn Sci. 2013; 17: 648–665.
4. Wagstyl Konrad, Ronan Lisa, Goodyer Ian M, Fletcher Paul C. Cortical thickness gradients in structural hierarchies. Neuroimage. 2015; 111: 241–250.
5. Mitchell Joseph S B, Mount David M, Papadimitriou Christos H. The Discrete Geodesic Problem. SIAM J Comput. 1987; 16: 647–668.
6. Gorgolewski Krzysztof, Burns Christopher D, Madison Cindee, Clark Dav, Halchenko Yaroslav O. Nipype: a flexible, lightweight and extensible neuroimaging data processing framework in Python. Frontiers in Neuroinformatics. 2011; 5.
7. Abraham Alex,re, Pedregosa Fabian, Eickenberg Michael, Gervais Philippe, Mueller Andreas, Kossaifi Jean, Gramfort Alex,re, Thirion Bertr, Varoquaux Gaël. Machine learning for neuroimaging with scikit-learn. Frontiers in Neuroinformatics. 2014; 8: 1–10.

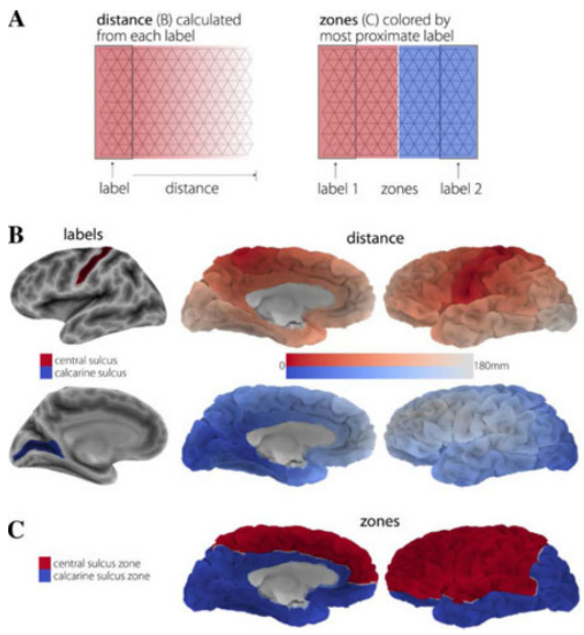

Fig. 14 (abstract A17). a Schematic illustrating the distance (**b**) and zone (**c**) analyses. **b** FreeSurfer labels from the central and calcarine sulci depicted on the individual inflated surface (left), and the exact geodesic distance from the two labels presented on an individual pial surface (right). **c** Zones delineated based on proximity to the central (red) or calcarine (blue) sulci

A18

Sharing data in the cloud

David O'Connor[1,2], Daniel J. Clark[2], Michael P. Milham[1,2], R. Cameron Craddock[1,2]
[1]Center for Biomedical Imaging and Neuromodulation, Nathan Kline Institute for Psychiatric Research, Orangeburg, NY, USA; [2]Center for the Developing Brain, Child Mind Institute, New York, NY, USA
Correspondence: David O'Connor (david.oconnor@childmind.org) – Center for Biomedical Imaging and Neuromodulation, Nathan Kline Institute for Psychiatric Research, Orangeburg, NY, USA
GigaScience 2016, **5(Suppl 1):**A18

Introduction

Cloud computing resources, such as Amazon Web Services (AWS) [http://aws.amazon.com], provide pay-as-you-go access to high-performance computer resources and dependable data storage solutions for performing large scale analyses of neuroimaging data [1]. These are particularly attractive for researchers at small universities and in developing countries who lack the wherewithal to maintain their own high performance computing systems. The objective of this project is to upload data from the 1000 Functional Connectomes Project (FCP) [2] and International Neuroimaging Datasharing Initiatives (INDI) [3] grass-roots data sharing initiatives into a Public S3 Bucket that has been generously provided by AWS. This will make the data more quickly accessible for AWS-based analysis of these data, but will also improve the speed and availability of access to this data for analyses performed outside of the cloud. To begin with, we focused on the following collections:

- The autism brain imaging data exchange *(ABIDE)* consists of structural MRI and resting state functional MRI from 1113 individuals (164 F, 948 M, 6–64 years old, 539 with autism spectrum disorders, 573 typical controls) aggregated from 20 different studies [4]
- The *ADHD-200* contains structural MRI and resting state functional MRI from 973 individuals (352 F, 594 M, 7–21 years old, 362 with attention deficit hyperactivity disorder (ADHD), 585 typically developing controls) collected from 8 sites [5]
- The *Consortium for Reliability and Reproducibility (CoRR)* consists of 3,357 structural MRI, 5,093 resting state fMRI, 1,302 diffusion MRI, and 300 cerebral blood flow scans from 1629 subjects (673 F, 956 M, 6–84 years old, all typical controls) acquired in a variety of test-retest designs at 35 sites [6]
- The *Enhanced Nathan Kline Institute - Rockland Sample (ENKI-RS)* consists of structural MRI, resting state functional MRI, diffusion MRI, cerebral blood flow, and a variety of task functional MRI scans and deep phenotyping on over 700 participants from across the lifespan and a variety of phenotypes acquired at a single site [7] The acquisition of this collection is ongoing.
- The *Addiction Connectome Preprocessed Initiative (ACPI)* [http://fcon_1000.projects.nitrc.org/indi/ACPI/html/index.html] consists of 216 structural MRI and 252 functional MRI from 192 subjects (44 F, 148 M, 18–50 years old) from three datasets generated by NIDA investigators.

Approach

Data for the ADHD-200, ABIDE, CoRR, and Rockland Sample data collections are currently downloadable from NITRC [http://fcon_1000.projects.nitrc.org/] as a series of large (>2GB) tar files. The process of uploading the data involved downloading and extracting the data from these tar files, organizing the individual images to the standardized INDI format [http://fcon_1000.projects.nitrc.org/indi/indi_data_contribution_guide.pdf] and then uploading the data to S3. We developed a S3 upload script in python using the Boto AWS software development kit [https://aws.amazon.com/sdk-for-python/] to facilitate this process. We also developed a download script in python that provides basic query functionality for selecting the data to download from a spreadsheet describing the data.

Results

The entirety of the CoRR, ABIDE, ACPI, and ADHD-200 data collections and ENKIRS data for 427 individuals were uploaded during the OHBM Hackathon event. The data are available as individual files to make it easily indexable by database infrastructures such as COINS [8] LORIS [9] and others. Additionally, this makes it easy for the users to download just the data that they want. The data in the bucket can be browsed and downloaded using a GUI based S3 file transfer software such as Cyberduck [http://cyberduck.io] (see Fig. 14), or using the Boto Python library [https://github.com/FCP-INDI/INDI-Tools]. One can connect to the bucket using the configuration shown in Fig. 15. The data is structured as follows: bucketname/data/Projects/ProjectName/DataType. For example you can access raw data from the ENKI-RS, as shown in Fig. 15, by specifying the following path in CyberDuck: https://s3.amazon.com/fcp-indi/data/Projects/RocklandSample/RawData

Conclusions

Uploading data shared through the FCP and INDI initiatives improves its accessibility for cloud-based and local computation. Future efforts for this project will include uploading the remainder of the FCP and INDI data and organizing the data in the new brain imaging data structure (BIDS) format [10].

Availability of supporting data

More information about this project can be found at: https://github.com/DaveOC90/INDI-Organization-Scripts

Competing interests

None.

Author's contributions

DO performed quality control, and uploaded the data. DJC wrote code to interact with AWS, preprocessed and uploaded data. MPM and RCC lead the data collection and sharing projects. All of the authors contributed to writing the project report.

Acknowledgements

Report from 2015 OHBM Hackathon (HI). The authors would like to thank the organizers and attendees of the OHBM Brainhack in Hawaii. This project was made possible by the S3 public bucket generously provided by Amazon Web Services.

A functional connectome phenotyping dataset including cognitive state and personality measures

Mendes, N., Oligschlaeger, S., Lauckner, M. E., Golchert, J., Huntenburg, J. M., Falkiewicz, M., ... Margulies, D. S. (under review). Scientific Data.

Preprint available on bioRxiv `http://dx.doi.org/10.1101/164764`

SCIENTIFIC DATA

Tracking no: SDATA-17-00391

A functional connectome phenotyping dataset including cognitive state and personality measures

Authors: Natacha Mendes (Max-Planck Institute for Human Cognitive and Brain Sciences), Sabine Oligschläger (Max-Planck Institute for Human Cognitive and Brain Sciences), Mark Lauckner (Max-Planck Institute for Human Cognitive and Brain Sciences), Johannes Golchert (Max-Planck Institute for Human Cognitive and Brain Sciences), Julia Huntenburg (Max-Planck Institute for Human Cognitive and Brain Sciences), Marcel Falkiewicz (Max Planck Institute for Human Cognitive and Brain Sciences), Melissa Ellami (Max-Planck Institute for Human Cognitive and Brain Sciences), Sarah Krause (Max-Planck Institute for Human Cognitive and Brain Sciences), Blazej Baczkowski (Max-Planck Institute for Human Cognitive and Brain Sciences), Roberto Cozatl (Max-Planck Institute for Human Cognitive and Brain Sciences), Anastasia Osoianu (Max-Planck Institute for Human Cognitive and Brain Sciences), Deniz Kumral (Max-Planck Institute for Human Cognitive and Brain Sciences), Jared Pool (Max-Planck Institute for Human Cognitive and Brain Sciences), Laura Golz (Max-Planck Institute for Human Cognitive and Brain Sciences), Maria Dreyer (Max-Planck Institute for Human Cognitive and Brain Sciences), Philipp Haueis (Max-Planck Institute for Human Cognitive and Brain Sciences), Rebecca Jost (Max-Planck Institute for Human Cognitive and Brain Sciences), Yelyzaveta Kramarenko (Max-Planck Institute for Human Cognitive and Brain Sciences), Haakon Engen (MRC Cognitive and Brain Sciences Unit, University of Cambridge), Katharina Ohrnberger (Max-Planck Institute for Human Cognitive and Brain Sciences), Krzysztof Gorgolewski (Stanford University), Nicolas Farrugia (LabSTICC-IMT), Anahit Babayan (Max Planck Institute for Human Cognitive and Brain Sciences), Andrea Reiter (Max Planck Institute for Human Cognitive and Brain Sciences), H. Lina Schaare (Max Planck Institute for Human Cognitive and Brain Sciences), Janis Reinelt (Max Planck Institute for Human Cognitive and Brain Sciences), Josefin Röbbig (Max Planck Institute for Human Cognitive and Brain Sciences), Marie Uhlig (Max Planck Institute for Human Cognitive and Brain Sciences), Miray Erbey (Max Planck Institute for Human Cognitive and Brain Sciences), Michael Gaebler (Max Planck Institute for Human Cognitive and Brain Sciences), Jonathan Smallwood (University of York), Arno Villringer (Max Planck Institute for Human Cognitive and Brain Sciences), and Daniel Margulies (Max Planck Institute for Human Cognitive and Brain Sciences)

Abstract:
The dataset enables exploration of higher-order cognitive faculties, self-generated mental experience, and personality features in relation to the intrinsic functional architecture of the brain. We provide multimodal magnetic resonance imaging (MRI) data and a broad set of state and trait phenotypic assessments: mind-wandering, personality traits, and cognitive abilities. Specifically, 194 healthy participants (between 20 and 75 years of age) filled out 31 questionnaires, performed 7 tasks, and reported 4 probes of in-scanner mind-wandering. The scanning session included four 15.5-min resting-state functional MRI runs using a multiband EPI sequence and a high-resolution structural scan using a 3D MP2RAGE sequence. This dataset constitutes one part of the MPI-Leipzig Mind-Brain-Body database.

Datasets:

Repository Name	Dataset Title	Dataset Accession Number	URL	Reviewer Passcode
OpenfMRI	MPI-Leipzig_Mind-Brain-Body	ds000221	https://openfmri.org/dataset/ds000221/	
Functional Connectomes Project International Neuroimaging Data-Sharing Initiative	MPI	MPI	http://fcon_1000.projects.nitrc.org/indi/retro/MPI.html	

A functional connectome phenotyping dataset including cognitive state and personality measures

Natacha Mendes[1]*, Sabine Oligschläger[1,2,3], Mark E. Lauckner[1], Johannes Golchert[1], Julia M. Huntenburg[1,4], Marcel Falkiewicz[1], Melissa Ellamil[1], Sarah Krause[1], Blazej M. Baczkowski[1,2,3], Roberto Cozatl[5] , Anastasia Osoianu[1,6], Deniz Kumral[7,8], Jared Pool[1], Laura Golz[9,10] , Maria Dreyer[7], Philipp Haueis[1,8], Rebecca Jost[1], Yelyzaveta Kramarenko[1], Haakon Engen[11,12] , Katharina Ohrnberger[1,8], Krzysztof J. Gorgolewski[13], Nicolas Farrugia[14], Anahit Babayan[7], Andrea Reiter[7,15], H. Lina Schaare[2,7], Janis Reinelt[7], Josefin Röbbig[7], Marie Uhlig[2,7], Miray Erbey[7], Michael Gaebler[7,8], Jonathan Smallwood[16], Arno Villringer[7,8], Daniel S. Margulies[1]*

1. Max Planck Research Group for Neuroanatomy & Connectivity, Max Planck Institute for Human Cognitive and Brain Sciences, Leipzig, Germany.
2. International Max Planck Research School NeuroCom, Leipzig, Germany.
3. Faculty of Biosciences, Pharmacy and Psychology, University Leipzig, Leipzig, Germany.
4. Neurocomputation and Neuroimaging Unit, Department of Education and Psychology, Freie Universität Berlin, Berlin, Germany
5. Database management, Max Planck Institute for Human Cognitive and Brain Sciences, Leipzig, Germany.
6. Department of Psychology, Technische Universität Dresden, Dresden, Germany.
7. Department of Neurology, Max Planck Institute for Human Cognitive and Brain Sciences, Leipzig, Germany.
8. MindBrainBody Institute, Berlin School of Mind and Brain, Humboldt-Universität zu Berlin, Germany.
9. Max Planck Research Group Cognitive and Affective Control of Behavioural Adaptation, Max Planck Institute for Human Cognitive and Brain Sciences, Leipzig, Germany.
10. Universitäre Psychiatrische Kliniken Basel, Switzerland.
11. Department of Social Neuroscience, Max Planck Institute for Human Cognitive and Brain Sciences, Leipzig, Germany.
12. MRC Cognition and Brain Sciences Unit, Cambridge University, Cambridge, United Kingdom.
13. Department of Psychology, Stanford University, Stanford, California 94305, USA.
14. LabSTICC-IMT Atlantique-campus de Brest, France.
15. Lifespan Developmental Neuroscience, Department of Psychology, Technische Universität Dresden, Dresden, Germany.
16. Department of Psychology, University of York, York, UK.

* Correspondence: mendes@cbs.mpg.de or margulies@cbs.mpg.de

Abstract

The dataset enables exploration of higher-order cognitive faculties, self-generated mental experience, and personality features in relation to the intrinsic functional architecture of the brain. We provide multimodal magnetic resonance imaging (MRI) data and a broad set of state and trait phenotypic assessments: mind-wandering, personality traits, and cognitive abilities. Specifically, 194 healthy participants (between 20 and 75 years of age) filled out 31 questionnaires, performed 7 tasks, and reported 4 probes of in-scanner mind-wandering. The scanning session included four 15.5-min resting-state functional MRI runs using a multiband EPI sequence and a high-resolution structural scan using a 3D MP2RAGE sequence. This dataset constitutes one part of the MPI-Leipzig Mind-Brain-Body database.

Background & Summary

Understanding the unique features of brain organization giving rise to distinct patterns of behavior, cognition, and mental experience remains one of the key research questions in the emerging field of human functional connectomics[1]. Functional connectivity has become a prominent method for investigating phenotypic differences across individuals[2,3]. However, there is ever greater need for validation of findings across independent datasets. The dataset presented here joins several others in contributing to this research agenda[4-6] and provides an additional resource for cross-site validation studies.

We acquired a wide range of self-reported personality measures as well as features of self-generated mental experience. In addition, a core magnetic resonance imaging (MRI) dataset—including one-hour of resting-state functional MRI (rs-fMRI) data—was acquired on 194 healthy participants. Questionnaires and behavioral measures were acquired over several follow-up sessions.

This dataset constitutes one part of the MPI-Leipzig Mind-Brain-Body database. It enables exploration of individual variance across cognitive and emotional phenotypes in relation to the brain. All MRI data were acquired on the same Siemens Verio 3Tesla MRI scanner.

Methods

Participants

In total, datasets from 194 native German-speaking participants are included (94 female, mean age = 34 years, median age = 27, SD = 16 years; Fig. 1). All participants were scanned on a 3 Tesla magnetic resonance imaging (MRI) scanner (Siemens Magnetom Verio) for the acquisition of one structural and four rs-fMRI scans. In addition, extensive questionnaire and task performance data were acquired from each participant. A subset of participants (N=109) were also included in a complementary data acquisition.

[Fig. 1 about here]

Recruitment and inclusion criteria

Prospective participants were initially recruited by the Leipzig Study for Mind-Body-Emotion Interactions project. Additional participants were recruited through online and poster advertisements. All participants were prescreened via telephone to determine their eligibility for the current study (Table 1). Participants fulfilling the eligibility criteria (including medical screening for MRI-scanning and neurological history) were invited to Max Planck Institute for Human Cognitive and Brain Sciences (MPI-CBS) where they were screened for past and present psychiatric disorders using the Structured Clinical Interview for DSM-IV (SCID-I[7]). After meeting eligibility criteria, participants received detailed information regarding the study.

All participants fulfilled the MRI safety requirements of the MPI-CBS (Supplementary Table 1), provided written informed consent (including agreement to their data being shared anonymously) prior to their participation in the study. Participants received monetary compensation for their participation. The study protocol was approved by the ethics committee at the medical faculty of the University of Leipzig (097/15-ff).

[Table 1 about here]

Data acquisition and protocol overview

Participants were required to complete: 1) four functional MRI scans within one scanning session and, if not previously acquired, one structural scan; 2) a battery of personality, mind-wandering, and emotional reactivity questionnaires spread over five appointments, and 3) a set of cognitive control, synesthesia, and creativity tasks spread over two appointments.

[Table 2 about here]

The data acquisition took place over five appointments over a two-year period (see Table 2):

- Day 1: We acquired data on a set of questionnaires that were completed at MPI-CBS (Tables 2 and 3).
- Day 2: We sent personalized links to participants, who could complete the set of online questionnaires at their convenience (Tables 2 and 3).
- Day 3: Participants were scanned at the Day Clinic for Cognitive Neurology, University of Leipzig. Before entering the scanner, participants completed a pen-and-paper practice trial of the short version of the New York Cognition Questionnaire[8]. While in the scanner, and immediately after each of the four resting state runs, participants received the computerized version of the same questionnaire. Immediately after the scanning session participants received additional questionnaires and a set of tasks (Tables 2 and 3).
- Day 4: The Abbreviated Math Anxiety Scale[9] and the NEO Personality Inventory-Revised[10-12] were completed online at the participant's convenience (Tables 2 and 3).
- Day 5: We acquired data on a set of questionnaires and tasks that were administered at MPI-CBS. Tasks were conducted using pen-and-paper, computer-administered, as well as Limesurvey[98] (version 2.00+) interfaces (Tables 2 and 3).

Within each set of questionnaires and tasks, the order of presentation of questionnaires and tasks was randomized across participants. If participants failed to complete a given questionnaire it was excluded from data analysis. Due to dropout, not all participants completed the full set of questionnaires and tasks.

[Table 3 about here]

Drug screening prior to MRI data acquisition

Each of the participants was instructed not to use illicit drugs within two weeks of the scanning appointment. Participants were also requested to abstain from alcohol and caffeine consumption, as well as nicotine on the night prior to the scanning day and on the day of scanning. Before the beginning of the MRI session, participants' urine was biochemically screened with a MULTI 8/2 strip test (Diagnostik Nord, Schwerin, Germany) for the presence of buprenorphine (cutoff 10ng/mL), amphetamine (cutoff 1000ng/mL), benzodiazepine (300ng/mL), cocaine (cutoff 300ng/mL), methamphetamine (1000ng/mL), morphine/heroine (cutoff 300ng/mL), methadone (cutoff 300ng/mL), THC (cutoff 50ng/mL). Cutoff levels are those recommended by the American National Institute on Drug Abuse (NIDA[13]). Participants provided informed consent on the use of the urine strip test and agreed to its anonymous data sharing, prior to their participation in the study.

MRI data acquisition

All magnetic resonance imaging (MRI) data was acquired using a whole-body 3 Tesla scanner (Magnetom Verio, Siemens Healthcare, Erlangen, Germany) equipped with a 32-channel Siemens head coil at the Day Clinic for Cognitive Neurology, University of Leipzig. For each participant the following scans were obtained: 1) a high-resolution structural scan, 2) four rs-fMRI scans, 3) two gradient echo fieldmaps and, 4) two pairs of spin echo images with reversed phase encoding direction. A low-resolution structural image of each participant was acquired using a FLAIR sequence for clinical screening.

Structural scan

The high-resolution structural image was acquired using a 3D MP2RAGE sequence[14] with the following parameters: voxel size = 1.0 mm isotropic, FOV = 256 x 240 x 176 mm , TR = 5000 ms, TE = 2.92 ms, TI1 = 700 ms, TI2 = 2500 ms, flip angle 1 = 4°, flip angle 2 = 5°, bandwidth = 240 Hz/Px, GRAPPA acceleration with iPAT factor 3 (32 reference lines), pre-scan normalization, duration = 8.22 min. From the two images produced by the MP2RAGE sequence at different inversion times (inv1 and inv2), a quantitative T1 map (t1map), and a uniform T1-weighted image (t1w) were generated. Importantly, the latter image is purely T1-weighted, whereas standard T1-weighted image, for example acquired with the MPRAGE sequence, also contain contributions of proton density and T2*. It should be taken into account that such differences can affect morphometric measures[15].

For one participant, the structural scan is MPRAGE instead of MP2RAGE (the T1-weighted image file names contain the sequence type) with voxel size = 1 mm isotropic, FoV = 256 x 240 x 176, TR = 2300 ms, TE = 2.98 ms, TI = 900 ms, flip angle = 9°, bandwidth = 238 Hz/Px.

Resting-state scans

Four rs-fMRI scans were acquired in axial orientation using T2*-weighted gradient-echo echo planar imaging (GE-EPI) with multiband acceleration, sensitive to blood oxygen level-dependent (BOLD) contrast[16,17]. Sequences were identical across the four runs, with the exception of alternating slice orientation and phase-encoding direction, to vary the spatial distribution of distortions and signal loss. Thus, the y-axis was aligned parallel to the AC-PC axis for runs 1 and

2, and parallel to orbitofrontal cortex for runs 2 and 4. The phase-encoding direction was A–P for runs 1 and 3, and P–A for runs 2 and 4. Further parameters were set as follows for all four runs: voxel size = 2.3 mm isotropic, FOV = 202 x 202 mm², imaging matrix = 88 x 88, 64 slices with 2.3 mm thickness, TR = 1400 ms, TE = 39.4 ms, flip angle = 69°, echo spacing = 0.67 ms, bandwidth = 1776 Hz/Px, partial fourier 7/8, no pre-scan normalization, multiband acceleration factor = 4, 657 volumes, duration = 15 min 30 s. During the resting-state scans, participants were instructed to remain awake with their eyes open and to fixate on a crosshair.

Scans for distortion correction

Two prominent methods exist to correct for geometric distortions in EPI images: fieldmaps, which represent the degree of distortion as calculated from two phase images with different echo times[18,19], and reverse phase encoding, in which pairs of "blip-up blip-down" images are acquired with opposite phase encoding direction — thus opposite distortions — and used to model a middle distortion-free image[20,21]. This dataset contains scans required for both methods to accommodate different preprocessing approaches and facilitate method comparison. Before each pair of resting-state runs with the same y-axis orientation (see above), the following scans were acquired in the same orientation as the subsequent resting-state scans: a pair of spin echo images (voxel size = 2.3 mm isotropic, FOV = 202 x 202 mm², imaging matrix = 88 x 88, 64 slices with 2.3 mm thickness, TR = 2200 ms, TE = 52 ms, flip angle = 90°, echo spacing = 0.67 ms, phase encoding = AP / PA, bandwidth = 1776 Hz/Px, partial fourier 6/8, no pre-scan normalization, duration = 0.20 min each), and a gradient echo fieldmap (voxel size = 2.3 mm isotropic, FOV = 202 x 202 mm², imaging matrix = 88 x 88, 64 slices with 2.3 mm thickness, TR = 680 ms, TE1 = 5.19 ms, TE2 = 7.65 ms, flip angle = 60°, bandwidth = 389 Hz/Px, prescan normalization, no partial fourier, duration = 2.03 min).

Additional scans

109 subjects also took part in a complementary protocol. Therefore, additional modalities will be available for these subjects. Modalities include high-resolution T2-weighted (108 subjects), diffusion-weighted (109), 3D FLAIR (47), phases and magnitudes of gradient-echo images suitable for Susceptibility-Weighted Imaging (SWI), and Quantitative Susceptibility Mapping (QSM) (45 subjects), as well as an additional 15-minute resting-state scan for all 109 subjects.

MRI data preprocessing

To enhance data usability we provide preprocessed data from 189 subjects (five participants did not have all four resting-state scans available, and were excluded from preprocessing). Data from five participants were further excluded due to failure at the preprocessing stage. The raw MRI data of these subjects are not corrupted, and are therefore available in the main database. Preprocessing pipelines were implemented using Nipype[22] and are described in more detail below. All code is openly available (https://github.com/NeuroanatomyAndConnectivity/pipelines/tree/master/src/lsd_lemon). Importantly, the preprocessing performed here is just one out of a multitude of possible pipelines that could be conceived for this dataset. The decisions taken at individual processing steps will not be suitable for every application. Users are strongly advised to familiarize themselves with

the details of the workflow before adopting the preprocessed data for their study. We also encourage users to subscribe to the mailing list for updates and discussions regarding the preprocessing pipelines used here (http://groups.google.com/group/resting_state_preprocessing).

Structural data

The background of the uniform T1-weighted image was removed using CBS Tools[23], and the masked image was used for cortical surface reconstruction using FreeSurfer's full version of recon-all[24,25]. A brain mask was created based on the FreeSurfer segmentation results. Diffeomorphic nonlinear registration as implemented in ANTs SyN algorithm[26] was used to compute a spatial transformation between the individual's T1-weighted image and the MNI152 1mm standard space.

To remove identifying information from the structural MRI scans, a mask for defacing was created from the MP2RAGE images using CBS Tools[23]. This mask was subsequently applied to all anatomical scans.

Functional data

The first five volumes of each resting-state run were excluded. Transformation parameters for motion correction were obtained by rigid-body realignment to the first volume of the shortened time series using FSL MCFLIRT[27]. The fieldmap images were preprocessed using the fsl_prepare_fieldmap script. A temporal mean image of the realigned time series was rigidly registered to the fieldmap magnitude image using FSL FLIRT[28] and unwarped using FSL FUGUE[29] to estimate transformation parameters for distortion correction. The unwarped temporal mean was rigidly coregistered to the subject's structural scan using FreeSurfer's boundary-based registration algorithm[30], yielding transformation parameters for coregistration. The spatial transformations from motion correction, distortion correction, and coregistration were then combined and applied to each volume of the original time series in a single interpolation step. The time series were masked using the brain mask created from the structural image (see above). The six motion parameters and their first derivatives were included as nuisance regressors in a general linear model (GLM), along with regressors representing outliers as identified by Nipype's rapidart algorithm (http://nipy.org/nipype/interfaces/generated/nipype.algorithms.rapidart.html), as well as linear and quadratic trends. To remove physiological noise from the residual time series, we followed the aCompCor approach as described by Behzadi and colleagues[31]. Masks of the white matter and cerebrospinal fluid were created by applying FSL FAST[32] to the T1-weighted image, thresholding the resulting probability images at 99%, eroding by one voxel and combining them to a single mask. Of the signal of all voxels included in this mask, the first six principal components were included as additional regressors in a second GLM, run on the residual time series from the first GLM. The denoised time series were temporally filtered to a frequency range between 0.01 and 0.1 Hz using FSL, mean centered and variance normalized using Nitime[33]. The fully preprocessed time series of all for runs were temporally concatenated. To facilitate analysis in standard space, the previously derived transformation was used to project the full-length time series into MNI152 2mm space. The preprocessed data are made available in

the subjects' native structural space and MNI standard space, along with the subject's brain mask and all regressors used for denoising.

Data security and data anonymization procedures

Data for all participants was stored on our instance of the eXtensible Neuroimaging Archive Toolkit (XNAT[34]) v.1.6.5. at the MPI-CBS. Access to the initial project was restricted (via XNAT's private project mode) to members of the Neuroanatomy & Connectivity Group at MPI-CBS for initial curation and quality assessment of data. All data comprised in the MPI-Leipzig Mind-Brain-Body database were derived from MPI-CBS so data import into XNAT was done from a local secured network.

A specially customized XNAT uploader was used to upload all participants' data to XNAT. The native DICOM format was used for MRI data, whilst a standard ASCII (*.csv, *.txt) format was employed to upload all other experimental data such as surveys, test batteries, and demographical data.

The anonymization measures applied to the MRI data consisted of removal of DICOM header tags containing information which could lead to the identification of test subjects as well as the defacing of all structural (NIFTI) scans. Specific surveys and test batteries containing sensitive information are only available via the restricted project in XNAT for which access needs to be applied for (see the Usage Notes section below).

Code availability

All code that was implemented for data acquisition and processing is available online (https://neuroanatomyandconnectivity.github.io/opendata/). Data handling and computation of summary measures were implemented in Python. The pipeline used for MRI preprocessing is also available (https://github.com/NeuroanatomyAndConnectivity/pipelines/tree/v2.0/src/lsd_lemon, release v2.0).

The tasks that the participants received were implemented using the Python package PsychoPy2 Experiment Builder v1.81.03[35,36], OpenSesame 0.27.4[37], and Presentation® software (Version 16.5, Neurobehavioral Systems, Inc., Berkeley, CA, www.neurobs.com). We provide the respective source codes of the Adaptive Visual and Auditory Oddball Target Detection Task [e.g.,38; c.f.,39](Oddball; https://github.com/NeuroanatomyAndConnectivity/opendata/tree/master/scripts), Conjunctive Continuous Performance Task[40] (CCPT; https://github.com/NeuroanatomyAndConnectivity/ConjunctiveContinuousPerformanceTask), and Emotional Task Switching[adapted from 41; see 42] (ETS; https://github.com/NeuroanatomyAndConnectivity/opendata/tree/master/scripts).

Data Records

Survey and task data

A comprehensive list of behavioral and questionnaire data are given in Supplementary Table 2. Data from all questionnaires are released as summary scores. Results of questionnaires without summary scores are released as raw item scores, namely: Multi-Gender Identity Questionnaire [adapted from 43] (MGIQ), Mobile Phone Usage[44] (MPU), Facebook Intensity Scale[45] (FBI), New York Cognition Questionnaire[46] (NYC-Q), and the short version of the New York Cognition Questionnaire[8] (Short-NYC-Q). Task data for the CCPT[40], ETS [adapted from 41; see 42], and oddball task [e.g.,38; c.f.,39] are available via subject-specific csv files. Accompanying specifications and information for each questionnaire and task are given in txt file format.

A basic demographic summary is provided together with general information on data acquisition. The metafile includes gender, age (5-year bins), body mass index, handedness, current or past diagnosed psychiatric disorder(s), result of the drug test on day of scanning, and formal education.

MRI data

The dataset is organized in concordance with the Brain Imaging Data Structure (BIDS) format[47]. This facilitates data analysis, for example with BIDS-Apps[48] (http://bids-apps.neuroimaging.io). BIDS-Apps encapsulate standard MRI analysis tools within an application that understands the BIDS format and allows to automatically access relevant data and metadata.

MRI data are currently available from three locations:

1. OpenfMRI.org platform also hosts the raw data (accession number ds000221):
   https://www.openfmri.org/dataset/ds000221/

2. International Neuroimaging Data-sharing Initiative (INDI):
   http://fcon_1000.projects.nitrc.org/indi/retro/MPI.html

3. Gesellschaft für wissenschaftliche Datenverarbeitung mbH Göttingen (GWDG):
   https://www.gwdg.de/
   Raw and preprocessed data at this location is accessible through web browser (https://ftp.gwdg.de/pub/misc/MPI-Leipzig_Mind-Brain-Body/) and a fast FTP connection (ftp://ftp.gwdg.de/pub/misc/MPI-Leipzig_Mind-Brain-Body/). In the case the location of the data changes in the future, the location of the dataset can be resolved with PID 21.11101/0000-0004-2CD6-A (e.g., https://hdl.handle.net/21.11101/0000-0004-2CD6-A)

Technical Validation

All datasets were manually assessed for missing or corrupt data. Further quality control of the data was applied to the MRI and behavioral measures, as described below.

MRI data quality assessment

Preprocessed MRI data were assessed for quality using the mriqc package[49] 8 (the code was adapted from https://github.com/chrisfilo/mriqc and can be found at https://github.com/NeuroanatomyAndConnectivity/pipelines/tree/master/src/lsd_lemon, release v2.0), implemented in Python. mriqc creates a report for each individual scan based on assessment of movement parameters, coregistration, and temporal signal-to-noise (tSNR) calculations. For comparison, all individual-level scores are displayed with respect to the group-level distribution. We visually inspected the quality assessment reports for each subject to ensure adequate coregistration and fieldmap correction.

As motion during the resting-state fMRI scan poses a substantial source of noise[50], we characterized motion for each run as the mean and maximum framewise displacement (Fig. 2). Overall, the summary of motion parameters demonstrates that the data are largely of sufficient quality, with 89.2% of runs showing less than one voxel (2.3 mm) maximum framewise displacement, and a mean framewise displacement of 0.18 mm (SD = 0.08 mm).

[Fig. 2 about here]

Fieldmap correction provides an approach to correct for distortions due to susceptibility artifacts. While unable to recover signal loss, the correction of such nonlinear distortions improves coregistration between scan types, and group-level alignment[51]. As an example, we present a single dataset, pre- and post-fieldmap correction, in Fig. 3. As expected, fieldmap correction primarily shifted voxels within ventral regions.

[Fig. 3 about here]

Temporal signal-to-noise (tSNR), which is calculated on the voxel-level as the mean signal divided by the standard deviation, offers a general overview of the local differences across the brain. We observed lower tSNR in ventral regions, including the orbitofrontal and temporal cortex (Fig. 4).

[Fig. 4 about here]

Behavioral measures quality assessment

Fifteen questionnaires without a published German version were in-house translated (English-German). To ensure general usability of the translated questionnaires, their reliability was estimated using Cronbach's Alpha coefficient (see Table 4). For comparison, the Cronbach's Alpha coefficients from the original questionnaires are also reported in Table 4.
Internal consistency of the majority of questionnaires was acceptable, with an average Cronbach's Alpha of 0.78, thus showing that the German translations of those specific questionnaires are reproducible and valid. However, three questionnaires (Short Dark Triad[79; original by 80], Body Consciousness Questionnaire[54], and the Creative Achievement Questionnaire[63]) and four scales (two scales of the Five Facets of Mindfulness Questionnaire[66], one scale of the

Metacognition Questionnaire[73], and one scale of the Involuntary Musical Imagery Scale[72]) showed modest reliability, with Cronbach's Alpha coefficient < 0.70, and should be interpreted with caution.

[Table 4 about here]

Usage Notes

The MRI dataset can be accessed at www.openfmri.org, http://fcon_1000.projects.nitrc.org, or https://www.gwdg.de/ and the behavioral data is available at www.nitrc.org (http://nitrc.org/projects/mpilmbb/). The following data are publicly available: 1) MRI data (structural and functional), 2) general demographic of the studied population, 3) summary scores and/or indexes of the questionnaires and tasks, and 4) raw scores of the measures that do not possess summary scores and have not been classified as sensitive. All MRI datasets are made available in NIFTI format, and all anatomical scans have been defaced.

The dataset, protocols, and software used in the acquisition and processing of the data are documented, curated, and available for research purposes. For access to the behavioral data, users must first agree to the terms of data usage.

Additional access to sensitive behavioral measures

Individual behavioral scores and sensitive phenotypic measures may be made available upon request to the corresponding authors. The completion of additional data license and confidentiality forms will be required in advance of further data access.

Acknowledgements

This work was partially supported by the Volkswagen Foundation (AZ.: 89 440). We thank Shameem Wagner and Elizabeth Kelly for assistance in the preparation of the manuscript.

Author contributions

Conception, design, and preparation of the manuscript: D.S.M., J.G., J.M.H., M.E.L., M.F., N.M., S.O.
Behavioral data analyses: J.G., M.E.L., S.O.
MRI data preprocessing: J.M.H., M.E.L.
Quality Control of MRI data: D.S.M., J.G., J.M.H., M.E.L., S.O.
Contributions to study design: B.M.B., H.E., J.P., J.S., K.J.G., K.O., N.F.
Participant recruitment: A.O., J.G., M.E.L., N.M., P.H., R.J., S.K., Y.K.
Data acquisition: D.K., J.G., J.P., L.G., M.D., M.E.L., N.M., S.K., S.O.
Data curation: M.F., R.C.
Data contributions: A.B., A.R., A.V., D.K., H.L.S., J.R., J.R., M.E., M.G., M.U.
All authors provided critical feedback and approval of the manuscript.

Competing interests

The authors declare no competing financial interests.

References

1 Kelly, C., Biswal, B. B., Craddock, R. C., Castellanos, F. X. & Milham, M. P. Characterizing variation in the functional connectome: promise and pitfalls. *Trends Cogn Sci.* **16,** 181-188 (2012).

2 Smith, S. M. *et al.* A positive-negative mode of population covariation links brain connectivity, demographics and behavior. *Nat. Neurosci.* **18,** 1565-1567 (2015).

3 Vaidya, C. J. & Gordon, E. M. Phenotypic variability in resting-state functional connectivity: current status. *Brain Connect* **3,** 99-120 (2013).

4 Nooner, K. B. *et al.* The NKI-Rockland sample: a model for accelerating the pace of discovery science in psychiatry. *Front Neurosci* **6,** 152 (2012).

5 Holmes, A. J. *et al.* Brain Genomics Superstruct Project initial data release with structural, functional, and behavioral measures. *Scientific data* **2** (2015).

6 Van Essen, D. C. *et al.* The WU-Minn human connectome project: an overview. *Neuroimage* **80,** 62-79 (2013).

7 Wittchen, H.-U., Kessler, R. C., Zhao, S. & Abelson, J. Reliability and clinical validity of UM-CIDI DSM-III-R generalized anxiety disorder. *J Psychiatr Res* **29,** 95-110 (1995).

8 Ruby, F. J., Smallwood, J., Engen, H. & Singer, T. How self-generated thought shapes mood—the relation between mind-wandering and mood depends on the socio-temporal content of thoughts. *PloS One* **8**, e77554 (2013).

9 Hopko, D. R., Mahadevan, R., Bare, R. L. & Hunt, M. K. The abbreviated math anxiety scale (AMAS) construction, validity, and reliability. *Assessment* **10**, 178-182 (2003).

10 Ostendorf, F. & Angleitner, A. *NEO-Persönlichkeitsinventar (revidierte Form, NEO-PI-R) nach Paul T. Costa und Robert R. McCrae*. (Hogrefe, 2004).

11 Costa, P. T. & McCrae, R. R. *The NEO personality inventory manual*. (Psychological Assessment Resources., 1985).

12 Costa, P. T. & McCrae, R. R. *Revised NEO personality inventory (NEO PI-R) and NEP five-factor inventory (NEO-FFI): professional manual*. (Psychological Assessment Resources Lutz, FL, 1992).

13 Hawks, R. L. & Chiang, C. N. *Urine testing for drugs of abuse*. (National Institute on Drug Abuse Rockville, MD, 1986).

14 Marques, J. P. *et al.* MP2RAGE, a self bias-field corrected sequence for improved segmentation and T 1-mapping at high field. *Neuroimage* **49,** 1271-1281 (2010).

15 Lorio, S. *et al.* Neurobiological origin of spurious brain morphological changes: A quantitative MRI study. *Hum Brain Mapp* **37,** 1801-1815 (2016).

16 Feinberg, D. A. *et al.* Multiplexed echo planar imaging for sub-second whole brain FMRI and fast diffusion imaging. *PloS One* **5,** e15710 (2010).

17 Moeller, S. *et al.* Multiband multislice GE-EPI at 7 tesla, with 16-fold acceleration using partial parallel imaging with application to high spatial and temporal whole-brain fMRI. *Magn Reson Med* **63,** 1144-1153 (2010).

18 Jezzard, P. & Balaban, R. S. Correction for geometric distortion in echo planar images from B0 field variations. *Magn Reson Med* **34,** 65-73 (1995).

19 Reber, P. J., Wong, E. C., Buxton, R. B. & Frank, L. R. Correction of off resonance-related distortion in echo-planar imaging using EPI-based field maps. *Magn Reson Med* **39,** 328-330 (1998).

20 Chang, H. & Fitzpatrick, J. M. A technique for accurate magnetic resonance imaging in

the presence of field inhomogeneities**.** *IEEE Trans Med Imaging* **11,** 319-329 (1992).
21 Andersson, J. L., Skare, S. & Ashburner, J. How to correct susceptibility distortions in spin-echo echo-planar images: application to diffusion tensor imaging. *Neuroimage* **20,** 870-888 (2003).
22 Gorgolewski, K. *et al.* Nipype: a flexible, lightweight and extensible neuroimaging data processing framework in python. *Front Neuroinform* **5,** 13 (2011).
23 Bazin, P.-L. *et al.* A computational framework for ultra-high resolution cortical segmentation at 7Tesla. *Neuroimage* **93,** 201-209 (2014).
24 Dale, A. M., Fischl, B. & Sereno, M. I. Cortical surface-based analysis: I. Segmentation and surface reconstruction. *Neuroimage* **9,** 179-194 (1999).
25 Fischl, B., Sereno, M. I. & Dale, A. M. Cortical surface-based analysis: II: inflation, flattening, and a surface-based coordinate system. *Neuroimage* **9,** 195-207 (1999).
26 Avants, B. B. *et al.* A reproducible evaluation of ANTs similarity metric performance in brain image registration. *Neuroimage* **54,** 2033-2044 (2011).
27 Jenkinson, M., Bannister, P., Brady, M. & Smith, S. Improved optimization for the robust and accurate linear registration and motion correction of brain images. *Neuroimage* **17,** 825-841 (2002).
28 Jenkinson, M. & Smith, S. A global optimisation method for robust affine registration of brain images. *Med Image Anal* **5,** 143-156 (2001).
29 Jenkinson, M., Beckmann, C. F., Behrens, T. E., Woolrich, M. W. & Smith, S. M. Fsl. *Neuroimage* **62,** 782-790 (2012).
30 Greve, D. N. & Fischl, B. Accurate and robust brain image alignment using boundary-based registration. *Neuroimage* **48,** 63-72 (2009).
31 Behzadi, Y., Restom, K., Liau, J. & Liu, T. T. A component based noise correction method (CompCor) for BOLD and perfusion based fMRI. *Neuroimage* **37,** 90-101 (2007).
32 Zhang, Y., Brady, M. & Smith, S. Segmentation of brain MR images through a hidden Markov random field model and the expectation-maximization algorithm. *IEEE Trans Med Imaging* **20**, 45-57 (2001).
33 Rokem, A., Trumpis, M. & Perez, F. in *Proceedings of the 8th Python in Science Conference (SciPy 2009)*. (eds G. Varoquaux, S. van der Walt, & J. Millman) 68-75.
34 Marcus, D. S., Olsen, T. R., Ramaratnam, M. & Buckner, R. L. The extensible neuroimaging archive toolkit. *Neuroinformatics* **5,** 11-33 (2007).
35 Peirce, J. W. PsychoPy—psychophysics software in Python. *J. Neurosci. Methods* **162,** 8-13 (2007).
36 Peirce, J. W. Generating stimuli for neuroscience using PsychoPy. *Front Neuroinform* **2** (2008).
37 Mathôt, S., Schreij, D. & Theeuwes, J. OpenSesame: An open-source, graphical experiment builder for the social sciences. *Behav Res Methods* **44,** 314-324 (2012).
38 Huettel, S. A. & McCarthy, G. What is odd in the oddball task?: Prefrontal cortex is activated by dynamic changes in response strategy. *Neuropsychologia* **42,** 379-386 (2004).
39 Golchert, J. *et al.* Individual variation in intentionality in the mind-wandering state is reflected in the integration of the default-mode, fronto-parietal, and limbic networks. *Neuroimage* **146,** 226-235 (2017).
40 Shalev, L., Ben-Simon, A., Mevorach, C., Cohen, Y. & Tsal, Y. Conjunctive continuous

performance task (CCPT)—a pure measure of sustained attention. *Neuropsychologia* **49,** 2584-2591 (2011).
41 Whitmer, A. J. & Banich, M. T. Inhibition versus switching deficits in different forms of rumination. *Psychol Sci* **18,** 546-553 (2007).
42 Hildebrandt, L. K., McCall, C., Engen, H. G. & Singer, T. Cognitive flexibility, heart rate variability, and resilience predict fine-grained regulation of arousal during prolonged threat. *Psychophysiology* **53,** 880-890 (2016).
43 Joel, D., Tarrasch, R., Berman, Z., Mukamel, M. & Ziv, E. Queering gender: studying gender identity in 'normative'individuals. *Psychol Sex* **5,** 291-321 (2014).
44 Gorgolewski, K. Mobile phone usage. (developed in-house).
45 Ellison, N. B., Steinfield, C. & Lampe, C. The benefits of Facebook "friends": Social capital and college students' use of online social network sites. *J Comput Mediat Commun* **12,** 1143-1168 (2007).
46 Gorgolewski, K. J. *et al.* A correspondence between individual differences in the brain's intrinsic functional architecture and the content and form of self-generated thoughts. *PloS One* **9,** e97176 (2014).
47 Gorgolewski, K. J. *et al.* The brain imaging data structure, a format for organizing and describing outputs of neuroimaging experiments. *Scientific data* **3,** 160044 (2016).
48 Gorgolewski, K. J. *et al.* BIDS Apps: Improving ease of use, accessibility and reproducibility of neuroimaging data analysis methods. *bioRxiv***,** 079145 (2016).
49 Esteban, O. *et al.* MRIQC: Predicting Quality in Manual MRI Assessment Protocols Using No-Reference Image Quality Measures. *bioRxiv***,** 111294 (2017).
50 Power, J. D. *et al.* Methods to detect, characterize, and remove motion artifact in resting state fMRI. *Neuroimage* **84,** 320-341 (2014).
51 Jezzard, P. Correction of geometric distortion in fMRI data. *Neuroimage* **62,** 648-651 (2012).
52 Derryberry, D. & Reed, M. A. Anxiety-related attentional biases and their regulation by attentional control. *J Abnorm Psychol* **111,** 225 (2002).
53 Achenbach, T. M. & Rescorla, L. A. Manual for the ASEBA adult forms & profiles. (Research Center for Children, Youth, & Families, University of Vermont, Burlington, VT, USA, 2003).
54 Miller, L. C., Murphy, R. & Buss, A. H. Consciousness of body: private and public. **J** *Pers Soc Psychol* **41,** 397 (1981).
55 Beck, A. T., Ward, C. H., Mendelson, M., Mock, J. & ERBAUGH, J. An inventory for measuring depression. *Arch. Gen. Psychiatry* **4,** 561-571 (1961).
56 Beck, A. T., Steer, R. A. & Brown, G. K. Beck depression inventory-II. *San Antonio* **78**, 490-498 (1996).
57 Hautzinger, M., Bailer, M., Worall, H. & Keller, F. BDI: Beck-Depressions-Inventar, Testhandbuch, 2. überarbeitete Auflage. *Bern: Verlag Hans Huber* (1995).
58 Carver, C. S. & White, T. L. Behavioral inhibition, behavioral activation, and affective responses to impending reward and punishment: The BIS/BAS Scales. *J Pers Soc Psychol* **67,** 319 (1994).
59 Strobel, A., Beauducel, A., Debener, S. & Brocke, B. Eine deutschsprachige Version des BIS/BAS-Fragebogens von Carver und White. *Zeitschrift für Differentielle und diagnostische Psychologie* (2001).
60 Gray, J. A. Precis of the neuropsychology of anxiety: An enquiry into the functions of the

septo-hippocampal system. *Behav Brain Sci* **5,** 469-534 (1982).
61 Gray, J. A. in *A Model for Personality* (ed Hans J. Eysenck) 246-276 (Springer Berlin Heidelberg, 1981).
62 Farmer, R. & Sundberg, N. D. Boredom proneness—the development and correlates of a new scale. *J Pers Assess* **50,** 4-17 (1986).
63 Carson, S. H., Peterson, J. B. & Higgins, D. M. Reliability, validity, and factor structure of the creative achievement questionnaire. *Creat Res J* **17,** 37-50 (2005).
64 Johns, M. W. A new method for measuring daytime sleepiness: the Epworth sleepiness scale. *Sleep* **14,** 540-545 (1991).
65 Bloch, K. E., Schoch, O. D., Zhang, J. N. & Russi, E. W. German version of the Epworth sleepiness scale. *Respiration* **66,** 440-447 (1999).
66 Baer, R. A., Smith, G. T., Hopkins, J., Krietemeyer, J. & Toney, L. Using self-report assessment methods to explore facets of mindfulness. *Assessment* **13,** 27-45 (2006).
67 Schaal, N. K., Bauer, A.-K. R. & Müllensiefen, D. Der Gold-MSI: replikation und validierung eines fragebogeninstrumentes zur messung musikalischer erfahrenheit anhand einer deutschen stichprobe. *Music Sci* **18,** 423-447 (2014).
68 Müllensiefen, D., Gingras, B., Musil, J. & Stewart, L. Measuring the facets of musicality: The Goldsmiths Musical Sophistication Index (Gold-MSI). *Pers Individ Dif* **60,** S35 (2014).
69 Zigmond, A. S. & Snaith, R. P. The hospital anxiety and depression scale. *Acta Psychiatr Scand* **67,** 361-370 (1983).
70 Herrmann-Lingen, C., Buss, U. & Snaith, P. *Hospital Anxiety and Depression Scale-Deutsche Version (HADS-D).* (Huber, 1995).
71 Young, K. S. Internet addiction: The emergence of a new clinical disorder. *Cyberpsychol Behav* **1,** 237-244 (1998).
72 Floridou, G. A., Williamson, V. J., Stewart, L. & Müllensiefen, D. The Involuntary Musical Imagery Scale (IMIS). *Psychomusicology: Music, Mind, and Brain* **25,** 28 (2015).
73 Wells, A. & Cartwright-Hatton, S. A short form of the metacognitions questionnaire: properties of the MCQ-30. *Behav Res Ther* **42,** 385-396 (2004).
74 Sadeghi, H., Hajloo, N., Babayi, K. & Shahri, M. The relationship between metacognition and obsessive beliefs, and procrastination in students of Tabriz and Mohaghegh Ardabili Universities, Iran. *Iran J Psychiatry Behav Sci* **8,** 42 (2014).
75 Ophir, E., Nass, C. & Wagner, A. D. Cognitive control in media multitaskers. *Proc. Natl. Acad. Sci. U.S.A.* **106,** 15583-15587 (2009).
76 Kuhl, J. & Kazén, M. *Persönlichkeits-Stil-und Störungs-Inventar: PSSI; Manual*. (Hogrefe, 2009).
77 Tangney, J. P., Baumeister, R. F. & Boone, A. L. High self-control predicts good adjustment, less pathology, better grades, and interpersonal success. *J Pers.* **72,** 271-324 (2004).
78 Bertrams, A. & Dickhäuser, O. Messung dispositioneller Selbstkontroll-Kapazität: Eine deutsche Adaptation der Kurzform der Self-Control Scale (SCS-KD). *Diagnostica* **55,** 2-10 (2009).
79 Paulhus, D. L. Dark triad of personality (D3-short). *Measurement instrument database for the social sciences* (2013).
80 Jones, D. N. & Paulhus, D. L. Introducing the short dark triad (SD3) a brief measure of

dark personality traits. *Assessment* **21**, 28-41 (2014).
81 Carriere, J. S., Seli, P. & Smilek, D. Wandering in both mind and body: individual differences in mind wandering and inattention predict fidgeting. *Can J Exp Psychol* **67,** 19 (2013).
82 Crowne, D. P. & Marlowe, D. A new scale of social desirability independent of psychopathology. *J Consult Psychol.* **24,** 349 (1960).
83 Stöber, J. Die Soziale-Erwünschtheits-Skala-17 (SES-17): Entwicklung und erste Befunde zu Reliabilität und Validität. (1999).
84 O'malley, P. M. & Bachman, J. G. Self-esteem and education: Sex and cohort comparisons among high school seniors. *J Pers Soc Psychol* **37,** 1153 (1979).
85 Stöber, J. Tuckman procrastination scale-Deutsch (TPS-D). *Unveröffentlichtes Manuskript* (1995).
86 Tuckman, B. W. The development and concurrent validity of the procrastination scale. *Educ Psychol Meas* **51,** 473-480 (1991).
87 Whiteside, S. P. & Lynam, D. R. The five factor model and impulsivity: Using a structural model of personality to understand impulsivity. *Pers Individ Dif* **30,** 669-689 (2001).
88 Lynam, D. R., Smith, G. T., Whiteside, S. P. & Cyders, M. A. The UPPS-P: Assessing five personality pathways to impulsive behavior. *West Lafayette, IN: Purdue University* (2006).
89 McCarthy-Jones, S. & Fernyhough, C. The varieties of inner speech: links between quality of inner speech and psychopathological variables in a sample of young adults. *Conscious Cogn* **20,** 1586-1593 (2011).
90 Silvia, P. J. *et al.* Assessing creativity with divergent thinking tasks: Exploring the reliability and validity of new subjective scoring methods**.** *Psychol Aesthet Creat Arts* **2,** 68 (2008).
91 Guilford, J., Christensen, P., Merrifield, P. & Wilson, R. Alternate uses: Manual of instructions and interpretation. *Orange, CA: Sheridan Psychological Services* (1978).
92 Landmann, N. *et al.* Entwicklung von 130 deutschsprachigen Compound Remote Associate (CRA)-Worträtseln zur Untersuchung kreativer Prozesse im deutschen Sprachraum. *Psychologische Rundschau* (2014).
93 Lee, C. S., Huggins, A. C. & Therriault, D. J. A measure of creativity or intelligence? Examining internal and external structure validity evidence of the Remote Associates Test. *Psychol Aesthet Creat Arts* **8**, 446 (2014).
94 Eagleman, D. M., Kagan, A. D., Nelson, S. S., Sagaram, D. & Sarma, A. K. A standardized test battery for the study of synesthesia. *J. Neurosci. Methods* **159**, 139-145 (2007).
95 Jankowska, D. M. & Karwowski, M. Measuring creative imagery abilities. *Front Psychol* **6**, 1591 (2015).
96 Young, K. S. Internet addiction: symptoms, evaluation and treatment. *Innovations in clinical practice: A source book* **17**, 19-31 (1999).
97 Streiner, D. L. Starting at the beginning: an introduction to coefficient alpha and internal consistency. *J Pers Assess* **80**, 99-103 (2003).
98 Limesurvey GmbH. / LimeSurvey: An Open Source survey tool /LimeSurvey GmbH, Hamburg, Germany. URL http://www.limesurvey.org

Data Citation

1. Nooner, K.B., Colcombe, S.J., Tobe, R.H., Mennes, M., Benedict, M.M., Moreno, A.L., Panek, L.J., Brown, S., Zavitz, S.T., Li, Q., Sikka, S., Gutman, D., Bangaru, S., Schlachter, R.T., Kamiel, S.M., Anwar, A.R., Hinz, C.M., Kaplan, M.S., Rachlin, A.B., Adelsberg, S., Cheung, B., Khanuja, R., Yan, C., Craddock, C.C., Calhoun, V., Courtney, W., King, M., Wood, D., Cox, C.L., Kelly, A.M., Di Martino, A., Petkova, E., Reiss, P.T., Duan, N., Thomsen, D., Biswal, B., Coffey, B., Hoptman, M.J., Javitt, D.C., Pomara, N., Sidtis, J.J., Koplewicz, H.S., Castellanos, F.X., Leventhal, B.L., Milham, M.P. *Enhanced Nathan Kline Institute-Rockland Sample* http://fcon_1000.projects.nitrc.org/indi/enhanced/ (2012)

2. Holmes, A. J. *Brain Genomics Superstruct Project (GSP) LONI Image Data Archive* http://neuroinformatics.harvard.edu/gsp/loni (2014)

3. Van Essen, D.C., Smith, S.M., Barch, D.M., Behrens, T.E., Yacoub, E., Ugurbil, K. *WU-Minn HCP Consortium*. https://www.humanconnectome.org/# (2013)

Figure Legends

Figure 1. Age distribution. Age distribution (5-year bins) of the participants split by gender.

Figure 2. Quality assessment of resting-state fMRI scans. Distribution of motion (maximum and mean framewise displacement).

Figure 3. Example impact of fieldmap correction.

Figure 4. Temporal signal-to-noise (tSNR). Group-level variance in temporal signal-to-noise (tSNR) across the brain. tSNR values are lower in ventral regions including orbitofrontal and temporal cortex.

Figure 1. Age distribution (5-year bins) of the participants split by gender.

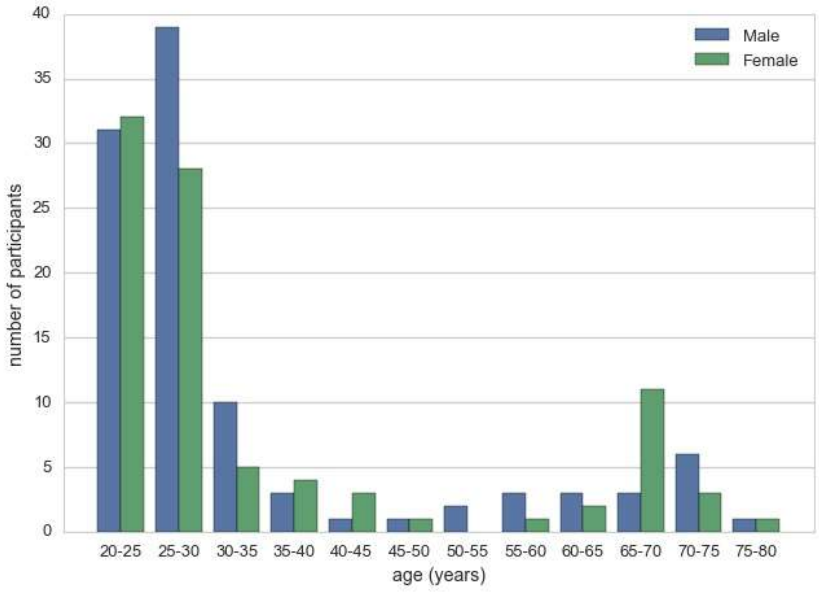

Figure 2. Quality assessment of resting-state fMRI scans.

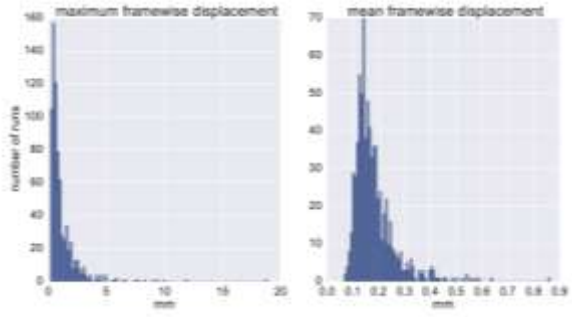

Figure 3. Example impact of fieldmap correction.

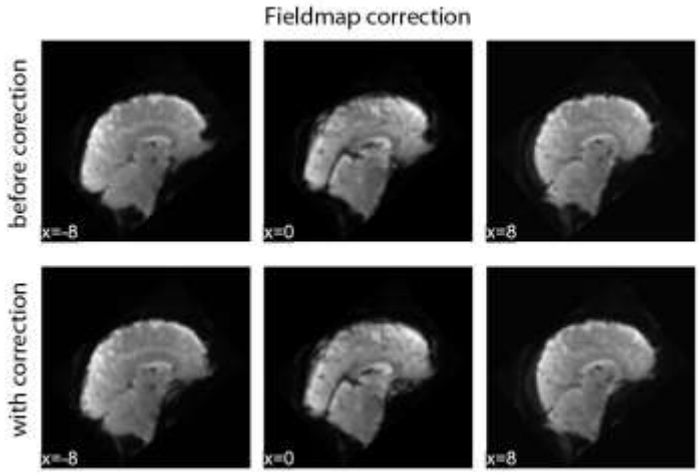

Figure 4. Temporal Signal-to-Noise (tSNR).

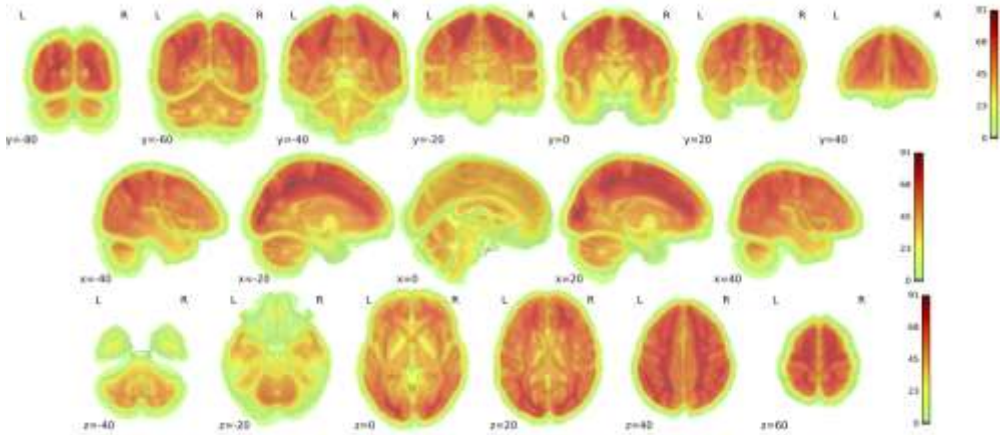

A Systematic Relationship Between Functional Connectivity and Intracortical Myelin in the Human Cerebral Cortex

Huntenburg, J.M., Bazin, P.-L., Goulas, A., Tardif, C.L., Villringer, A., Margulies, D.S. (2017). Cerebral Cortex, 27 (2), 981-997.

http://dx.doi.org/10.1093/cercor/bhx030

Gradients of connectivity distance are anchored in primary cortex

Oligschlaeger, S., Huntenburg, J.M., Golchert, J., Lauckner, M.E., Bonnen, T., Margulies, D.S. (2016). Brain Structure and Function (222)(5).

http://dx.doi.org/10.1007/s00429-016-1333-7

Situating the default-mode network along a principal gradient of macroscale cortical organization

Margulies, D.S., Ghosh, S.S., Goulas, A., Falkiewicz, M., Huntenburg, J.M., Langs, G., Bezgin, G., Eickhoff, S.B., Castellanos, F.X., Petrides, M., Jefferies, E., Small- wood, J. (2016). Proceedings of the National Academy of Sciences USA, 113 (44), 12574-12579. http://dx.doi.org/10.1073/pnas.1608282113

Situating the default-mode network along a principal gradient of macroscale cortical organization

Daniel S. Margulies[a,1], Satrajit S. Ghosh[b,c], Alexandros Goulas[d], Marcel Falkiewicz[a], Julia M. Huntenburg[a,e], Georg Langs[f,g], Gleb Bezgin[h], Simon B. Eickhoff[i,j], F. Xavier Castellanos[k,l], Michael Petrides[m], Elizabeth Jefferies[n,o], and Jonathan Smallwood[n,o]

[a]Max Planck Research Group for Neuroanatomy & Connectivity, Max Planck Institute for Human Cognitive and Brain Sciences, Leipzig 04103, Germany; [b]McGovern Institute for Brain Research, Massachusetts Institute of Technology, Cambridge, MA 02139; [c]Department of Otolaryngology, Harvard Medical School, Cambridge, MA 02115; [d]Department of Computational Neuroscience, University Medical Center Hamburg-Eppendorf, Hamburg 20246, Germany; [e]Neurocomputation and Neuroimaging Unit, Department of Education and Psychology, Free University of Berlin, Berlin 14195, Germany; [f]Department of Biomedical Imaging and Image-Guided Therapy, Computational Imaging Research Laboratory, Medical University of Vienna, Vienna A-1090, Austria; [g]Computer Science and Artificial Intelligence Laboratory, Massachusetts Institute of Technology, Cambridge, MA 02139; [h]McConnell Brain Imaging Centre, Montreal Neurological Institute, McGill University, Montreal, QC, Canada H3A 2B4; [i]Institute for Neuroscience and Medicine, Research Center Jülich, Juelich 52428, Germany; [j]Institute of Clinical Neuroscience and Medical Psychology, Heinrich Heine University, Duesseldorf 40225, Germany; [k]Child Study Center, Department of Child and Adolescent Psychiatry, New York University Langone Medical Center, New York, NY 10016; [l]Nathan Kline Institute for Psychiatric Research, Orangeburg, NY 10962; [m]Cognitive Neuroscience Unit, Montreal Neurological Institute, McGill University, Montreal, QC, Canada H3A 2B4; [n]Department of Psychology, University of York, York YO10 5DD, United Kingdom; and [o]York Neuroimaging Centre, University of York, York YO10 5DD, United Kingdom

Edited by Peter L. Strick, University of Pittsburgh, Pittsburgh, PA, and approved September 9, 2016 (received for review May 27, 2016)

Understanding how the structure of cognition arises from the topographical organization of the cortex is a primary goal in neuroscience. Previous work has described local functional gradients extending from perceptual and motor regions to cortical areas representing more abstract functions, but an overarching framework for the association between structure and function is still lacking. Here, we show that the principal gradient revealed by the decomposition of connectivity data in humans and the macaque monkey is anchored by, at one end, regions serving primary sensory/motor functions and at the other end, transmodal regions that, in humans, are known as the default-mode network (DMN). These DMN regions exhibit the greatest geodesic distance along the cortical surface—and are precisely equidistant—from primary sensory/motor morphological landmarks. The principal gradient also provides an organizing spatial framework for multiple large-scale networks and characterizes a spectrum from unimodal to heteromodal activity in a functional metaanalysis. Together, these observations provide a characterization of the topographical organization of cortex and indicate that the role of the DMN in cognition might arise from its position at one extreme of a hierarchy, allowing it to process transmodal information that is unrelated to immediate sensory input.

topography | connectivity | cortical organization | default-mode network | gradients

A key assumption in neuroscience is that the topographical structure of the cerebral cortex provides an organizing principle that constrains its cognitive processes. Recent advances in the field of human connectomics have revealed multiple large-scale networks (1–3), each characterized by distinct functional profiles (4). Some are related to basic primary functions, such as movement or perceiving sounds and images; some serve well-documented, domain-general functions, such as attention or cognitive control (5–8); and some have functional characteristics that remain less well-understood, such as the default-mode network (DMN) (9, 10). Although the topography of these distinct distributed networks has been described using multiple methods (1–3), the reason for their particular spatial relationship and how this constrains their function remain unclear.

Advances in mapping local processing streams have revealed spatial gradients that support increasingly abstract levels of representation, often extending along adjacent cortical regions in a stepwise manner (11). In the visual domain, for example, the ventral occipitotemporal object stream transforms simple visual features, coded by neurons in primary visual cortex, into more complex visual descriptions of objects in anterior inferior temporal cortical regions and ultimately, contributes to multimodal semantic representations in the middle temporal cortex and the most anterior temporal cortex that capture the meaning of what we see, hear, and do (12–15). Similarly, in the prefrontal cortex, a rostral–caudal gradient has been proposed, whereby goals become increasingly abstract in anterior areas more distant from motor cortex, because they are increasingly removed from selection processes that operate on specific motor representations (5, 16–19). Much like the function–structure correspondence elucidated by topographic maps within sensory and motor areas (20, 21), these processing gradients provide a systematic mapping between spatial position and a functional spectrum of increasingly abstract representations (22).

Processing gradients have proven useful for understanding the relation between specific regions and function in separate domains: Mesulam (23) observed that the emergence of more abstract functional classes of cortex may follow a similar trajectory, hypothesizing that abstract categories emerge from the convergence of information across modalities (Fig. 1*C*). This notion has recently been extended by Buckner and Krienen (24), who proposed the "tethering hypothesis," arguing that association cortex gains its functional attributes through its increasing spatial distance from the constraints that determine the functional specialization of

Significance

We describe an overarching organization of large-scale connectivity that situates the default-mode network at the opposite end of a spectrum from primary sensory and motor regions. This topography, based on the differentiation of connectivity patterns, is also embedded in the spatial distance along the cortical surface between these respective systems. In addition, this connectivity gradient accounts for the respective positions of canonical networks and captures a functional spectrum from perception and action to more abstract cognitive functions. These results suggest that the default-mode network consists of regions at the top of a representational hierarchy that describe the current cognitive landscape in the most abstract terms.

Author contributions: D.S.M., M.P., E.J., and J.S. designed research; D.S.M. performed research; D.S.M., S.S.G., M.F., J.M.H., G.L., G.B., and S.B.E. contributed new reagents/analytic tools; D.S.M. analyzed data; and D.S.M., S.S.G., A.G., M.F., J.M.H., G.L., G.B., S.B.E., F.X.C., M.P., E.J., and J.S. wrote the paper.

The authors declare no conflict of interest.

This article is a PNAS Direct Submission.

Freely available online through the PNAS open access option.

[1]To whom correspondence should be addressed. Email: margulies@cbs.mpg.de.

This article contains supporting information online at www.pnas.org/lookup/suppl/doi:10.1073/pnas.1608282113/-/DCSupplemental.

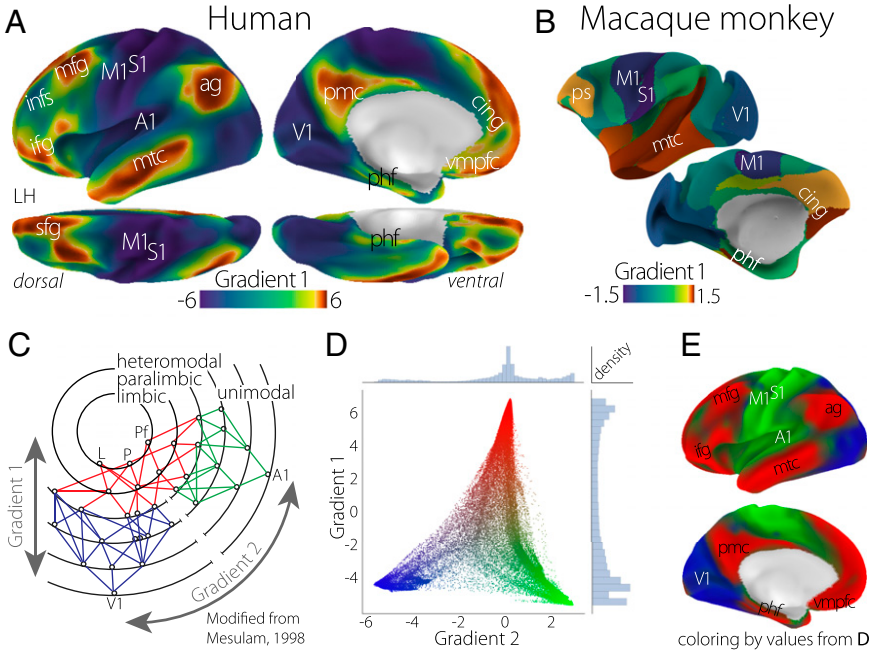

Fig. 1. The principal gradient of connectivity in both the (*A*) human and (*B*) macaque monkey cortices shows a spectrum between unimodal regions (dark blue) and transmodal regions (sienna), which in the human cortex, peaks in regions corresponding to the DMN. The proximity of colors can be interpreted as greater similarity of connectivity patterns. (*C*) The illustration of connectivity organization suggested by Mesulam (23) proposes a hierarchy of processing from distinct unimodal areas to integrative transmodal areas. Labels Gradient 1 and Gradient 2, which were not included in the original figure, correspond to the results in *D*. Modified from ref. 23. (*D*) A scatter plot of the first two connectivity embedding gradients. Gradient 1 extends between primary sensorimotor and transmodal regions (red). Gradient 2 separates somatomotor and auditory cortex (green) from visual cortex (blue). Histograms depicting the distribution of values are presented on the respective axes. (*E*) Colors from the scatter plot are presented on the cortical surface for anatomical orientation. A1, primary auditory; ag, angular gyrus; cing, anterior cingulate cortex; ifg, inferior frontal gyrus; infs, intermediate frontal sulcus; L, limbic; M1, primary motor; mfg, middle frontal gyrus; mtc, middle temporal cortex; P, parietal; Pf, prefrontal; phf, parahippocampal formation; pmc, posteromedial cortex; ps, principal sulcus; S1, primary somatosensory; sfg, superior frontal gyrus; V1, primary visual; vmpfc, ventromedial prefrontal cortex.

primary cortex. These viewpoints suggest that there may be macroscale gradients that integrate information across multiple domains into progressively more abstract representations, in which local gradients within specific cortical systems could be situated and understood.

One large-scale cortical system with function that remains unclear is the DMN. Initially identified through its tendency to deactivate during externally oriented tasks (25), the DMN has since been shown to activate in tasks that depend on information retrieved from memory, such as remembering the past or thinking about the future, or considering the mental states of others (reviews are in refs. 10 and 26). The DMN is also known to play a role in states that are less related to ongoing environmental events, such as daydreaming and mind wandering (27–30), and contributes to lapses in external processing (31). A consensus view on the role of the DMN in human cognition is still lacking, however, because of the increasing number of cognitive domains in which it has been implicated. As well as playing an active role during states, such as autobiographical memory retrieval, social cognition, and future thinking, the DMN has recently been shown to operate in concert with regions implicated in cognitive control during complex working memory tasks (32–36). This emerging evidence illustrates that the DMN is not tied to a specific form of informational content, leading to suggestions that it acts as a hub that integrates representational information across the cortex (30, 37).

To understand the topographic organization of the cerebral cortex at the macroscale (38), we explore how the principal variance in cortical connectivity relates to the topography of structure and function by addressing four key questions. (*i*) Is there a macroscale gradient of connectivity in the human brain that reflects the systematic integration across modalities in a hierarchical fashion? (*ii*) Does this macroscale organization relate to the geometric structure of the cortex? (*iii*) Does the organization captured by the principal gradient account for the spatial distribution of large-scale networks and the associated functions across the cortex? (*iv*) Do these observations provide a framework for understanding the functional role of the DMN in cognition?

Results

We began our analysis by characterizing the components describing the maximum variance in functional connectivity patterns—the extent to which nodes agree in the spatial distribution of correlations—across the human cerebral cortex (Fig. 1 and Fig. S1). The functional connectivity matrix consisted of 91,282 cortical and subcortical "grayordinates" with a resolution of 2 mm from the preprocessed dense connectome S900 release of the Human Connectome Project (HCP) (39). These data were based on 1 h of resting-state fMRI data acquired from 820 healthy adult individuals. No further processing of the connectivity matrices beyond those already implemented by the HCP, which included minimal spatial smoothing of 2 mm FWHM (40), was conducted.

Rather than delineating discrete network parcellations, we implemented a method that captures gradients in connectivity patterns over space—a cortical feature termed "connectopies" (41). This method, known as diffusion embedding (42), allows local and long distance connections to be projected into a common space more effectively than approaches that use linear dimensionality reduction, such as principal component analysis (*SI Materials and Methods*). The resultant components, which we describe here as "gradients," are unitless and identify the position of nodes along the respective embedding axis that encodes the dominant differences in nodes' connectivity patterns.

The Principal Gradient in Humans and Macaque Monkeys. The principal gradient (Fig. 1*A*), which accounts for the greatest variance in connectivity in the human brain (Fig. S2), is anchored at one end by the primary and unimodal visual, somatosensory/motor, and auditory regions. At the other end are regions including the angular gyrus, rostral anterior cingulate, posteromedial cortex, middle temporal gyrus, and middle and superior frontal gyri—regions that, in humans, are collectively described as the DMN. Regions situated between the two extreme ends of the principal gradient include the inferior frontal sulcus, the intraparietal sulcus, and the inferior temporal sulcus, constituting heteromodal integration and higher-order cognitive regions.

The initial proposal of Mesulam (23) was motivated by tract-tracing studies conducted in the macaque monkey. To determine whether our method would generalize to these forms of data, we performed the same embedding analysis on a publicly available database of tract-tracing studies conducted in the macaque monkey. The principal gradient of the macaque monkey cerebral cortex is presented in Fig. 1*B* and similar to the human functional connectivity-based results, anchored at one end by visual and somatosensory/motor regions and at the other end by higher-order transmodal regions in the temporal lobe and the medial and lateral prefrontal cortexes. The cross-species correspondence of the principal gradient suggests that this axis of connectivity variation is phylogenetically conserved and may represent a primary dimension of cortical expansion (43).

The topography of the principal gradient in both the human and macaque monkey is consistent with the claim that cortical connectivity is organized along a dimension spanning primary/unimodal and transmodal regions—a hypothesis that is summarized schematically along the Gradient 1 dimension in Fig. 1*C*. However, for this spectrum to indicate hierarchical integration across distinct modalities, the following connectivity component should distinguish between primary modalities as indicated by the dimension Gradient 2 in Fig. 1*C*.

Consistent with the hypothesis by Mesulam (23) (Fig. 1*C*), the component accounting for the second-most variance in connectivity in the human brain differentiates regions solely within the unimodal end of the principal gradient (Fig. 1*D*). One end of the spectrum is characterized by regions of the occipital cortex implicated in processing visual input, whereas the opposite end includes the somatosensory and motor regions surrounding the central sulcus as well as the auditory regions of the temporal perisylvian region (Fig. 1*E*). The convergence described by the first two connectivity gradients across sensory/motor modalities and toward a singular set of nodes within transmodal cortex is consistent with the claim that the principal gradient is organized along a dimension that integrates unimodal regions in a hierarchical manner (Fig. 1*C*). Moreover, the principal gradient, anchored at one end by the DMN, contains within it several local processing gradients that have already been described within the temporal and frontal lobes (12–15, 17–19). Additional gradients describing progressively less connectivity variance are available in Fig. S1.

DMN Peaks of the Principal Gradient Are Equidistant from Primary Areas. Having characterized the topography of a principal gradient in connectivity, we next investigated whether it is related to the intrinsic geometry of the cortex. To do so, we examined whether regions at the extreme of the DMN end occupy spatial locations that are maximally distant along the cortical surface from unimodal regions. We selected seven peak cortical nodes across the DMN clusters of the principal gradient and calculated the minimum geodesic distance from all other nodes to any of these "seed" nodes (additional description of methods is in *SI Materials and Methods*).

Fig. 2 shows that cortical distance reproduces many features of the spatial embedding of the principal gradient. Four of the peak DMN nodes are equidistant from the central sulcus, which is the topographical landmark of primary somatosensory/motor cortex. Likewise, we observe a similar correspondence with the calcarine sulcus, marking the location of primary visual cortex. More generally, distance clearly increases with lower principal gradient values, with an especially rapid transition in the connectivity gradient between 25 and 40 mm and plateaus at the extremes (Fig. 2*B*). This relationship is, nevertheless, captured by a linear fit ($R^2 = 0.55$). It is noteworthy that unimodal regions are at least 40 mm from the DMN peaks. In similar analyses of macaque monkey cortical distance (Fig. S3), we observed a comparable distance threshold for unimodal regions. In sum, this analysis shows that the principal connectivity gradient reflects macrostructural features of cortical organization: the nodes corresponding to one extreme end of the gradient—core regions of the DMN—are maximally distant from regions that directly govern perception and action.

The Principal Gradient Captures the Spatial Layout of Large-Scale Networks. We next examined the extent to which the principal gradient captures the macroscale layout of intrinsic functional connectivity networks. Despite the high reproducibility of large-scale resting-state networks (1, 44–46), there is no clear overarching spatial schema to explain the transition of one network to another. We examined the widely used seven-network parcellation by Yeo et al. (2) with respect to the position of each network along the principal gradient (Fig. 3*A*). [Results using the 17-network parcellation from ref. 2 are presented in Fig. S4.]

Fig. 3 shows that networks are not randomly distributed along this dimension: instead, as shown in the box plots in Fig. 3*B*, cortical nodes from the same network tend to cluster at similar positions. Importantly, the DMN identified in this parcellation (Fig. 3, red) occupies one extreme position along the principal gradient and is maximally separated from visual (Fig. 3, purple) and motor (Fig. 3, blue) networks, which are at the other extreme. One exception is the limbic network (Fig. 3, beige), which includes an extensive range of values. However, the spatial distribution of

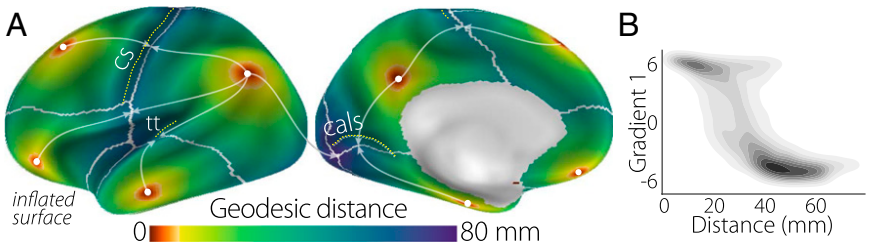

Fig. 2. (*A*) The minimum geodesic distance (in millimeters) from each point on the cortical surface to seven seed nodes located in the positive peaks of the principal gradient. Morphological landmarks of primary areas denoted by white dotted lines, such as the central sulcus (cs; somatosensory/motor), calcarine sulcus (cals; visual), and transverse temporal gyrus (tt; auditory), are equidistant from the surrounding DMN peaks (illustrated by arrows). Gray lines mark the calculated equidistant line. (*B*) The contour scatter plot shows the negative relationship between geodesic distance from seven positive peak locations and the principal gradient ($R^2 = 0.55$).

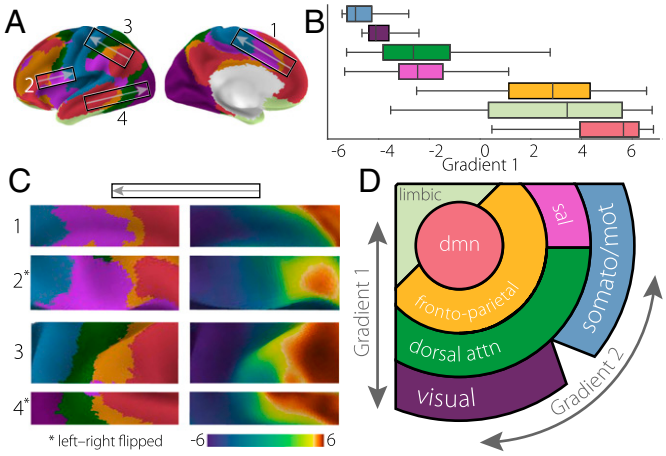

Fig. 3. (*A*) The principal gradient values from each of seven networks (2) are presented as (*B*) box plots ordered by the mean value. (*C*) Illustrative cutouts taken from *A* to show the repeated patterns of network spatial adjacency captured by the principal gradient. Arrows in *A* indicate the corresponding orientation of the cutouts. (*D*) A schematic of the spatial relationships of canonical resting-state networks (2) applying the schema suggested in ref. 23 presented in Fig. 1*C*. dmn, default-mode network; dorsal attn, dorsal attention network; sal, salience network; somato/mot, somatosensory/motor network.

this network may be accounted for by low signal to noise within the original data used for parcellation (2), and it may, thus, not accurately reflect the connectivity of its constituent regions.

This analysis, therefore, shows that the principal gradient of connectivity provides a framework for the spatial ordering of large-scale networks. In addition, the principal gradient captures similar, repeating transitions between these networks, which occur across cortical lobes (Fig. 3*C*). We represent this consistent arrangement as a schematic illustration in Fig. 3*D*. Notably, outlier gradient values for each network are located predominantly at their boundaries (Fig. S5), suggesting that, in some cases, the principal gradient describes gradual connectivity transitions that are obscured by discrete network parcellation.

Distribution of Functions Along the Principal Gradient. Our final analysis explored whether the regions located at the DMN extreme of the gradient serve functions that are abstracted from perception and action. We conducted a metaanalysis using the NeuroSynth database (47) [Figs. S6 and S7 show corresponding analysis using the BrainMap database (48)] and examined the association between a list of topic terms with regions of interest created from five-percentile bins of the principal gradient. Topic terms were sorted by their weighted average position along the gradient, revealing a systematic shift in function. Fig. 4 shows that the unimodal end is characterized by terms depicting acting and perceiving, such as "motor," "visual perception," "multisensory processing," and "auditory processing," whereas the end characterized by the DMN emphasizes terms such as "social cognition," "verbal semantics," and "autobiographical memory"—tasks that rely on complex representations abstracted away from specific sensory and motor processes. Between the extremes, we observe domain-general functions, such as "cued attention," "inhibition," and "working memory," in regions corresponding to the dorsal attention and salience networks above (Fig. 3*D*).

Discussion

Our analysis characterized a principal gradient of cortical organization in the human connectome, which is anchored at one end by systems implicated in perceiving and acting, and at the other end by transmodal association regions, corresponding in humans to the DMN (Fig. 1). A comparative analysis using tract-tracing data from studies in the macaque monkey found a corresponding gradient, providing initial evidence that this axis of connectivity variation may be phylogenetically conserved. The observation that the principal gradient corresponds to the intrinsic geometry of the cortex—regions in the DMN have the greatest geodesic distance along the cortical surface from primary sensory/motor areas—further indicates this axis may provide a crucial blueprint for cortical organization (Fig. 2). We also found that large-scale networks are arranged along this axis, with the same transitions between consistently adjacent networks occurring throughout the cortex (Fig. 3). Finally, a task-based metaanalysis characterizing the functional attributes of this gradient showed a spectrum of increasing abstraction that follows the transition from unimodal cortex to the extreme end of the gradient in the DMN (Fig. 4).

The location of the DMN at one extreme end of the principal gradient provides an organizing principle for understanding its role in cognition. First, these findings provide anatomical support for why the DMN has been associated with processes that are unrelated to immediate stimulus input, such as daydreaming or mind wandering (27, 28, 30). The DMN is at a maximal distance from systems involved in perception and action in both functional connectivity and anatomical space, indicating that the neural activity in these regions is likely to be comparably insulated from direct environmental input (49, 50). Second, the location of the DMN as equidistant from all sensory/motor systems is aligned with its broad range of functions that requires integration between multiple sensory systems, including episodic (51) and semantic memory (52–54), social cognition (55, 56), goal-directed working memory tasks (26, 32, 33, 35), and reward-guided decision making (57, 58). The two cardinal features of the DMN related to abstraction—stimulus independence and content heterogeneity—can be accounted for by its position at the end of a topographical hierarchy that is equidistant from unimodal systems, thus acting as a hub of integration across multiple sensory modalities (37) (Fig. 3*D*).

The principal gradient illustrates a broader topographic organization of large-scale connectivity (38) that accounts for the

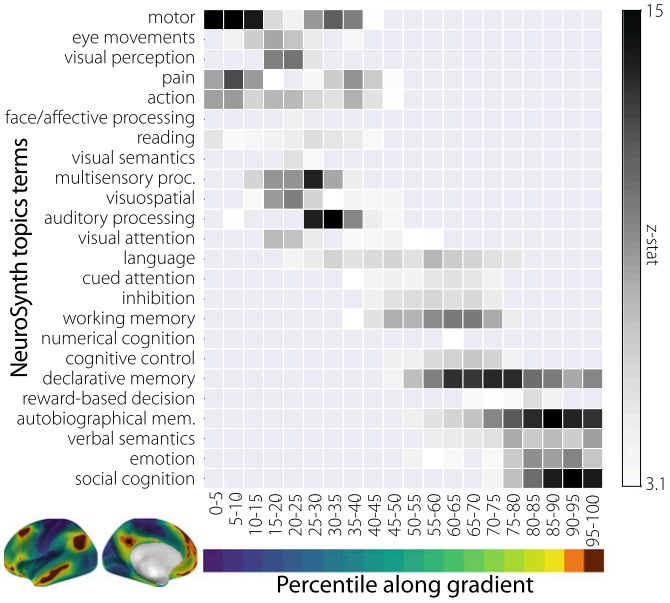

Fig. 4. NeuroSynth metaanalysis of regions of interest along the principal gradient using 24 topic terms. Terms are ordered by the weighted mean of their location along the gradient. Sensory processing terms are located at the top followed by domain-general cognitive functions and then, higher-order abstract cognitive and memory-related processes. Similar results using the BrainMap database are available in *SI Materials and Methods*. autobiographical mem., autobiographical memory; multisensory proc., multisensory processing.

NEUROSCIENCE

spatial arrangement of local processing streams throughout the cerebral cortex. Gradients in both the temporal and prefrontal cortexes are apparent in Fig. 1, showing that these hierarchies are not isolated local phenomena; they emerge as elements of a spectrum that begins within input–output systems and ends with the DMN. Notably, our results are consistent with a recent modification of the rostral–caudal processing gradient described within lateral frontal cortex (59, 60). Rather than the more rostral areas located farther along in the processing hierarchy (18, 19), two distinct hierarchical gradients of temporal- and feature-related abstraction converge in middle lateral prefrontal cortex (60). The consistency between the principal gradient and this revised lateral prefrontal hierarchy suggests that it may provide a source for future studies investigating the detailed topography of local processing streams.

In addition to incorporating local processing streams within a global framework, the principal gradient situates discrete large-scale connectivity networks along a continuous spectrum. With recent advances in multimodal cortical parcellation (61), this approach provides a complementary means to describe the gestalt of the cortical mosaic. Future studies are needed to better characterize the types of transitions between different patterns of large-scale connectivity and identify where processing occurs in a stepwise (11) or "gradiential" manner (22).

It is now widely accepted that the DMN is important, because it permits cognitive processing that is independent of the here and now. This capacity is adaptive, because it permits flexibility: more abstract representations of a stimulus enable the generation of alternative behaviors, allowing original and creative thoughts to emerge (62). Along those lines, a "positive–negative" axis of brain–behavior covariation describes a similar connectivity spectrum, distinguishing the DMN from sensory/motor regions (63). Beyond supporting states of creativity and planning (64, 65), the DMN has also been implicated in almost all psychiatric conditions (66), indicating that there may be costs as well as benefits from the capacity to apprehend the world as it might be rather than seeing it as it is right now.

Materials and Methods

The principal gradient was derived from human (39) and macaque (67, 68) connectivity matrices using diffusion embedding (42)—a nonlinear dimensionality reduction technique (Fig. 1). Geodesic distance along the cortical surface from peak nodes of the transmodal end of the principal gradient, presented in Fig. 2, was calculated using an exact distance algorithm (69, 70). For the comparison with canonical large-scale networks (Fig. 3), the principal gradient values were extracted from each of seven networks from ref. 2. Finally, binarized masks at five-percentile increments of the principal gradient were used as regions of interest in a NeuroSynth (47) metaanalysis (Fig. 4). Additional information regarding methods is available in *SI Materials and Methods* as well as Figs. S1–S7. All software used in this study is openly available at https://neuroanatomyandconnectivity.github.io/gradient_analysis/.

All MRI data used in this study were publicly available and anonymized. Participant recruitment procedures and informed consent forms, including consent to share deidentified data, were previously approved by the Washington University Institutional Review Board as part of the HCP (39).

ACKNOWLEDGMENTS. Data were provided by the HCP, and the Washington University, University of Minnesota, and Oxford University Consortium (Principal Investigators David Van Essen and Kamil Ugurbil; Grant 1U54MH091657) funded by 16 NIH Institutes and Centers that support the NIH Blueprint for Neuroscience Research, and the McDonnell Center for Systems Neuroscience at Washington University. S.S.G. was partially supported by NIH Grants 1R01EB020740-01A1, 1P41EB019936-01A1, 3R01MH092380-04S2, and 1U01MH108168-01. M.P. was supported by Canadian Institutes of Health Research Foundation Grant FDN-143212. E.J. was supported by Biotechnology and Biological Sciences Research Council (BB/J006963/1) and European Research Council Grant 283530-SEMBIND. J.S. was supported by European Research Council Grant WANDERINGMINDS–646927 and a grant from the John Templeton Foundation "Prospective Psychology Stage 2: A Research Competition" (to Martin Seligman). G.L. is supported by NIH National Institute of Biomedical Imaging and Bioengineering Neuroimaging Analysis Center P41EB015902; NIH National Institute of Neurological Disorders and Stroke R01NS086905; and Austrian Science Fund [Fonds zur Förderung wissenschaftlicher Forschung (FWF)] I2714-B31, KLI 544-B27, and Jubiläumsfonds der Österreichischen Nationalbank 15356. S.B.E. is supported by the National Institute of Mental Health (R01-MH074457), the Helmholtz Portfolio Theme "Supercomputing and Modeling for the Human Brain," and the European Union Seventh Framework Programme (FP7/2007-2013) under Grant Agreement 604102. The opinions expressed in this publication are those of the authors and do not necessarily reflect the views of the John Templeton Foundation.

1. Damoiseaux JS, et al. (2006) Consistent resting-state networks across healthy subjects. *Proc Natl Acad Sci USA* 103(37):13848–13853.
2. Yeo BTT, et al. (2011) The organization of the human cerebral cortex estimated by intrinsic functional connectivity. *J Neurophysiol* 106(3):1125–1165.
3. Power JD, et al. (2011) Functional network organization of the human brain. *Neuron* 72(4):665–678.
4. Smith SM, et al. (2009) Correspondence of the brain's functional architecture during activation and rest. *Proc Natl Acad Sci USA* 106(31):13040–13045.
5. Petrides M (2005) Lateral prefrontal cortex: Architectonic and functional organization. *Philos Trans R Soc Lond B Biol Sci* 360(1456):781–795.
6. Duncan J (2010) The multiple-demand (md) system of the primate brain: Mental programs for intelligent behaviour. *Trends Cogn Sci* 14(4):172–179.
7. Cole MW, Yarkoni T, Repovs G, Anticevic A, Braver TS (2012) Global connectivity of prefrontal cortex predicts cognitive control and intelligence. *J Neurosci* 32(26):8988–8999.
8. Petrides M (2015) Lateral and dorsomedial prefrontal cortex and the control of cognition. *Brain Mapping: An Encyclopedic Reference, Volume 2: Anatomy and Physiology, Systems*, ed Toga AW (Academic, London), pp 417–422.
9. Greicius MD, Krasnow B, Reiss AL, Menon V (2003) Functional connectivity in the resting brain: A network analysis of the default mode hypothesis. *Proc Natl Acad Sci USA* 100(1):253–258.
10. Raichle ME (2015) The brain's default mode network. *Annu Rev Neurosci* 38:433–447.
11. Sepulcre J, Sabuncu MR, Yeo TB, Liu H, Johnson KA (2012) Stepwise connectivity of the modal cortex reveals the multimodal organization of the human brain. *J Neurosci* 32(31):10649–10661.
12. Mishkin M, Ungerleider LG (1982) Contribution of striate inputs to the visuospatial functions of parieto-preoccipital cortex in monkeys. *Behav Brain Res* 6(1):57–77.
13. Goodale MA, Milner AD (1992) Separate visual pathways for perception and action. *Trends Neurosci* 15(1):20–25.
14. Patterson K, Nestor PJ, Rogers TT (2007) Where do you know what you know? the representation of semantic knowledge in the human brain. *Nat Rev Neurosci* 8(12):976–987.
15. Visser M, Jefferies E, Embleton KV, Lambon Ralph MA (2012) Both the middle temporal gyrus and the ventral anterior temporal area are crucial for multimodal semantic processing: Distortion-corrected fMRI evidence for a double gradient of information convergence in the temporal lobes. *J Cogn Neurosci* 24(8):1766–1778.
16. Koechlin E, Ody C, Kouneiher F (2003) The architecture of cognitive control in the human prefrontal cortex. *Science* 302(5648):1181–1185.
17. Petrides M (2005) *From Monkey Brain to Human Brain. A Fyssen Foundation Symposium*, eds Dehaene S, Duhamel J-R, Hauser MD, Rizzolatti G (MIT Press, Cambridge, MA), pp 293–314.
18. Badre D (2008) Cognitive control, hierarchy, and the rostro-caudal organization of the frontal lobes. *Trends Cogn Sci* 12(5):193–200.
19. Badre D, D'Esposito M (2009) Is the rostro-caudal axis of the frontal lobe hierarchical? *Nat Rev Neurosci* 10(9):659–669.
20. Kaas JH (1997) Topographic maps are fundamental to sensory processing. *Brain Res Bull* 44(2):107–112.
21. Kaas JH (1987) The organization of neocortex in mammals: Implications for theories of brain function. *Annu Rev Psychol* 38:129–151.
22. Goldberg E (1989) Gradiental approach to neocortical functional organization. *J Clin Exp Neuropsychol* 11(4):489–517.
23. Mesulam MM (1998) From sensation to cognition. *Brain* 121(Pt 6):1013–1052.
24. Buckner RL, Krienen FM (2013) The evolution of distributed association networks in the human brain. *Trends Cogn Sci* 17(12):648–665.
25. Shulman GL, et al. (1997) Common blood flow changes across visual tasks. II. Decreases in cerebral cortex. *J Cogn Neurosci* 9(5):648–663.
26. Spreng RN, Grady CL (2010) Patterns of brain activity supporting autobiographical memory, prospection, and theory of mind, and their relationship to the default mode network. *J Cogn Neurosci* 22(6):1112–1123.
27. Mason MF, et al. (2007) Wandering minds: The default network and stimulus-independent thought. *Science* 315(5810):393–395.
28. Christoff K, Gordon AM, Smallwood J, Smith R, Schooler JW (2009) Experience sampling during fMRI reveals default network and executive system contributions to mind wandering. *Proc Natl Acad Sci USA* 106(21):8719–8724.
29. Stawarczyk D, Majerus S, Maquet P, D'Argembeau A (2011) Neural correlates of ongoing conscious experience: Both task-unrelatedness and stimulus-independence are related to default network activity. *PLoS One* 6(2):e16997.
30. Smallwood J, et al. (2016) Representing representation: Integration between the temporal lobe and the posterior cingulate influences the content and form of spontaneous thought. *PLoS One* 11(4):e0152272.
31. Weissman DH, Roberts KC, Visscher KM, Woldorff MG (2006) The neural bases of momentary lapses in attention. *Nat Neurosci* 9(7):971–978.
32. Vatansever D, Menon DK, Manktelow AE, Sahakian BJ, Stamatakis EA (2015) Default mode dynamics for global functional integration. *J Neurosci* 35(46):15254–15262.

33. Konishi M, McLaren DG, Engen H, Smallwood J (2015) Shaped by the past: The default mode network supports cognition that is independent of immediate perceptual input. *PLoS One* 10(6):e0132209.
34. Spreng RN, et al. (2014) Goal-congruent default network activity facilitates cognitive control. *J Neurosci* 34(42):14108–14114.
35. Crittenden BM, Mitchell DJ, Duncan J (2015) Recruitment of the default mode network during a demanding act of executive control. *eLife* 4:e06481.
36. Krieger-Redwood K, et al. (2016) Down but not out in posterior cingulate cortex: Deactivation yet functional coupling with prefrontal cortex during demanding semantic cognition. *Neuroimage* 141:366–377.
37. van den Heuvel MP, Sporns O (2013) Network hubs in the human brain. *Trends Cogn Sci* 17(12):683–696.
38. Jbabdi S, Sotiropoulos SN, Behrens TE (2013) The topographic connectome. *Curr Opin Neurobiol* 23(2):207–215.
39. Van Essen DC, et al. (2013) The WU-Minn human connectome project: An overview. *Neuroimage* 80:62–79.
40. Glasser MF, et al. (2013) The minimal preprocessing pipelines for the human connectome project. *Neuroimage* 80:105–124.
41. Haak KV, Marquand AF, Beckmann CF (2016) Connectopic mapping with resting-state fMRI. arXiv:1602.07100.
42. Coifman RR, et al. (2005) Geometric diffusions as a tool for harmonic analysis and structure definition of data: Diffusion maps. *Proc Natl Acad Sci USA* 102(21):7426–7431.
43. Hill J, et al. (2010) Similar patterns of cortical expansion during human development and evolution. *Proc Natl Acad Sci USA* 107(29):13135–13140.
44. Biswal BB, et al. (2010) Toward discovery science of human brain function. *Proc Natl Acad Sci USA* 107(10):4734–4739.
45. Wang D, et al. (2015) Parcellating cortical functional networks in individuals. *Nat Neurosci* 18(12):1853–1860.
46. Gordon EM, Laumann TO, Adeyemo B, Petersen SE (October 13, 2015) Individual variability of the system-level organization of the human brain. *Cereb Cortex*.
47. Yarkoni T, Poldrack RA, Nichols TE, Van Essen DC, Wager TD (2011) Large-scale automated synthesis of human functional neuroimaging data. *Nat Methods* 8(8):665–670.
48. Fox PT, Lancaster JL (2002) Opinion: Mapping context and content: The BrainMap model. *Nat Rev Neurosci* 3(4):319–321.
49. Kiebel SJ, Daunizeau J, Friston KJ (2008) A hierarchy of time-scales and the brain. *PLoS Comput Biol* 4(11):e1000209.
50. Friston K (2013) Life as we know it. *J R Soc Interface* 10(86):20130475.
51. Schacter DL, Addis DR (2007) The cognitive neuroscience of constructive memory: Remembering the past and imagining the future. *Philos Trans R Soc Lond B Biol Sci* 362(1481):773–786.
52. Binder JR, Desai RH, Graves WW, Conant LL (2009) Where is the semantic system? a critical review and meta-analysis of 120 functional neuroimaging studies. *Cereb Cortex* 19(12):2767–2796.
53. Jefferies E (2013) The neural basis of semantic cognition: Converging evidence from neuropsychology, neuroimaging and TMS. *Cortex* 49(3):611–625.
54. Constantinescu AO, O'Reilly JX, Behrens TEJ (2016) Organizing conceptual knowledge in humans with a gridlike code. *Science* 352(6292):1464–1468.
55. Amodio DM, Frith CD (2006) Meeting of minds: The medial frontal cortex and social cognition. *Nat Rev Neurosci* 7(4):268–277.
56. Amft M, et al. (2015) Definition and characterization of an extended social-affective default network. *Brain Struct Funct* 220(2):1031–1049.
57. Fellows LK (2011) Orbitofrontal contributions to value-based decision making: Evidence from humans with frontal lobe damage. *Ann N Y Acad Sci* 1239:51–58.
58. Chau BKH, Kolling N, Hunt LT, Walton ME, Rushworth MFS (2014) A neural mechanism underlying failure of optimal choice with multiple alternatives. *Nat Neurosci* 17(3):463–470.
59. Goulas A, Uylings HBM, Stiers P (2014) Mapping the hierarchical layout of the structural network of the macaque prefrontal cortex. *Cereb Cortex* 24(5):1178–1194.
60. Nee DE, D'Esposito M (March 21, 2016) The hierarchical organization of the lateral prefrontal cortex. *eLife*, 10.7554/eLife.12112.
61. Glasser MF, et al. (2016) A multi-modal parcellation of human cerebral cortex. *Nature* 536(7615):171–178.
62. Haggard P (2008) Human volition: Towards a neuroscience of will. *Nat Rev Neurosci* 9(12):934–946.
63. Smith SM, et al. (2015) A positive-negative mode of population covariation links brain connectivity, demographics and behavior. *Nat Neurosci* 18(11):1565–1567.
64. Spreng RN, Stevens WD, Chamberlain JP, Gilmore AW, Schacter DL (2010) Default network activity, coupled with the frontoparietal control network, supports goal-directed cognition. *Neuroimage* 53(1):303–317.
65. Beaty RE, et al. (2014) Creativity and the default network: A functional connectivity analysis of the creative brain at rest. *Neuropsychologia* 64:92–98.
66. Broyd SJ, et al. (2009) Default-mode brain dysfunction in mental disorders: A systematic review. *Neurosci Biobehav Rev* 33(3):279–296.
67. Stephan KE, et al. (2001) Advanced database methodology for the Collation of Connectivity data on the Macaque brain (CoCoMac). *Philos Trans R Soc Lond B Biol Sci* 356(1412):1159–1186.
68. Bakker R, Wachtler T, Diesmann M (2012) CoCoMac 2.0 and the future of tract-tracing databases. *Front Neuroinform* 6:30.
69. Mitchell JSB, Mount DM, Papadimitriou CH (1987) The discrete geodesic problem. *SIAM J Comput* 16(4):647–668.
70. O'Rourke J (1999) Computational geometry column 35. *Int J Comp Geom Appl* 9(4-5): 513–515.
71. Marcus DS, et al. (2011) Informatics and data mining tools and strategies for the human connectome project. *Front Neuroinform* 5:4.
72. Fischl B (2012) FreeSurfer. *Neuroimage* 62(2):774–781.
73. Jenkinson M, Bannister P, Brady M, Smith S (2002) Improved optimization for the robust and accurate linear registration and motion correction of brain images. *Neuroimage* 17(2):825–841.
74. Jenkinson M, Beckmann CF, Behrens TEJ, Woolrich MW, Smith SM (2012) FSL. *Neuroimage* 62(2):782–790.
75. Van Essen DC, Glasser MF, Dierker DL, Harwell J, Coalson T (2012) Parcellations and hemispheric asymmetries of human cerebral cortex analyzed on surface-based atlases. *Cereb Cortex* 22(10):2241–2262.
76. Van Essen DC (2004) Surface-based approaches to spatial localization and registration in primate cerebral cortex. *Neuroimage* 23(Suppl 1):S97–S107.
77. Von Bonin G, Bailey P (1947) *The Neocortex of Macaca Mulatta* (University of Illinois Press, Champaign, IL).
78. Bezgin G, Vakorin VA, van Opstal AJ, McIntosh AR, Bakker R (2012) Hundreds of brain maps in one atlas: Registering coordinate-independent primate neuro-anatomical data to a standard brain. *Neuroimage* 62(1):67–76.
79. Lafon S, Lee AB (2006) Diffusion maps and coarse-graining: A unified framework for dimensionality reduction, graph partitioning, and data set parameterization. *IEEE Trans Pattern Anal Mach Intell* 28(9):1393–1403.
80. Ye AQ, et al. (2015) The intrinsic geometry of the human brain connectome. *Brain Inform* 2(4):197–210.
81. Atasoy S, Donnelly I, Pearson J (2016) Human brain networks function in connectome-specific harmonic waves. *Nat Commun* 7:10340.
82. Von Luxburg U (2007) A tutorial on spectral clustering. *Stat Comput* 17(4):395–416.
83. Tenenbaum JB, De Silva V, Langford JC (2000) A global geometric framework for nonlinear dimensionality reduction. *Science* 290(5500):2319–2323.
84. Langs G, Golland P, Tie Y, Rigolo L, Golby AJ (2010) Functional geometry alignment and localization of brain areas. *Adv Neural Inf Process Syst* 1:1225–1233.
85. Langs G, Tie Y, Rigolo L, Golby AJ, Golland P (2010) Localization of language areas in brain tumor patients by functional geometry alignment. *Proceedings of the MICCAI Workshop on Computational Imaging Biomarkers for Tumors*, eds Shen D, et al. (Beijing, China). Available at www.spl.harvard.edu/publications/item/view/2112. Accessed September 9, 2016.
86. Langs G, Menze BH, Lashkari D, Golland P (2011) Detecting stable distributed patterns of brain activation using gini contrast. *Neuroimage* 56(2):497–507.
87. Langs G, et al. (2011) Learning an atlas of a cognitive process in its functional geometry. *Inf Process Med Imaging* 22:135–146.
88. Langs G, et al. (2014) Decoupling function and anatomy in atlases of functional connectivity patterns: Language mapping in tumor patients. *Neuroimage* 103:462–475.
89. Langs G, Golland P, Ghosh SS (2015) Predicting activation across individuals with resting-state functional connectivity based multi-atlas label fusion. *Medical Image Computing and Computer-Assisted Intervention–MICCAI 2015,* Lecture Notes in Computer Science, eds Navab N, Hornegger J, Wells WM, Frangi AF (Springer, Berlin), Vol 9350, pp 313–320.
90. Fox PT, Lancaster JL, Laird AR, Eickhoff SB (2014) Meta-analysis in human neuroimaging: Computational modeling of large-scale databases. *Annu Rev Neurosci* 37:409–434.
91. Laird AR, et al. (2011) Behavioral interpretations of intrinsic connectivity networks. *J Cogn Neurosci* 23(12):4022–4037.
92. Rottschy C, et al. (2013) Differentiated parietal connectivity of frontal regions for "what" and "where" memory. *Brain Struct Funct* 218(6):1551–1567.

Large-Scale Gradients in Human Cortical Organization. Trends in Cognitive Sciences

Huntenburg, J. M., Bazin, P.-L., & Margulies, D. S. (2017). Published online ahead of print December 01, 2017

http://dx.doi.org/10.1016/j.tics.2017.11.002